



Calhoun: The NPS Institutional Archive
DSpace Repository

Theses and Dissertations

1. Thesis and Dissertation Collection, all items

2004-03

Performance analysis of the IEEE 802.11A
WLAN standard optimum and sub-optimum
receiver in frequency-selective, slowly fading
Nakagami channels with AWGN and pulsed
noise jamming

Kalogrias, Christos

Monterey California. Naval Postgraduate School

<http://hdl.handle.net/10945/1666>

Copyright is reserved by the copyright owner

Downloaded from NPS Archive: Calhoun



<http://www.nps.edu/library>

Calhoun is the Naval Postgraduate School's public access digital repository for research materials and institutional publications created by the NPS community. Calhoun is named for Professor of Mathematics Guy K. Calhoun, NPS's first appointed -- and published -- scholarly author.

Dudley Knox Library / Naval Postgraduate School
411 Dyer Road / 1 University Circle
Monterey, California USA 93943



NAVAL POSTGRADUATE SCHOOL

MONTEREY, CALIFORNIA

THESIS

PERFORMANCE ANALYSIS OF THE IEEE 802.11A WLAN STANDARD
OPTIMUM AND SUB-OPTIMUM RECEIVER IN FREQUENCY-
SELECTIVE, SLOWLY FADING NAKAGAMI CHANNELS WITH AWGN
AND PULSED NOISE JAMMING

by

Christos Kalogrias

March 2004

Thesis Advisor:
Second Reader:

Clark Robertson
Don Wadsworth

Approved for public release; distribution is unlimited

THIS PAGE INTENTIONALLY LEFT BLANK

REPORT DOCUMENTATION PAGE			<i>Form Approved OMB No. 0704-0188</i>	
Public reporting burden for this collection of information is estimated to average 1 hour per response, including the time for reviewing instruction, searching existing data sources, gathering and maintaining the data needed, and completing and reviewing the collection of information. Send comments regarding this burden estimate or any other aspect of this collection of information, including suggestions for reducing this burden, to Washington headquarters Services, Directorate for Information Operations and Reports, 1215 Jefferson Davis Highway, Suite 1204, Arlington, VA 22202-4302, and to the Office of Management and Budget, Paperwork Reduction Project (0704-0188) Washington DC 20503.				
1. AGENCY USE ONLY (Leave blank)		2. REPORT DATE March 2004	3. REPORT TYPE AND DATES COVERED Master's Thesis	
4. TITLE AND SUBTITLE: Performance analysis of the IEEE 802.11a WLAN standard Optimum and Sub-optimum receiver in frequency-selective, slowly fading Nakagami channels with AWGN and pulsed noise jamming.			5. FUNDING NUMBERS	
6. AUTHOR(S) Christos Kalogrias				
7. PERFORMING ORGANIZATION NAME(S) AND ADDRESS(ES) Naval Postgraduate School Monterey, CA 93943-5000			8. PERFORMING ORGANIZATION REPORT NUMBER	
9. SPONSORING /MONITORING AGENCY NAME(S) AND ADDRESS(ES) N/A			10. SPONSORING/MONITORING AGENCY REPORT NUMBER	
11. SUPPLEMENTARY NOTES The views expressed in this thesis are those of the author and do not reflect the official policy or position of the Department of Defense or the U.S. Government.				
12a. DISTRIBUTION / AVAILABILITY STATEMENT Approved for public release; distribution is unlimited.			12b. DISTRIBUTION CODE	
13. ABSTRACT (maximum 200 words) The objective of this thesis is to investigate the performance of the orthogonal frequency division multiplexing (OFDM) based IEEE 802.11a wireless local area network (WLAN) standard receiver when the signal is transmitted over a frequency selective, slow fading Nakagami channel in a worst case, pulse-noise jamming environment. The different combinations of modulation type (both binary and non-binary modulation) and convolutional code rate specified by the WLAN standard, are examined. Receiver performance with Viterbi soft decision decoding (SDD) is analyzed for additive white Gaussian noise (AWGN) alone as well as for AWGN plus pulse-noise jamming (PNJ). The performance of the IEEE 802.11a WLAN standard receiver is examined both for the scenario where perfect side information is assumed (optimum receiver) and when it is not (sub-optimum receiver). For the sub-optimum receiver scenario, the receiver performance is examined both when noise-normalization is utilized and when only linear combining is utilized. The analysis indicates that the receiver performance is severely affected by the pulse-noise jamming environment for the linear combining scenario; however, the sub-optimum receiver performance is significantly improved when noise-normalization is implemented.				
14. SUBJECT TERMS IEEE 802.11a WLAN Standard, Nakagami Fading Channel, OFDM, Soft Decision Decoding, Pulse-Noise Jamming, Perfect Side Information, Noise-Normalization			15. NUMBER OF PAGES 169	
			16. PRICE CODE	
17. SECURITY CLASSIFICATION OF REPORT Unclassified	18. SECURITY CLASSIFICATION OF THIS PAGE Unclassified	19. SECURITY CLASSIFICATION OF ABSTRACT Unclassified	20. LIMITATION OF ABSTRACT UL	

THIS PAGE INTENTIONALLY LEFT BLANK

Approved for public release; distribution is unlimited

PERFORMANCE ANALYSIS OF THE IEEE 802.11A WLAN STANDARD OPTIMUM AND SUB-OPTIMUM RECEIVER IN FREQUENCY-SELECTIVE, SLOWLY FADING NAKAGAMI CHANNELS WITH AWGN AND PULSED NOISE JAMMING

Christos Kalogrias
Lieutenant, Hellenic Navy
Bachelor of Engineering, Hellenic Naval Academy, 1994

Submitted in partial fulfillment of the
requirements for the degree of

**MASTER OF SCIENCE IN ELECTRICAL ENGINEERING
and
MASTER OF SCIENCE IN SYSTEMS ENGINEERING**

from the

**NAVAL POSTGRADUATE SCHOOL
March 2004**

Author: Christos Kalogrias

Approved by: Clark Robertson
Thesis Advisor

Don Wadsworth
Second Reader

John P. Powers
Chairman, Department of Electrical and Computer Engineering

Dan C. Boger
Chairman, Department of Information Sciences

THIS PAGE INTENTIONALLY LEFT BLANK

ABSTRACT

Wide local area networks (WLAN) are increasingly important in meeting the needs of next generation broadband wireless communications systems for both commercial and military applications. Under IEEE 802.11a 5GHz WLAN standard, OFDM was chosen as the modulation scheme for transmission because of its well-known ability to avoid multi-path effects while achieving high data rates. The objective of this thesis is to investigate the performance of the *IEEE 802.11a* WLAN standard receiver over flat fading Nakagami channels in a worst case, pulse-noise jamming environment, for the different combinations of modulation type (binary and non-binary modulation) and code rate specified by the WLAN standard. Receiver performance with Viterbi soft decision decoding (SDD) will be analyzed for additive white Gaussian noise (AWGN) alone and for AWGN plus pulse-noise jamming. Moreover, the performance of the *IEEE 802.11a* WLAN standard receiver will be examined both in the scenario where perfect side information is considered to be available (optimum receiver) and when it is not (sub-optimum receiver). In the sub-optimum receiver scenario, the receiver performance is examined both when noise-normalization is utilized and when it is not. The receiver performance is severely affected by the pulse-noise jamming environment, especially in the sub-optimum receiver scenario. However, the sub-optimum receiver performance is significantly improved when noise-normalization is implemented.

THIS PAGE INTENTIONALLY LEFT BLANK

TABLE OF CONTENTS

I.	INTRODUCTION.....	1
A.	BACKGROUND	1
B.	OBJECTIVE	1
C.	RELATED RESEARCH	2
D.	THESIS OUTLINE.....	3
II.	BACKGROUND INFORMATION FOR THE IEEE 802.11A WLAN STANDARD	5
A.	OFDM TRANSMISSION TECHNIQUE	5
B.	DATA ERROR CORRECTION MANAGEMENT	7
1.	Forward Error Correction (FEC) Coding.....	8
2.	Viterbi Decoding	9
C.	COMMUNICATION MULTI-PATH CHANNEL.....	10
D.	IEEE 802.11A COMMUNICATION SCHEME	14
1.	IEEE 802.11A TRANSMITTER	15
2.	IEEE 802.11A RECEIVER.....	15
E.	PERFORMANCE ANALYSIS OF MQAM.....	16
III.	PERFORMANCE ANALYSIS OF THE IEEE 802.11A OPTIMUM RECEIVER	25
A.	IEEE 802.11A OPTIMUM RECEIVER.....	25
B.	PERFORMANCE ANALYSIS IN A FADING CHANNEL WITH AWGN.....	29
1.	BPSK/QPSK Modulation	29
a.	<i>Data Rates of 6 and 12 Mbps.....</i>	<i>34</i>
b.	<i>Data Rates of 9 and 18 Mbps.....</i>	<i>34</i>
2.	Non-Binary Modulation	35
a.	<i>Data Rate of 24 Mbps.....</i>	<i>40</i>
b.	<i>Data Rate of 36 Mbps.....</i>	<i>41</i>
c.	<i>Data Rate of 48 Mbps.....</i>	<i>42</i>
d.	<i>Data Rate of 54 Mbps.....</i>	<i>43</i>
3.	Conclusions on the Effect of AWGN on the 802.11a Optimum Receiver.....	44
C.	PERFORMANCE ANALYSIS WITH A HOSTILE PULSED-NOISE JAMER	46
1.	BPSK/QPSK Modulation	47
a.	<i>Data Rates of 6 and 12 Mbps.....</i>	<i>55</i>
b.	<i>Data Rates of 9 and 18 Mbps.....</i>	<i>59</i>
2.	Non-Binary Modulation	60
a.	<i>Data Rate of 24 Mbps.....</i>	<i>61</i>
b.	<i>Data Rate of 36 Mbps.....</i>	<i>63</i>
c.	<i>Data Rate of 48 Mbps.....</i>	<i>64</i>
d.	<i>Data Rate of 54 Mbps.....</i>	<i>67</i>

3.	Conclusions on the Effect of PNJ on the 802.11a Optimum Receiver.....	68
IV.	PERFORMANCE ANALYSIS OF THE IEEE 802.11A SUB-OPTIMUM RECEIVER	73
A.	THE IEEE 802.11A SUB-OPTIMUM RECEIVER	73
B.	PERFORMANCE ANALYSIS IN A FADING CHANNEL WITH AWGN.....	75
1.	BPSK/QPSK Modulation	76
a.	<i>Data Rates of 6 and 12 Mbps.....</i>	80
b.	<i>Data Rates of 9 and 18 Mbps.....</i>	82
2.	Non-Binary Modulation	83
a.	<i>Data Rate of 24 Mbps.....</i>	84
b.	<i>Data Rate of 36 Mbps.....</i>	85
c.	<i>Data Rate of 48 Mbps.....</i>	85
d.	<i>Data Rate of 54 Mbps.....</i>	86
3.	Conclusions on the Effect of AWGN on the 802.11a Sub-Optimum Receiver	87
C.	PERFORMANCE ANALYSIS WITH A HOSTILE PULSED NOISE JAMMER.....	88
1.	BPSK/QPSK Modulation	88
a.	<i>Data Rates of 6 and 12 Mbps.....</i>	94
b.	<i>Data Rates of 9 and 18 Mbps.....</i>	97
2.	Non-binary Modulation	99
a.	<i>Data Rate of 24 Mbps.....</i>	100
b.	<i>Data Rate of 36 Mbps.....</i>	102
c.	<i>Data Rate of 48 Mbps.....</i>	104
d.	<i>Data Rate of 54 Mbps.....</i>	105
3.	Conclusions on the Effect of PNJ on the 802.11a Sub-optimum Receiver.....	107
V.	PERFORMANCE ANALYSIS OF THE IEEE 802.11A SUB-OPTIMUM RECEIVER WITH NOISE-NORMALIZATION.....	111
A.	THE IEEE 802.11A NOISE-NORMALIZED SUB-OPTIMUM RECEIVER	111
B.	PERFORMANCE ANALYSIS IN A FADING CHANNEL WITH HOSTILE PNJ	113
1.	BPSK/QPSK Modulation	113
a.	<i>Data Rates of 6 and 12 Mbps.....</i>	117
b.	<i>Data Rates of 9 and 18 Mbps.....</i>	120
2.	Non-binary Modulation.....	121
a.	<i>Data Rate of 24 Mbps.....</i>	122
b.	<i>Data Rate of 36 Mbps.....</i>	122
c.	<i>Data Rate of 48 Mbps.....</i>	125
d.	<i>Data Rate of 54 Mbps.....</i>	125
3.	Conclusions on the Effect of a Hostile PNJ on an IEEE 802.11a Noise-Normalized Sub-optimum Receiver	127

VI.	CONCLUSIONS	135
A.	SUMMARY OF THESIS FINDINGS.....	135
1.	Conclusions on the Effect of AWGN	135
2.	Conclusions on the Effect of PNJ	136
B.	FUTURE WORK.....	138
C.	CLOSING COMMENTS	138
APPENDIX A.	THE TWO-SIDED LAPLACE TRANSFORM.....	139
	LIST OF REFERENCES	143
	INITIAL DISTRIBUTION LIST	145

THIS PAGE INTENTIONALLY LEFT BLANK

LIST OF FIGURES

Figure 1.	FDM communication technique spectral analysis [After Ref. 1.]	6
Figure 2.	OFDM communication technique spectral analysis [After Ref. 1.]	6
Figure 3.	The convolutional encoder with generator polynomials $g_0 = 133_8$, $g_1 = 171_8$ and constraint length $\nu = 7$ as specified by <i>IEEE 802.11a</i> WLAN standard [From Ref. 3.]	8
Figure 4.	The two types of fading channels [From Ref. 7.]	12
Figure 5.	BPSK performance for $r = 1/2$ and SDD, operating both in a severe ($0.5 \leq m \leq 1$) and a non-severe ($3 \leq m \leq 4$) fading environment.	14
Figure 6.	The IEEE 802.11a transmitter [After Ref. 3.]	15
Figure 7.	The IEEE 802.11a receiver [After Ref. 3.]	15
Figure 8.	Rectangular constellations of all modulation techniques utilized by the <i>IEEE 802.11a</i> WLAN standard [From Ref. 3.]	17
Figure 9.	The 16QAM square constellation with the decision regions and the corresponding limits [After Ref. 3.]	20
Figure 10.	Exact BER for 16QAM vs. the BER obtained by several approximate expressions.	23
Figure 11.	BPSK maximum likelihood receiver (MLR)	26
Figure 12.	802.11a receiver block diagram, optimized to operate with AWGN	29
Figure 13.	Optimum <i>802.11a</i> receiver for a Nakagami fading channel with AWGN for bit rates of 6 and 12 Mbps.	34
Figure 14.	Optimum <i>802.11a</i> receiver for a Nakagami fading channel with AWGN for bit rates of 9 and 18 Mbps.	35
Figure 15.	Optimum <i>802.11a</i> receiver in a Nakagami fading channel with AWGN for bit rate of 24 Mbps ($r = 1/2$).	41
Figure 16.	Optimum <i>802.11a</i> receiver in a Nakagami fading channel with AWGN for bit rate of 36 Mbps ($r = 3/4$).	42
Figure 17.	Optimum <i>802.11a</i> receiver in a Nakagami fading channel with AWGN for bit rate of 48 Mbps ($r = 2/3$).	43
Figure 18.	Optimum <i>802.11a</i> receiver in a Nakagami fading channel with AWGN for bit rate of 54 Mbps ($r = 3/4$).	44
Figure 19.	BER performance of the optimum <i>802.11a</i> receiver in severe Nakagami fading channel ($m = 1$) with AWGN for all specified bit rates.	45
Figure 20.	BER performance of the optimum <i>802.11a</i> receiver in a Nakagami fading channel ($m = 3$) with AWGN for all specified bit rates.	46
Figure 21.	BER performance of <i>802.11a</i> receiver optimized to operate with PNJ, estimated both analytically and numerically, for data rates of 6 and 12 Mbps	56
Figure 22.	BER performance of <i>802.11a</i> receiver optimized to operate with PNJ for various fading conditions and for data rates of 6 and 12 Mbps.	57
Figure 23.	BER performance of <i>802.11a</i> receiver optimized to operate with PNJ for different values of ρ ($0 < \rho \leq 1$) and for data rates of 6 and 12 Mbps.	58

Figure 24.	BER performance of <i>802.11a</i> receiver optimized to operate with PNJ for data rates of 9 and 18 Mbps.	59
Figure 25.	BER performance of <i>802.11a</i> receiver, optimized to operate with PNJ for different values of ρ ($0 < \rho \leq 1$) and for data rates of 9 and 18 Mbps.	60
Figure 26.	BER performance of <i>802.11a</i> receiver optimized to operate with PNJ for data rate of 24 Mbps.	62
Figure 27.	BER performance of <i>802.11a</i> receiver optimized to operate with PNJ for different values of ρ ($0 < \rho \leq 1$) and for data rate of 24 Mbps.	63
Figure 28.	BER performance of <i>802.11a</i> receiver optimized to operate with PNJ for data rate of 36 Mbps.	64
Figure 29.	BER performance of <i>802.11a</i> receiver optimized to operate with PNJ for different values of ρ ($0 < \rho \leq 1$) and for data rate of 36 Mbps.	65
Figure 30.	BER performance of <i>802.11a</i> receiver optimized to operate with PNJ for data rate of 48 Mbps.	66
Figure 31.	BER performance of <i>802.11a</i> receiver optimized to operate under PNJ for different values of ρ ($0 < \rho \leq 1$) and for data rate of 48 Mbps.	66
Figure 32.	BER performance of <i>802.11a</i> receiver optimized to operate with PNJ for data rate of 54 Mbps.	67
Figure 33.	BER performance of <i>802.11a</i> receiver optimized to operate with PNJ for different values of ρ ($0 < \rho \leq 1$) and for data rate of 54 Mbps.	68
Figure 34.	BER performance of the optimum <i>802.11a</i> receiver for a severe Nakagami fading channel ($m = 1$) with PNJ and $\rho = 0.5$ for all specified bit rates.	69
Figure 35.	BER performance of the optimum <i>802.11a</i> receiver for non-severe Nakagami fading channel ($m = 3$) with PNJ and for all specified bit rates. ...	70
Figure 36.	The <i>IEEE 802.11a</i> sub-optimum receiver	73
Figure 37.	Sub-optimum <i>IEEE 802.11a</i> receiver performance for a Nakagami fading channel with AWGN for bit rates of 6 and 12 Mbps.	81
Figure 38.	Sub-optimum <i>IEEE 802.11a</i> receiver performance for a Nakagami fading channel with AWGN for bit rates of 6 and 12 Mbps.	82
Figure 39.	Sub-optimum <i>IEEE 802.11a</i> receiver performance for a Nakagami fading channel with AWGN for bit rate of 24 Mbps.	84
Figure 40.	Sub-optimum <i>IEEE 802.11a</i> receiver performance for a Nakagami fading channel with AWGN for bit rate of 36 Mbps.	85
Figure 41.	Sub-optimum <i>IEEE 802.11a</i> receiver performance for a Nakagami fading channel with AWGN for bit rate of 48 Mbps.	86
Figure 42.	Sub-optimum <i>IEEE 802.11a</i> receiver performance for a Nakagami fading channel with AWGN for bit rate of 54 Mbps.	87
Figure 43.	BER performance of <i>IEEE 802.11a</i> sub-optimum receiver with PNJ for various fading conditions and for data rates of 6 and 12 Mbps.	95
Figure 44.	BER performance of <i>IEEE 802.11a</i> sub-optimum receiver with PNJ for various fading conditions and for data rates of 6 and 12 Mbps.	96
Figure 45.	BER performance of <i>IEEE 802.11a</i> sub-optimum receiver with PNJ for data rates of 9 and 18 Mbps.	98

Figure 46.	BER performance of <i>IEEE 802.11a</i> sub-optimum receiver with PNJ for various fading conditions and for data rates of 9 and 18 Mbps.....	99
Figure 47.	BER performance of <i>IEEE 802.11a</i> sub-optimum receiver with PNJ for a data rate of 24 Mbps.	101
Figure 48.	BER performance of <i>IEEE 802.11a</i> sub-optimum receiver with PNJ for different values of ρ ($0 < \rho \leq 1$) and for a data rate of 24 Mbps..	102
Figure 49.	BER performance of <i>IEEE 802.11a</i> sub-optimum receiver with PNJ for a data rate of 36 Mbps.	103
Figure 50.	BER performance of <i>IEEE 802.11a</i> sub-optimum receiver with PNJ for different values of ρ ($0 < \rho \leq 1$) and for a data rate of 36 Mbps.	103
Figure 51.	BER performance of <i>IEEE 802.11a</i> sub-optimum receiver with PNJ, for data rate of 48 Mbps.	104
Figure 52.	BER performance of <i>IEEE 802.11a</i> sub-optimum receiver with PNJ for different values of ρ ($0 < \rho \leq 1$) and for a data rate of 48 Mbps.	105
Figure 53.	BER performance of <i>IEEE 802.11a</i> sub-optimum receiver with PNJ for a data rate of 54 Mbps.	106
Figure 54.	BER performance of <i>IEEE 802.11a</i> sub-optimum receiver with PNJ for different values of ρ ($0 < \rho \leq 1$) and for a data rate of 54 Mbps.	107
Figure 55.	The <i>IEEE 802.11a</i> noise normalized sub-optimum receiver.	112
Figure 56.	Noise-normalized sub-optimum receiver BER vs. optimum receiver BER with PNJ without fading for data rates of 6 and 12 Mbps.	118
Figure 57.	BER performance of an <i>IEEE 802.11a</i> noise-normalized sub-optimum receiver with PNJ for data rates of 6 and 12 Mbps.	119
Figure 58.	BER performance of an <i>IEEE 802.11a</i> noise-normalized sub-optimum receiver with PNJ for various ρ and for data rates of 6 and 12 Mbps.	119
Figure 59.	BER performance of an <i>IEEE 802.11a</i> noise-normalized sub-optimum receiver with PNJ for data rates of 9 and 18 Mbps.	120
Figure 60.	BER performance of an <i>IEEE 802.11a</i> noise-normalized sub-optimum receiver with PNJ for various ρ and for data rates of 9 and 18 Mbps.	121
Figure 61.	BER performance of an <i>IEEE 802.11a</i> noise-normalized sub-optimum receiver with PNJ for data rate of 24 Mbps.	123
Figure 62.	BER performance of an <i>IEEE 802.11a</i> noise-normalized sub-optimum receiver with PNJ for various ρ and for data rate of 24 Mbps.	123
Figure 63.	BER performance of an <i>IEEE 802.11a</i> noise-normalized sub-optimum receiver with PNJ for data rate of 36 Mbps.	124
Figure 64.	BER performance of an <i>IEEE 802.11a</i> noise-normalized sub-optimum receiver with PNJ for various ρ and for data rate of 36 Mbps.	124
Figure 65.	BER performance of an <i>IEEE 802.11a</i> noise-normalized sub-optimum receiver with PNJ for data rate of 48 Mbps.	125
Figure 66.	BER performance of an <i>IEEE 802.11a</i> noise-normalized sub-optimum receiver with PNJ for various ρ and for data rate of 48 Mbps.	126
Figure 67.	BER performance of an <i>IEEE 802.11a</i> noise-normalized sub-optimum receiver with PNJ for data rate of 54 Mbps.	126

Figure 68.	BER performance of an <i>IEEE 802.11a</i> noise-normalized sub-optimum receiver with PNJ for various ρ and for data rate of 54 Mbps.....	127
Figure 69.	Noise-normalized sub-optimum receiver vs. linear-combining sub-optimum receiver with PNJ for $\rho = 0.1$ and 1.0 and for data rates of 6, 12 Mbps.	130
Figure 70.	Noise-normalized sub-optimum receiver vs. linear-combining sub-optimum receiver with PNJ for $\rho = 0.1$ and 1.0 and for data rates of 9, 18 Mbps.	130
Figure 71.	Noise-normalized sub-optimum receiver vs. linear-combining sub-optimum receiver with PNJ for $\rho = 0.1$ and 1.0 and for data rate of 24 Mbps.	131
Figure 72.	Noise-normalized sub-optimum receiver vs. linear-combining sub-optimum receiver with PNJ for $\rho = 0.1$ and 1.0 and for data rate of 36 Mbps.	131
Figure 73.	Noise-normalized sub-optimum receiver vs. linear-combining sub-optimum receiver with PNJ for $\rho = 0.1$ and 1.0 and for data rate of 48 Mbps.	132
Figure 74.	Noise-normalized sub-optimum receiver vs. linear-combining sub-optimum receiver with PNJ for $\rho = 0.1$ and 1.0 and for data rate of 54 Mbps.	132

LIST OF TABLES

Table 1.	Code rates and modulation techniques for the various data rates as they are specified by <i>IEEE 802.11a</i> WLAN standard [From ref. 3.].....	7
Table 2.	Weight structure of the best $r = 1/2$ and punctured $r = 2/3$ and $r = 3/4$ convolutional FEC [From Ref. 5.].....	10

THIS PAGE INTENTIONALLY LEFT BLANK

ACKNOWLEDGMENTS

This thesis is dedicated to my loving wife Niki for enduring my stress and absence during my research here at the Naval Postgraduate School. I am forever indebted to her for her love, consideration, and unrelenting support that continually inspired me to visualize reality from a different perspective.

I also wish to dedicate this thesis to my thoughtful and supportive parents, who taught me the values of education, diligence and conscientiousness.

I would like to express my sincere appreciation to my advisors Professor Clark Robertson and Professor Don Wadsworth. Without their support, coupled with clear explanations and supervision, this thesis would not have been possible.

Lastly, I must thank the Hellenic Navy, for providing an opportunity for me to pursue my postgraduate study here at the Naval Postgraduate School.

THIS PAGE INTENTIONALLY LEFT BLANK

EXECUTIVE SUMMARY

The performance of the *IEEE 802.11a* wide local area networks (WLAN) standard receiver over flat fading Nakagami channels in a worst case, pulse-noise jamming (PNJ) environment was investigated in this thesis for the different combinations of modulation type (binary and non-binary modulation) and code rate specified by the WLAN standard. The *IEEE 802.11a* WLAN standard is not only used commercially. It is also widely used in many military applications. The presence of hostile jamming is not uncommon in the modern military operational war-theater. Therefore, the analysis in this thesis gives useful information and conclusions about the performance of an already fielded communication system in a hostile environment. Prior to the analysis, the more important concepts utilized by the *IEEE 802.11a* WLAN standard are discussed in order to gain some perspective on how the WLAN standard operates. The concept of orthogonal-frequency-division-multiplexing (OFDM) transmission is discussed along with the error correction codes utilized by the standard.

Since the WLAN is designed to operate in a multi-path environment, the channel is modeled as a Nakagami channel because the Nakagami distribution gives the best fit to experimentally obtained results for data signals received in urban radio multi-path channels. Additionally, it has the advantage that it is more general than other statistical models since it embraces special cases such as when there is no line-of-sight (LOS) (i.e., Rayleigh distribution) and where LOS communication is available (i.e., Ricean distribution).

The *IEEE 802.11a* transmitter and receiver are also presented with a brief description of the processes performed. A very important point in our analysis is the assumption made that the side information generated by soft-decision-decoding (SDD) is maintained by each bit after the symbol de-mapping and bit deinterleaving. This assumption enables the performance analysis when non-binary modulation is implemented in conjunction with binary coding.

As a part of the preliminary analysis, the exact performance of M-ary quadrature-amplitude-modulation (MQAM) is also examined. This analysis results in determining

the most suitable upper bound on the probability of bit error, an upper bound widely used throughout the whole thesis.

Next, the performance of the *IEEE 802.11a* optimum receiver is examined for the scenario where perfect side information is assumed to be available. In this scenario both the amplitude of the information signal and the noise power for every received bit are considered to be known. The performance of the receiver, in terms of bit-error-rate (BER), is analyzed first when operating in additive-white-Gaussian-noise (AWGN) only with channel fading and is then generalized to the scenario when PNJ is also present. In both scenarios, it is found that the receiver performance in the presence of PNJ generally degrades as higher order modulation schemes are used, resulting in a tradeoff between data rate and BER. Additionally, it is found that the receiver performance in a fading environment is mostly affected by the code rate used; the higher the code rate the more severely is the receiver affected by the fading environment. It is also found that the worst jamming scenario for the optimum receiver is barrage jamming.

Next, a more practical type of receiver is examined. This receiver can be realized in practice since no perfect side information is assumed. The performance of this receiver, referred to as the sub-optimum receiver, is examined for a Nakagami fading channel and for no fading. The performance of the receiver, in terms of BER, is analyzed both when operating in only AWGN with channel fading and when PNJ is also present. Our analysis finds that the sub-optimum receiver is significantly worse, especially for low SIR, even in the case of no fading. Also, it is proven that the worst case occurs when the jammer operates for a small fraction of time, focusing the jamming power only to a small percentage of the received bits.

The last topic examined is how noise-normalization affects sub-optimum receiver performance. The performance of this receiver, named the noise-normalized sub-optimum receiver, is examined only when hostile PNJ is present. In our analysis, a form of side information is assumed, meaning that at every instance the noise power corrupts every received bit is either known or can accurately be measured. It is found that noise-normalization significantly improves the sub-optimum receiver performance for low signal-to-interference-ratio (SIR), while it has no effect for larger SIR. The worst case sce-

nario for the noise-normalized sub-optimum receiver is, as in the optimum receiver scenario, barrage jamming.

Summarizing, our analysis indicates that the optimum receiver results in the best performance in PNJ. On the other hand, the more practical sub-optimum receiver with linear combining results in significantly worse performance, especially when SIR is small. This disadvantage for low SIR can be compensated for by the implementation of noise-normalization.

THIS PAGE INTENTIONALLY LEFT BLANK

I. INTRODUCTION

A. BACKGROUND

The ability to communicate with other people, and to exchange data quickly and securely, has always been of great importance. Particularly during the past ten years, much research effort has been focused on the development of a wireless communication scheme that can provide all the useful services that are already available by wire. For this reason, wireless local area networks (WLAN) are very important in meeting the needs for reliable wireless communication for both commercial and military applications. Particularly, for military applications the presence of hostile jamming is not uncommon. Therefore, the analysis of the performance of WLANs operating in a jamming environment is of great importance.

One of the most promising wireless communications standards is *IEEE 802.11a*, that was adopted by the Standards of the Institute of Electrical and Electronics Engineers in 1999. The *IEEE 802.11a* WLAN standard utilizes different modulation techniques to support various data rates for signals transmitted over a restricted bandwidth. For low data rates, binary phase-shift-keying (BPSK) and quadrature-phase-shift-keying (QPSK) are used, while non-binary modulation (i.e., quadrature-amplitude-modulation (16QAM) and 64QAM) is used to improve channel capacity and achieve higher data rates. Channel capacity is further increased by implementing orthogonal frequency-division-multiplexing (OFDM). The OFDM technique allows the transmission of multiple carriers over the same bandwidth. OFDM is also used to avoid inter-symbol interference and performance degradation when operating in fading environments. Finally, communication integrity is increased by the implementation of forward-error-correction coding (FEC) and Viterbi soft-decision-decoding (SDD). The implementation of coding results in lower bit-error-rates (BER) and provides the means for higher, reliable data-rate transmission.

B. OBJECTIVE

The objective of this thesis was to study and analyze the performance of receivers designed to the specifications of the *IEEE 802.11a* WLAN standard in the presence of

additive-white-Gaussian-noise (AWGN) and hostile pulsed-noise-jamming (PNJ). In order to obtain more realistic and practical results, the communication system was considered to operate in a multi-path environment. The multi-path environment was modeled as a frequency-selective, slowly-fading Nakagami channel. This type of channel better models the characteristics of the indoor environment, where *IEEE 802.11a* WLAN standard compliant systems are used. The bit-error rate (BER) was studied for both binary and non-binary modulation, with binary FEC and Viterbi SDD. Furthermore, for completeness, the BER analysis is performed for both optimum and sub-optimum *IEEE 802.11a* receivers. In the optimum receiver case, perfect side information was assumed (i.e., the amplitude of the information signal and the noise power for every received bit are known). For the sub-optimum receiver (more practical), no side information is assumed.

C. RELATED RESEARCH

The *IEEE 802.11a* WLAN standard is a proven and widely used communication scheme. The performance of systems designed to comply with this standard operating in different conditions has been the topic of many different studies [1, 2]. These studies investigated the performance of *IEEE 802.11a* WLAN systems in various multi-path environments (i.e., Rayleigh, Ricean, Nakagami fading channels) for AWGN. Little research has been done on the effect of hostile PNJ. In addition, all previous studies [1, 2] on the effect of PNJ assumed either BPSK or QPSK with SDD or 16QAM and 64QAM with hard-decision-decoding (HDD).

In this thesis, the performance of *IEEE 802.11a* WLAN compliant systems are analyzed for all possible data rates, including the analysis of combining a binary FEC with non-binary modulation (MQAM) in a fading channel under the effect of hostile PNJ. Additionally, in order to obtain more practical conclusions, both optimum and sub-optimum *IEEE 802.11a* receivers are considered. Finally, performance of the sub-optimum receiver with noise normalization is also studied.

The *IEEE 802.11a* WLAN standard is not only used commercially. It is also widely used in many military applications. The presence of hostile jamming is not uncommon in the modern military operational war-theater. Therefore, the analysis in this

thesis gives useful information and conclusions about the performance of an already fielded communication system in a hostile environment. These conclusions may be even more useful since the more practical sub-optimum receiver is also analyzed.

D. THESIS OUTLINE

After this introduction, this thesis is organized into five remaining chapters. In Chapter II all relative concepts utilized by the *IEEE 802.11a* WLAN standard are discussed, such as the OFDM transmission technique, error correction coding techniques, multi-path channels, the *IEEE 802.11a* transmitter and receiver, and MQAM modulation. This is necessary in order to gain some perspective on how the WLAN standard operates. In Chapter III the performance of the *IEEE 802.11a* optimum receiver when the signal is transmitted over a Nakagami fading channel is examined. The performance of the receiver, in terms of BER, is analyzed initially when operating in an AWGN channel, and then the analysis is expanded to the more general PNJ scenario. In Chapter IV a more practical type of receiver is examined. The performance this receiver, referred to as the sub-optimum receiver, is examined for a Nakagami fading channel both when operating with AWGN only as well as when PNJ is present. Next, in Chapter V the performance of the sub-optimum receiver examined in Chapter IV is examined when noise-normalization is utilized. The performance of this receiver, named the noise-normalized sub-optimum receiver, is examined only when hostile PNJ is present since when only AWGN is present the noise-normalization has no effect. This study concludes with Chapter VI and a brief review of the results obtained in the previous chapters, followed by recommendations for further research. Finally, in Appendix A, a technique is presented for numerical computation of the inverse Laplace transform.

THIS PAGE INTENTIONALLY LEFT BLANK

II. BACKGROUND INFORMATION FOR THE IEEE 802.11A WLAN STANDARD

One of the most promising wireless communications standards is *IEEE 802.11a*, adopted by the Standards Committee of the Institute of Electrical and Electronics Engineers in 1999. This low power WLAN standard is implemented mainly within buildings and offices and has the ability to transfer data at high rates. The *802.11a* WLAN standard utilizes different binary and non-binary modulation techniques (i.e., BPSK, QPSK, and MQAM) to support various data rates in restricted bandwidth. The bandwidth efficiency is further increased by implementing orthogonal frequency-division multiplexing (OFDM), which also rejects inter-symbol interference effectively when operating in fading environments. Finally, communication integrity is increased by the implementation of forward-error-correction coding (FEC) and Viterbi soft-decision-decoding (SDD). All these concepts, utilized by *IEEE 802.11a* WLAN standard, are discussed in Chapter II to gain some perspective on how the WLAN standard operates. This knowledge is necessary in order to examine the performance of the *IEEE 802.11a* receiver for various fading conditions and for different types of interference.

A. OFDM TRANSMISSION TECHNIQUE

In order to achieve a more bandwidth efficient communication scheme, the *IEEE 802.11a* standard specifies the use of OFDM transmission. OFDM is an advanced version of the traditional frequency-division multiplexing (FDM) technique and enables the transmission of multiple carriers in parallel, so-called sub-carriers, where each sub-carrier carries a portion of the transmitted message.

FDM is a multiplexing technique whereby each frequency channel carries a distinct, separate signal. These signals are all transmitted simultaneously. This parallel transmission can result in channel cross-talk (CCT) and inter-symbol interference (ISI), especially when the communication signal is transmitted over a multi-path channel. In order to compensate for CCT and ISI, each sub-carrier occupies a separate portion of the spectrum as it is shown in Figure 1. The addition of a guard band to each sub-channel is

necessary to reduce the CCT and ISI even more. However, it is obvious that this use of the given spectrum is not the optimum, since a portion of the spectrum (guard bands) is not occupied by the waveform.

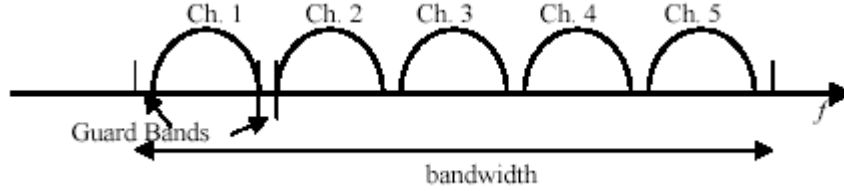


Figure 1. FDM communication technique spectral analysis [After Ref. 1.].

Contrary to FDM, OFDM uses overlapped sub-carriers to divide the given frequency spectrum into a number of overlapping sub-channels, which yields a more effective use of the available bandwidth, as shown in Figure 2. The realization of this technique is possible only by using orthogonal sub-carriers. Orthogonality between sub-carriers prevents CCT since any two orthogonal sub-carriers are uncorrelated over a symbol duration. So in OFDM each sub-carrier is spaced at intervals of $1/T_s$ where T_s is the symbol duration for each sub-carrier. Moreover, since the data are transmitted in parallel over several low-rate sub-carriers, the lower sub-carrier data rates result in a longer symbol duration for each sub-carrier. As a result, a smaller percentage of the symbol duration is affected by ISI.

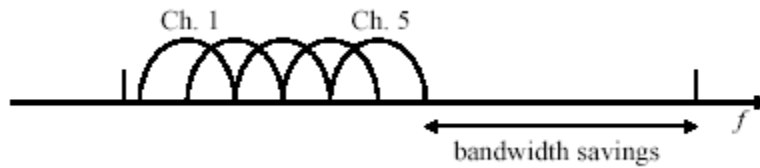


Figure 2. OFDM communication technique spectral analysis [After Ref. 1.].

An other advantage of OFDM is that it performs better when the data signal is transmitted over a multi-path channel. The use of multiple carriers spreads the transmitted signal over the whole available spectrum. Consequently, interference in a small number of sub-carriers affects only a portion of the information.

In the *IEEE 802.11a* standard, the use of 52 sub-carriers is specified. However, four pilot sub-carriers are used to assist timing and carrier tracking tasks during data transmission. Hence, the remaining 48 sub-carriers are used to carry the data sequence. Additionally, the use of a $0.8\text{--}\mu\text{s}$ guard interval is specified, the symbol duration (T_s) is $4\text{--}\mu\text{s}$, and the overall occupied bandwidth is 16.6 MHz [3].

B. DATA ERROR CORRECTION MANAGEMENT

The use of data encoding and de-coding is utilized by the *IEEE 802.11a* standard for two reasons. First, the use of various code rates along with different modulation techniques enables the transfer of data with various data rates. The possible data rates that can be achieved from the combination of code rates and modulation techniques are shown in Table 1 [3].

Table 1. Code rates and modulation techniques for the various data rates as they are specified by *IEEE 802.11a* WLAN standard [From ref. 3].

Data rate (Mbits/s)	Modulation	Coding rate (R)	Coded bits per subcarrier (N_{BPSC})	Coded bits per OFDM symbol (N_{CBPS})	Data bits per OFDM symbol (N_{DBPS})
6	BPSK	1/2	1	48	24
9	BPSK	3/4	1	48	36
12	QPSK	1/2	2	96	48
18	QPSK	3/4	2	96	72
24	16-QAM	1/2	4	192	96
36	16-QAM	3/4	4	192	144
48	64-QAM	2/3	6	288	192
54	64-QAM	3/4	6	288	216

Second, data encoding and its ability for error correction is utilized in order to increase the communication scheme integrity and channel capacity. Since for higher data

rates the use of non-binary modulation techniques is specified, the use of data encoding is necessary in order to improve the BER of the system, which is high for uncoded non-binary techniques [4].

1. Forward Error Correction (FEC) Coding

The *IEEE 802.11a* standard specifies the use of a convolutional encoder for data encoding. A convolutional code produces n coded bits from k data bits where each set of n coded bits is determined by the k data bits and between $(\nu-1)$ and $k(\nu-1)$ of the preceding bits. The parameter ν is the constraint length of the convolutional code. The code rate is $r = k/n$ and $1/r$ bits are generated for every data bit. A general convolutional encoder can be implemented with k shift-registers and n modulo-2 adders.

The convolutional encoder employed for the rate $r = 1/2$ code uses industry-standard generator polynomials $g_0 = 133_8$ and $g_1 = 171_8$ with constraint length $\nu = 7$. The convolutional encoder in Figure 3 consists of six linear shift registers interconnected to produce the non-catastrophic, $r = 1/2$ convolutional code.

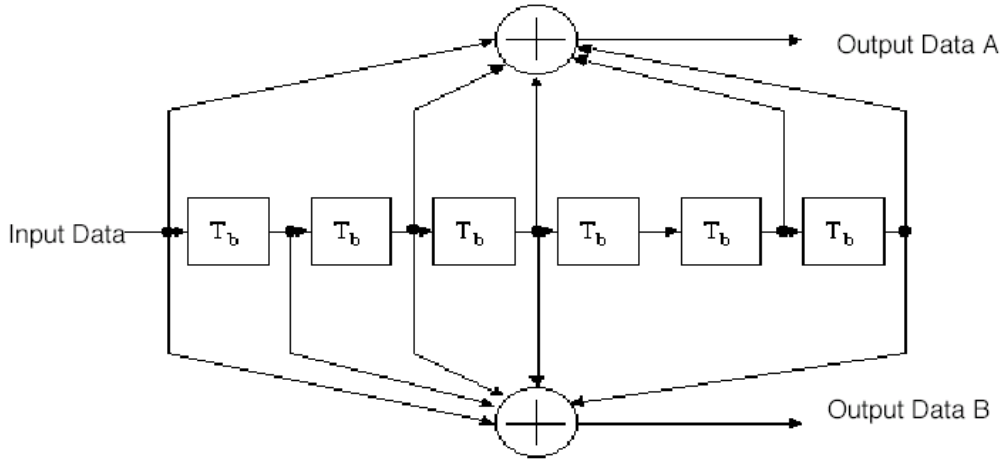


Figure 3. The convolutional encoder with generator polynomials $g_0 = 133_8$, $g_1 = 171_8$ and constraint length $\nu = 7$ as specified by *IEEE 802.11a* WLAN standard [From Ref. 3.].

The higher code rates of $r = 2/3$ and $r = 3/4$ specified in Table 1 are generated from the same encoder by puncturing. “Puncturing is a procedure for omitting some of the encoded bits in the transmitter (thus reducing the number of transmitted bits and increasing the coding rate) and inserting a dummy ‘zero’ metric into the convolutional decoder on the receive side in place of the omitted bits.” [3]. The specific puncture pattern specified for *IEEE 802.11a* compliant systems can be found in the standard [3].

2. Viterbi Decoding

The data decoding at the receiver is performed via the Viterbi decoding algorithm. The Viterbi algorithm is an extremely powerful and flexible means for decoding convolutional codes and is used to determine the maximum-likelihood code sequence associated with a given received sequence. The Viterbi algorithm decodes a convolutional code by choosing a path through the code trellis which yields a code sequence that differs from the received code sequence in the fewest possible places. The Viterbi algorithm searches all possible paths in the trellis in order to compute the path metrics. After the metrics have been obtained, the algorithm selects the path with the “best” metric. The metric selection depends on the specific implementation of the algorithm.

The *IEEE 802.11a* standard specifies the use of soft decision decoding (SDD) at the receiver. In SDD, the receiver takes advantage of the side information generated by the receiver bit decision circuitry. In SDD the channel reliability information can be used to improve the performance of the error control system. Rather than simply assign a zero or a one to each received binary signal, a more flexible approach is taken. Four or more decision regions are established, ranging from a “strong-one” decision to a “strong-zero” decision. Intermediate values are given to signals for which the decision is less clear. In the *IEEE 802.11a* standard, eight decision regions are specified. This is equivalent to using three bits to represent the receiver matched filter outputs instead of the usual one.

When convolutional FEC is implemented with Viterbi SDD, there is no analytic expression for BER. However, an upper bound can be used, and it is given by [4]

$$P_b < \frac{1}{k} \sum_{d=d_{free}}^{\infty} B_d P_d \quad (2.1)$$

where d_{free} is the free distance of the convolutional code, B_d is the total number of information bit ones on all weight- d paths, P_d is the probability of selecting a weight- d output sequence as the transmitted code sequence, and k is the number of information bits. The quantities B_d and d_{free} are parameters of the convolutional code. Those parameters for the code specified for the *802.11a* WLAN standard are presented in Table 2.

Table 2. Weight structure of the best $r = 1/2$ and punctured $r = 2/3$ and $r = 3/4$ convolutional FEC [From Ref. 5].

Rates	d_{free}	$B_{d_{free}}$	$B_{d_{free}+1}$	$B_{d_{free}+2}$	$B_{d_{free}+3}$	$B_{d_{free}+4}$
$r = 1/2$	10	36	0	211	0	1404
$r = 2/3$	6	3	81	402	1487	6793
$r = 3/4$	5	42	252	1903	11995	72115

The probability P_d of selecting a weight- d output sequence as the transmitted code sequence is determined by the modulation type used and the nature of the interference that affects the received signal. The goal of this thesis is to estimate the probability P_d for all the modulation schemes specified by the *802.11a* WLAN standard and for various fading conditions and types of interference.

C. COMMUNICATION MULTI-PATH CHANNEL

As already mentioned at the beginning of Chapter II, the *IEEE 802.11a* WLAN standard is mainly implemented within big buildings and offices. Usually, under these operational conditions there is no line-of-sight (LOS) between the transmitter and the receiver. Furthermore, due to many reflections from the ground and other surrounding structures, the received signal contains multiple delayed versions of the transmitted signal. This phenomenon is referred to as *multi-path propagation*. Consequently, the *IEEE 802.11a* WLAN waveform is destined to operate within multi-path environments. This

assumption is included in our analysis, and the performance of the WLAN standard is examined when operating in the multi-path environment.

The best model for a certain communication scheme depends on its bandwidth and the environment in which the communication occurs. In this thesis the communication channel is modeled as a Nakagami channel, where at each instance the amplitude of the received signal, a_c , is modeled as a Nakagami- m random variable. A Nakagami channel gives the best fit to experimentally obtained results for data signals received in urban radio multi-path channels [4]. Additionally, it has the advantage that it is more general than other statistical models since it embraces special cases such as when there is no LOS (i.e., Rayleigh distribution) and where LOS communication is available (i.e., Rician distribution).

The Nakagami- m probability density distribution (PDF), which is a function of two parameters, is given by [4]

$$f_{A_c}(a_c) = \frac{2}{\Gamma(m)} \left(\frac{m}{\Omega} \right)^m a_c^{2m-1} e^{-\frac{ma_c^2}{\Omega}} \quad (2.2)$$

where $\Gamma(m)$ is the Gamma function defined as

$$\Gamma(m) = \int_0^\infty t^{m-1} e^{-t} dt, \quad m \geq 0, \quad (2.3)$$

Ω is defined as

$$\Omega = E[A_c^2] \quad (2.4)$$

the parameter m , the fading figure, is defined as the ratio of moments

$$m = \frac{\Omega^2}{E[(A_c^2 - \Omega)^2]}, \quad m \geq 0.5 \quad (2.5)$$

and A_c is the expected value of the random variable a_c .

The values that the fading figure m takes reflect how severe a fading environment is. For small values of m (i.e., $0.5 \leq m \leq 1$) the fading conditions are severe, while for bigger values of m the fading conditions are less severe. As $m \rightarrow \infty$, no fading is present.

Since the communication scheme studied is designed to operate indoors, our analysis covers severe to moderate fading conditions of $0.5 \leq m \leq 4$. It can be shown that for $m = 1$, the PDF in Equation (2.2) is equivalent to the Rayleigh PDF [4].

Another categorization of the communication channel is whether it is a frequency-selective or a flat-fading channel. A channel is characterized by comparing the channel bandwidth W to the coherence bandwidth B_c . The coherence bandwidth is defined in [6] as “the range of frequencies over which two frequency components have a strong potential for amplitude correlation”. A communication channel is characterized as frequency-selective if

$$B_c \leq W. \quad (2.6)$$

By the same token a channel is characterized as flat-fading if

$$B_c > W. \quad (2.7)$$

These two different types of channel are illustrated in Figure 4.

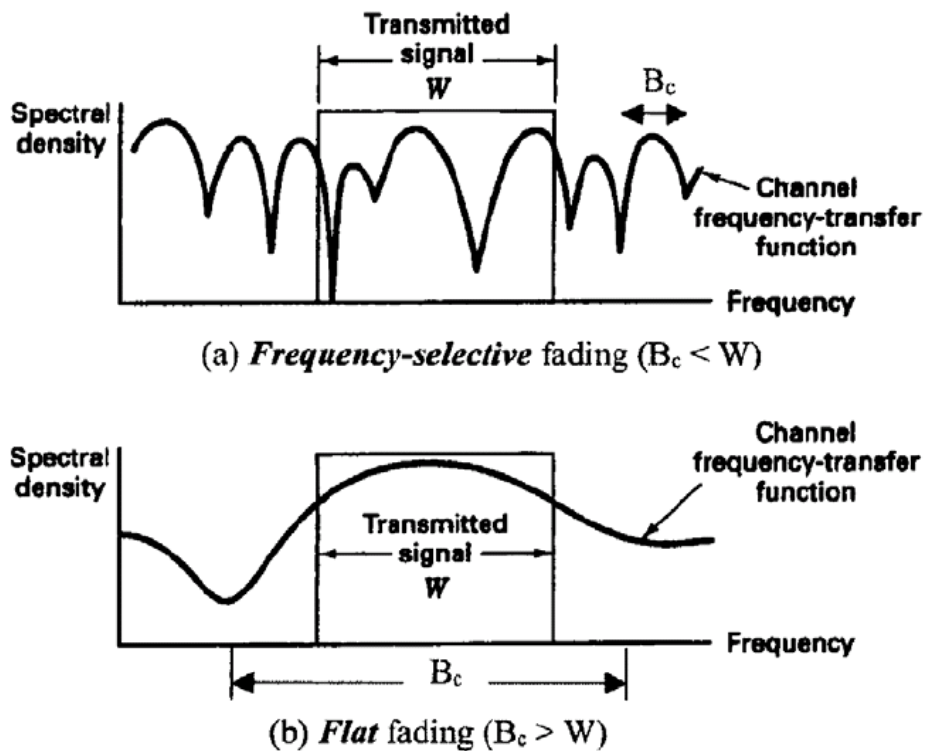


Figure 4. The two types of fading channels [From Ref. 7.].

From Figure 4, it is clear that a frequency-selective channel affects a transmitted signal more than does a flat fading channel. In real life applications, the indoor environments are generally frequency-selective channels.

However, the *IEEE 802.11a* standard specifies the transmission of an OFDM signal over the communication channel. We have already seen that with OFDM high data rate transmissions are divided up into 48 low data rate sub-carriers transmitted in parallel. As a result, the bandwidth of each data sub-carrier is significantly smaller ($1/48$ times) than the system bandwidth. Therefore, the sub-carrier signal bandwidth is now sufficiently small relative to the channel coherence bandwidth to be considered flat. As a result, in our analysis each independent sub-carrier is assumed to be transmitted over a flat fading channel. This assumption allows the theoretical study of the problem and useful, realistic conclusions can be derived.

As a consequence, when we examine the performance of the *IEEE 802.11a* receiver we need to examine each sub-carrier BER independently and then average over all 48 sub-carriers. Since the 48 sub-carriers are considered to be independent, the fading effect of each one generally has a different fading factor m . However, when the WLAN is operating in a particular indoor environment, the variation of the fading figure m is not expected to be large. In a severe fading environment, reasonable values of m are $0.5 \leq m \leq 1$, while in a non-severe environment, reasonable values are $3 \leq m \leq 4$. In order to investigate the effect of various values of m on the communication system, we plot in Figure 5 the average BER of the receiver for both severe ($0.5 \leq m \leq 1$) and non-severe ($3 \leq m \leq 4$) fading conditions along with the BER obtained for the limiting values of m (i.e., $m = 0.5, 1.5$ and $m = 3, 4$). The BER is obtained by the analysis made in [1] for BPSK operating in AWGN with $r = 1/2$ FEC and SDD and is presented in section III.B.

From Figure 5 we can see that the average BER curve lies between the BERs obtained for the limiting cases of m . It is obvious that the average performance curve in the severe fading case ($0.5 \leq m \leq 1$) lies closer to the BER obtained for $m = 0.5$ and is upper bounded by it. In other words the average receiver performance is dominated by the per-

formance of the sub-carriers with the smaller m . Additionally, when $3 \leq m \leq 4$, the difference between the various BERs is insignificant.

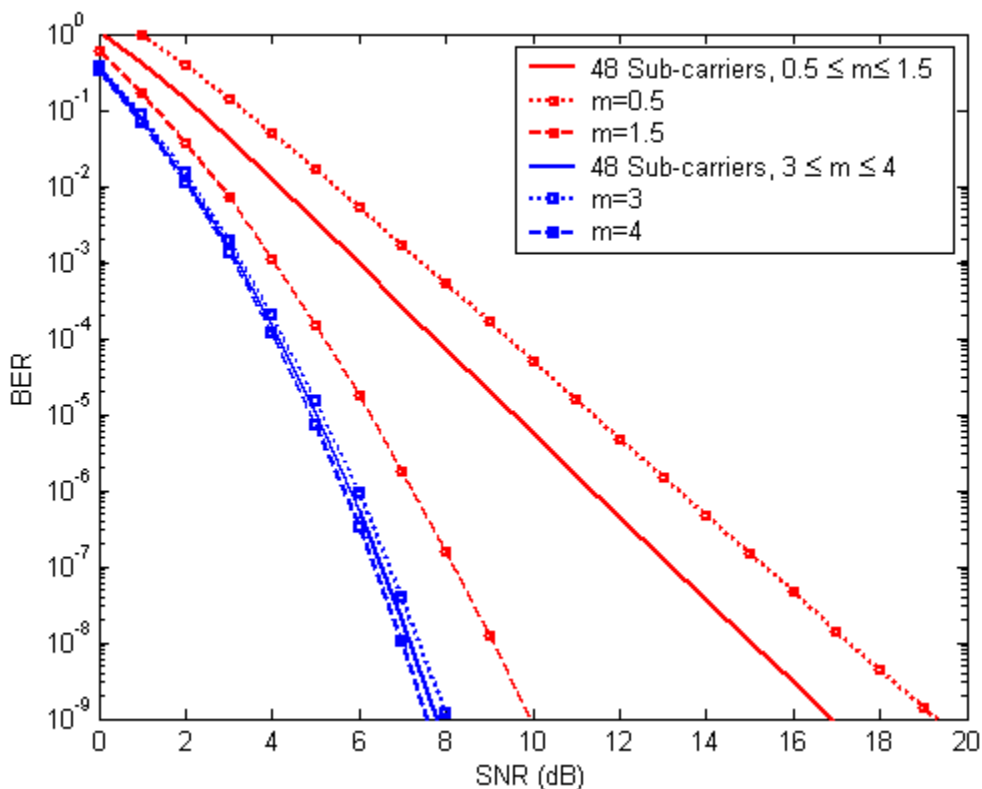


Figure 5. BPSK performance for $r = 1/2$ and SDD, operating both in a severe ($0.5 \leq m \leq 1$) and a non-severe ($3 \leq m \leq 4$) fading environment.

As result, in our future analysis we assume, without any loss of generality, that all sub-carriers operate under similar fading conditions with the same fading figure m . Moreover, in order to cover all possible scenarios in our analysis, the values of m that are considered are $m = 0.5, 1, 2, 3$, and 4 .

D. IEEE 802.11A COMMUNICATION SCHEME

The *IEEE 802.11a* standard transmitter and receiver and the method of implementation of OFDM are presented next.

1. IEEE 802.11A TRANSMITTER

A diagram of the *IEEE 802.11a* transmitter that implements the OFDM transmission technique is illustrated in Figure 4.

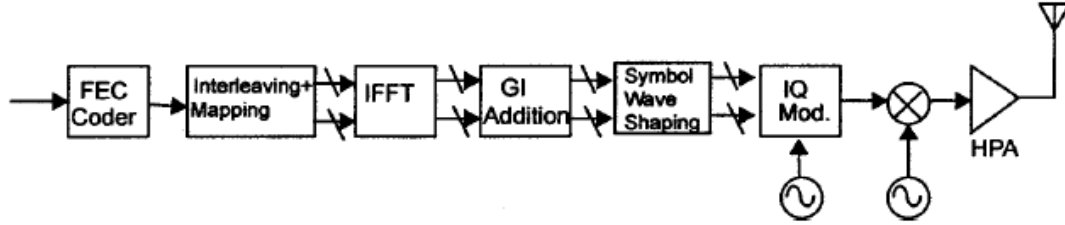


Figure 6. The IEEE 802.11a transmitter [After Ref. 3].

At the front of the transmitter, the raw data stream is coded and interleaved. The interleaver spreads sequential coded bits out in time in such a way that a bursty channel is transformed at the receiver into a channel having independent errors that can be corrected by the error correction code. The interleaved bits are mapped into binary (BPSK) or non-binary (MQAM) symbols according to the data rate that is desired. Next, the guard interval with a cyclic extension is added. Symbol wave shaping follows. The I/Q modulation process generates the in-phase and quadrature components of the signal that are summed to generate a single waveform. This waveform is then translated into a higher frequency range (the 5 GHz band for *802.11a* applications) for amplification and final transmission [3].

2. IEEE 802.11A RECEIVER

A diagram of the *IEEE 802.11a* receiver, that receives and recovers the OFDM transmitted signal is illustrated in Figure 5.

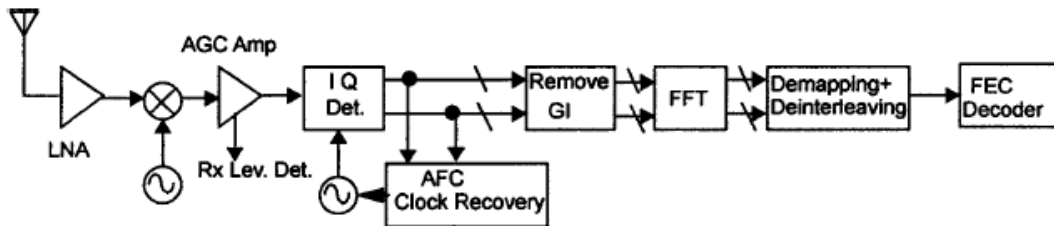


Figure 7. The IEEE 802.11a receiver [After Ref. 3].

At the receiver, the reverse procedure described in the previous section is performed. The signal after the local oscillator is amplified by a low noise amplifier (LNA) to boost the signal strength and the in-phase and quadrature components are recovered. After removing the guard interval with the cyclic extension, the signal is de-mapped and de-interleaved. At this point the transmitted symbols have been converted into bits that are inserted into the de-coder to perform the error correction process [3].

As we have previously discussed, the *IEEE 802.11a* standard specifies the use of soft decision decoding (SDD) at the receiver. By implementing SDD, the receiver takes advantage of the side information generated by the receiver bit decision circuitry. However, this information is carried along with the transmitted symbols. In the analysis made in this thesis, it is assumed that the generated side information is maintained by each bit after the symbol de-mapping and bit interleaving. This being the case, a performance analysis is possible when a non-binary modulation technique is implemented along with binary coding.

E. PERFORMANCE ANALYSIS OF MQAM

As discussed previously, the *802.11a* WLAN standard utilizes different binary and non-binary modulation techniques (i.e., BPSK, QPSK, and MQAM) to support various data rates in a restricted bandwidth. In order to transfer data at high rates, the use of MQAM is specified. MQAM is a non-binary, memoryless modulation technique in which one of M different symbols is transmitted per symbol time using two orthogonal carriers. MQAM can be thought of as a discrete form of double-sideband, suppressed-carrier amplitude modulation with quadrature-carrier multiplexing. The channel waveform for MQAM can be represented by

$$s(t) = \sqrt{2}A_{i_m} \cos(\omega_c t) - \sqrt{2}A_{q_m} \sin(\omega_c t) \quad (2.8)$$

where A_{i_m} and A_{q_m} are the amplitudes of the in-phase and quadrature components of the carrier, respectively, and ω_c is the carrier frequency.

In this modulation technique, the m^{th} symbol is represented by the combination of the amplitudes A_{i_m} and A_{q_m} . Therefore, M-QAM is completely defined by its constella-

tion, which graphically represents the M possible symbols as dots on a Cartesian plot. The coordinates (x, y) of each constellation dot are the amplitudes A_{i_m} and A_{q_m} of the corresponding symbol. The constellation that is specified by the *IEEE 802.11a* standard is the rectangular constellation, presented in Figure 1, for all the modulation schemes used by the WLAN standard.

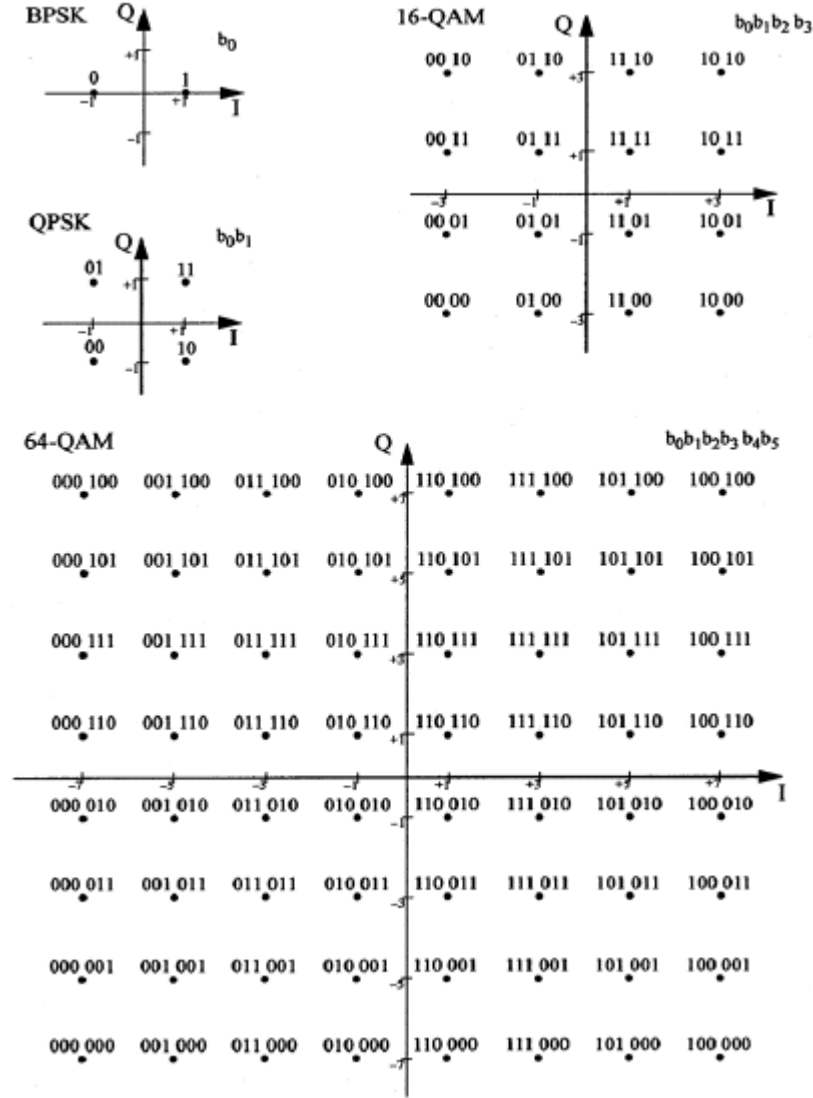


Figure 8. Rectangular constellations of all modulation techniques utilized by the *IEEE 802.11a* WLAN standard [From Ref. 3].

The robustness of a communication scheme is obtained by predicting the probability of symbol error (PSE). A symbol error occurs when a transmitted symbol, after

being received and demodulated, is not mapped to the correct decision region for that particular symbol. When MQAM with a square constellation is used, the PSE is given by [8]

$$P_s = 4 \left(1 - \frac{1}{\sqrt{M}}\right) Q \left(\sqrt{\frac{3qE_b}{(M-1)N_o}} \right) \left[1 - \left(1 - \frac{1}{\sqrt{M}}\right) Q \left(\sqrt{\frac{3qE_b}{(M-1)N_o}} \right) \right] \quad (2.9)$$

where $E_s = (M-1)E_o/3$ is the average energy per symbol, $E_o = 2A_o^2T_s$ is the energy of the lowest amplitude symbols, A_o is the amplitude of the smallest magnitude symbols, T_s is the symbol duration, and N_o is the one-sided noise power spectral density (PSD). Since each symbol contains $q = \log_2(M)$ bits, the average energy per bit is

$$E_b = \frac{E_s}{\log_2(M)} = \frac{E_s}{q}. \quad (2.10)$$

A way to minimize the probability of bit error (PBE) is by implementing *Gray Coding* [4]. The constellations shown in Figure 8 are Gray coded. In general there is no simple analytic expression for the PBE, so an approximation is used instead. With *Gray Coding*, the probability of bit error (PBE) is expressed as

$$P_b \approx \frac{P_s}{q} = \frac{4}{q} \left(1 - \frac{1}{\sqrt{M}}\right) Q \left(\sqrt{\frac{3qE_b}{(M-1)N_o}} \right) \left[1 - \left(1 - \frac{1}{\sqrt{M}}\right) Q \left(\sqrt{\frac{3qE_b}{(M-1)N_o}} \right) \right] \quad (2.11)$$

Other widely used expressions, valid when $E_b / N_o \gg 1$, are

$$P_{1_b} \approx \frac{4}{q} \left(1 - \frac{1}{\sqrt{M}}\right) Q \left(\sqrt{\frac{3qE_b}{(M-1)N_o}} \right) \quad (2.12)$$

and, when $M \gg 1$

$$P_{2_b} \approx \frac{4}{q} Q \left(\sqrt{\frac{3qE_b}{(M-1)N_o}} \right). \quad (2.13)$$

However, Equations (2.11), (2.12) and (2.13) yield optimistic results. In order to determine the most accurate approximation for PBE, the exact PBE is estimated. Due to

the complexity of analysis as M gets large, the exact PBE for the uncoded 16QAM is obtained, and the results are generalized for all MQAM.

In the 16QAM case, using $M = 16$ and $q = 4$, Equations (2.9), (2.11), (2.12), and (2.13) can be rewritten as

$$P_s \approx 3Q\left(\sqrt{\frac{4 E_b}{5 N_o}}\right) - \frac{9}{4} \left[Q\left(\sqrt{\frac{4 E_b}{5 N_o}}\right) \right]^2, \quad (2.14)$$

$$P_b \approx \frac{3}{4} Q\left(\sqrt{\frac{4 E_b}{5 N_o}}\right) - \frac{9}{4} \left[Q\left(\sqrt{\frac{4 E_b}{5 N_o}}\right) \right]^2, \quad (2.15)$$

$$P_{1_b} \approx \frac{3}{4} Q\left(\sqrt{\frac{4 E_b}{5 N_o}}\right), \quad (2.16)$$

and

$$P_{2_b} \approx Q\left(\sqrt{\frac{4 E_b}{5 N_o}}\right), \quad (2.17)$$

respectively.

In order to determine the exact PBE for 16QAM, consider the square constellation in Figure 9. In Figure 9 the constellation is shown along with the corresponding decision regions and the limits that define those regions. For instance, when a received symbol is mapped into the decision region V_1 , it is detected as symbol 1111 , while when it is mapped into V_2 , it is detected as symbol 1110 .

Examining the constellation of the 16QAM in Figure 9, we can see that there exist three types of symbols. Four corner symbols (i.e., 0000, 1000, 1010, 0010), eight side symbols (i.e., 0110, 1110, 1011, 1001, 1100, 0100, 0001, 0011) and four interior symbols (i.e., 0111, 1111, 1101, 0101).

The exact PBE for the 16QAM constellation in Figure 9 is expressed as

$$P_b = \frac{4P_{b_{corner}} + 8P_{b_{side}} + 4P_{b_{int}}}{16} \quad (2.18)$$

where $P_{b_{corner}}$ is the probability that a corner symbol is mapped into a wrong decision region, $P_{b_{side}}$ is the probability that a side symbol is mapped into a wrong decision region, and $P_{b_{int}}$ is the probability that an interior symbol is mapped into a wrong decision region.

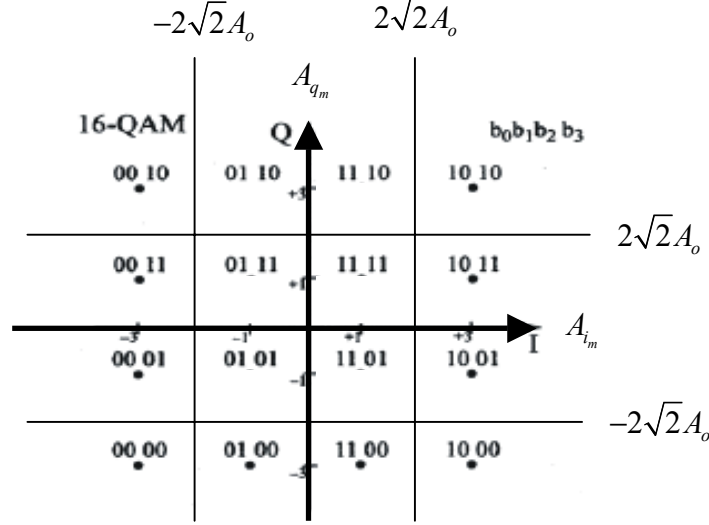


Figure 9. The 16QAM square constellation with the decision regions and the corresponding limits [After Ref. 3.].

The probability $P_{b_{corner}}$ that a corner symbol is mapped into a wrong decision region is examined first. Without loss of generality, it is assumed that the symbol 1010 that corresponds to decision region V_3 with limits $A_{i_m} \geq 2\sqrt{2}A_o$ and $A_{q_m} \geq 2\sqrt{2}A_o$ was transmitted. It is clear that the symbol in region V_3 differs in one bit from the symbols in regions V_2 and V_4 , differs in two bits from the symbol in region V_1 , and in average differs in three bits from the symbols in all remaining regions. Therefore, the probability $P_{b_{corner}}$ that a corner symbol is mapped into a wrong decision region is expressed as

$$\begin{aligned}
 P_{b_{corner}} &= \frac{1}{4} \Pr\{s \in V_2 / V_3\} + \frac{2}{4} \Pr\{s \in V_1 / V_3\} + \frac{1}{4} \Pr\{s \in V_4 / V_3\} \\
 &+ \frac{3}{4} \left[P_s - (\Pr\{s \in V_2 / V_3\} + \Pr\{s \in V_1 / V_3\} + \Pr\{s \in V_4 / V_3\}) \right]
 \end{aligned} \tag{2.19}$$

where by $\Pr\{s \in V_j / V_i\}$ we denote the probability that a symbol that corresponds to region V_i was transmitted but was mapped into decision region V_j , leading to an error detection, and P_s is given by Equation (2.14).

Since $\Pr\{s \in V_2 / V_3\} = \Pr\{s \in V_4 / V_3\}$, Equation (2.19) is written

$$P_{b_{corner}} = \frac{3}{4}P_s - \frac{1}{4}\Pr\{s \in V_1 / V_3\} - \Pr\{s \in V_2 / V_3\} \quad (2.20)$$

where we can easily show that

$$\Pr\{s \in V_1 / V_3\} = \left[Q\left(\sqrt{\frac{4}{5} \frac{E_b}{N_o}}\right) - Q\left(3\sqrt{\frac{4}{5} \frac{E_b}{N_o}}\right) \right]^2 \quad (2.21)$$

and

$$\Pr\{s \in V_2 / V_3\} = 1 - Q\left(\sqrt{\frac{4}{5} \frac{E_b}{N_o}}\right). \quad (2.22)$$

Combining Equations (2.14), (2.21), and (2.22) into (2.20), we get the exact probability $P_{b_{corner}}$ that a corner symbol is mapped into a wrong decision region.

Next the probability $P_{b_{side}}$ that a side symbol is mapped into a wrong decision region is examined. Without loss of generality, it is assumed that symbol 1110 that corresponds to decision region V_2 with limits $0 \leq A_{i_m} \leq 2\sqrt{2}A_o$ and $A_{q_m} \geq 2\sqrt{2}A_o$ was transmitted. Following an analogous procedure, the probability $P_{b_{side}}$ is given by

$$P_{b_{side}} = \frac{3}{4}P_s - \frac{2}{4}\Pr\{s \in V_1 / V_2\} - \frac{2}{4}\Pr\{s \in V_3 / V_2\} - \frac{3}{4}\Pr\{s \in V_4 / V_2\} - \frac{1}{4}\Pr\{s \in V_1 / V_2\} \quad (2.23)$$

where the probabilities $\Pr\{s \in V_j / V_i\}$ are found to be

$$\begin{aligned}
\Pr\{s \in V_1 / V_2\} &= \left[1 - 2Q\left(\sqrt{\frac{4 E_b}{5 N_o}}\right)\right] \left[Q\left(\sqrt{\frac{4 E_b}{5 N_o}}\right) - Q\left(3\sqrt{\frac{4 E_b}{5 N_o}}\right)\right], \\
\Pr\{s \in V_3 / V_2\} &= Q\left(\sqrt{\frac{4 E_b}{5 N_o}}\right) \left[1 - Q\left(\sqrt{\frac{4 E_b}{5 N_o}}\right)\right], \\
\Pr\{s \in V_4 / V_2\} &= Q\left(\sqrt{\frac{4 E_b}{5 N_o}}\right) \left[Q\left(\sqrt{\frac{4 E_b}{5 N_o}}\right) - Q\left(3\sqrt{\frac{4 E_b}{5 N_o}}\right)\right], \\
\Pr\{s \in V_6 / V_2\} &= \left[Q\left(\sqrt{\frac{4 E_b}{5 N_o}}\right) - Q\left(3\sqrt{\frac{4 E_b}{5 N_o}}\right)\right]^2.
\end{aligned} \tag{2.24}$$

Finally, the probability $P_{b_{\text{int}}}$ that an interior symbol is mapped into a wrong decision region is examined. Without loss of generality, it is assumed that symbol $IIII$ that corresponds to decision region V_1 with limits $0 \leq A_{i_m} \leq 2\sqrt{2}A_o$ and $0 \leq A_{q_m} \leq 2\sqrt{2}A_o$ was transmitted. The probability $P_{b_{\text{int}}}$ is given by

$$\begin{aligned}
P_{b_{\text{int}}} &= \frac{3}{4}P_s - \Pr\{s \in V_2 / V_1\} - \frac{1}{4}\Pr\{s \in V_3 / V_1\} \\
&\quad - \frac{2}{4}\Pr\{s \in V_5 / V_1\} - \Pr\{s \in V_6 / V_1\} - \frac{1}{4}\Pr\{s \in V_7 / V_1\}
\end{aligned} \tag{2.25}$$

where

$$\begin{aligned}
\Pr\{s \in V_2 / V_1\} &= 1 - 2Q\left(\sqrt{\frac{4 E_b}{5 N_o}}\right), \\
\Pr\{s \in V_3 / V_1\} &= \left[Q\left(\sqrt{\frac{4 E_b}{5 N_o}}\right)\right]^2, \\
\Pr\{s \in V_5 / V_1\} &= Q\left(\sqrt{\frac{4 E_b}{5 N_o}}\right) \left[Q\left(\sqrt{\frac{4 E_b}{5 N_o}}\right) - Q\left(3\sqrt{\frac{4 E_b}{5 N_o}}\right)\right], \\
\Pr\{s \in V_6 / V_1\} &= \left[1 - 2Q\left(\sqrt{\frac{4 E_b}{5 N_o}}\right)\right] \left[Q\left(\sqrt{\frac{4 E_b}{5 N_o}}\right) - Q\left(3\sqrt{\frac{4 E_b}{5 N_o}}\right)\right], \\
\Pr\{s \in V_7 / V_1\} &= \left[Q\left(\sqrt{\frac{4 E_b}{5 N_o}}\right) - Q\left(3\sqrt{\frac{4 E_b}{5 N_o}}\right)\right]^2.
\end{aligned} \tag{2.26}$$

Substituting Equations (2.19), (2.23), and (2.25) into (2.18), we get the exact probability of bit error for the 16QAM constellation specified by the *IEEE 802.11a* WLAN standard.

In Figure 10, the exact PBE given by Equation (2.18) is plotted along with the approximate expressions from Equations (2.15), (2.16), and (2.17). From Figure 10, it is clear that all expressions give very accurate results, especially for large values of SNR. However, when SNR is small, the most accurate approximation is obtained with Equation (2.17). Generalizing this assumption, we claim that the best expression for the PBE for MQAM is given by Equation (2.13), which is the general case, while Equation (2.17) is a special case obtained when $q = 4$ is used in Equation (2.13). So, in this thesis Equation (2.13) is used for the PBE of MQAM.

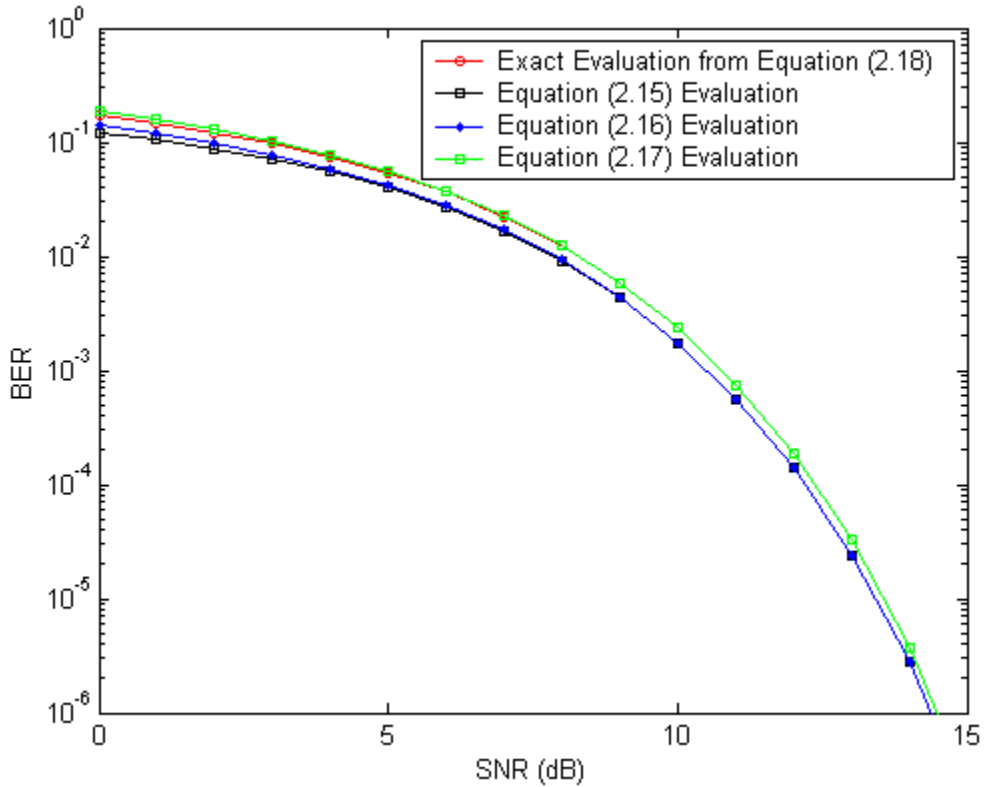


Figure 10. Exact BER for 16QAM vs. the BER obtained by several approximate expressions.

THIS PAGE INTENTIONALLY LEFT BLANK

III. PERFORMANCE ANALYSIS OF THE IEEE 802.11A OPTIMUM RECEIVER

The performance of the *802.11a* optimum receiver when the signal is transmitted over a Nakagami fading channel is examined in this chapter. For analysis purposes, perfect side information is assumed, meaning that both the amplitude of the information signal and the noise power for every received bit are considered to be known. The performance of the receiver, in terms of BER, is analyzed both when operating in AWGN channel with fading and when PNJ is also present.

A. IEEE 802.11A OPTIMUM RECEIVER

The *IEEE 802.11a* optimum receiver studied on this chapter is the receiver designed to maximize the likelihood ratio (LR) when soft decision decoding (SDD) is used. The LR is defined [9]

$$\Lambda(x_k) = \frac{\prod_{k=1}^d f_{X_k}(x_k / 1)}{\prod_{k=1}^d f_{X_k}(x_k / 0)} \quad (3.1)$$

where $f_{X_k}(x_k / 1)$ is the conditional probability density function (PDF) of the random variable x_k given than a bit “one” was transmitted, $f_{X_k}(x_k / 0)$ is the PDF of the random variable x_k given than a bit “zero” was transmitted, and d is the weight of the output sequence.

Since we implicitly assume an ideal interleaver at the transmitter and an ideal deinterleaver at the receiver, every received bit can be assumed to be independent. In other words, the channel is modeled as a memoryless channel. For memoryless channels and equally likely ones and zeros, the LR satisfies the inequality [7]

$$\Lambda(x_k) \begin{matrix} > \\ < \end{matrix} 1 \quad (3.2)$$

where Equation (3.2) is greater than one for a bit one and less than one for a bit zero.

For computational purposes, we use

$$\ln[\Lambda(x_k)] = \ln \left[\frac{\prod_{k=1}^d f_{X_k}(x_k/1)}{\prod_{k=1}^d f_{X_k}(x_k/0)} \right] \begin{matrix} > \\ < \end{matrix} 0. \quad (3.3)$$

A receiver that is designed to perform the detection decision based on the criterion of Equation (3.3) is called maximum-likelihood receiver (MLR).

In the special case of BPSK modulation, the MLR can be modeled as shown in Figure 11.

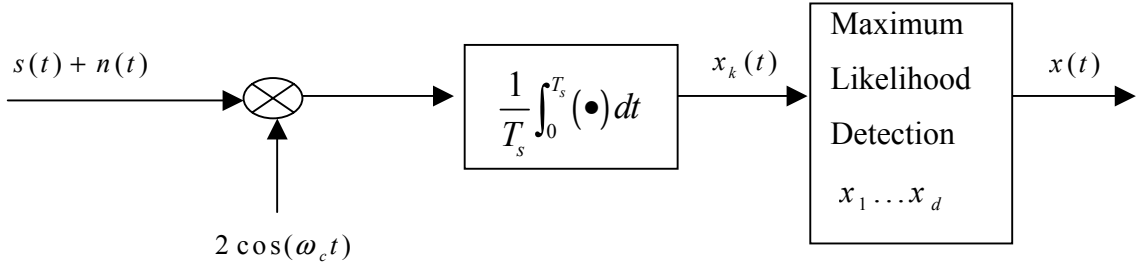


Figure 11. BPSK maximum likelihood receiver (MLR)

At the input of the receiver, the desired BPSK signal can be represented as $s(t) = \sqrt{2}a_c d(t) \cos(\omega_c t)$, where a_c is the amplitude of the received signal, $d(t)$ is the information waveform, T_s is the time duration of a symbol, and ω_c is the frequency of the sub-carrier signal.

The signal $x_k(t)$ at the integrator output represents those sequence bits that have been affected in a random way by the channel. The signal $x_k(t)$ can be modeled as Gaussian random variable (GRV). Therefore, we can write the PDFs $f_{X_k}(x_k/1)$ and $f_{X_k}(x_k/0)$ as

$$f_{X_k}(x_k/1) = \frac{1}{\sqrt{2\pi}\sigma_k} \exp \left[-\frac{(x_k - \sqrt{2}a_{c_k})^2}{2\sigma_k^2} \right] \quad (3.4)$$

and

$$f_{X_k}(x_k/0) = \frac{1}{\sqrt{2\pi}\sigma_k} \exp\left[-\frac{(x_k + \sqrt{2}a_{c_k})^2}{2\sigma_k^2}\right]. \quad (3.5)$$

Combining Equations (3.3), (3.4), and (3.5), we get the detection criterion for a BPSK MLR

$$\sum_{k=1}^d \frac{4\sqrt{2}a_{c_k} x_k}{2\sigma_k^2} \begin{matrix} > \\ < \end{matrix} 0 \quad (3.6)$$

or

$$\sum_{k=1}^d \frac{a_{c_k} x_k}{\sigma_k^2} \begin{matrix} > \\ < \end{matrix} 0. \quad (3.7)$$

For the optimum BPSK receiver the probability of making an incorrect detection P_b , when the decision statistic is modeled as Gaussian random variable (GRV), can be expressed as [4]

$$P_b = Q\left(\frac{\bar{X}}{\sigma_x}\right) = Q\left(\sqrt{\frac{\bar{X}^2}{\sigma_x^2}}\right), \quad (3.8)$$

where in this case \bar{X} and σ_x are the mean and variance of the random variable

$$x = \sum_{k=1}^d z_k \quad (3.9)$$

with

$$z_k = \frac{a_{c_k} x_k}{\sigma_k^2}. \quad (3.10)$$

Since x_k is a GRV, the random variable z_k can also be modeled as GRV. The PDF of z_k is obtained by performing the change of variables

$$f_{z_k}(z_k) = \left| \frac{dx_k}{dz_k} \right| f_{A_c}(x_k) \Big|_{x_k = \frac{z_k \sigma_k^2}{a_{c_k}}} \quad (3.11)$$

The resulting PDF of the GRV z_k is

$$f_{z_k}(z_k) = \frac{1}{\sqrt{2\pi} \left(\frac{a_{c_k}}{\sigma_k} \right)} \exp \left[-\frac{\left(z_k + \sqrt{2} \left(\frac{a_{c_k}}{\sigma_k} \right)^2 \right)^2}{2 \left(\frac{a_{c_k}}{\sigma_k} \right)^2} \right] \quad (3.12)$$

with mean

$$\overline{z_k} = \sqrt{2} \left(\frac{a_{c_k}}{\sigma_k} \right)^2 \quad (3.13)$$

and variance

$$\sigma_{z_k}^2 = \left(\frac{a_{c_k}}{\sigma_k} \right)^2. \quad (3.14)$$

Since the random variable x is the sum of d independent GRVs z_k and using Equations (3.13) and (3.14), we obtain the mean and variance of x as

$$\overline{X} = \sqrt{2} \sum_{k=1}^d \left(\frac{a_{c_k}}{\sigma_k} \right)^2 \quad (3.15)$$

and

$$\sigma_x^2 = \sum_{k=1}^d \left(\frac{a_{c_k}}{\sigma_k} \right)^2, \quad (3.16)$$

respectively.

Finally, substituting Equations (3.15) and (3.16) into (3.8), we obtain the probability of making an incorrect detection P_b for the optimum BPSK receiver as

$$P_b = Q \left(\sqrt{2 \sum_{k=1}^d \frac{a_{c_k}^2}{\sigma_k^2}} \right). \quad (3.17)$$

B. PERFORMANCE ANALYSIS IN A FADING CHANNEL WITH AWGN

The performance of the optimum receiver when the signal is transmitted over a fading channel with AWGN is examined here for all possible sub-carrier modulations as specified in the *802.11a* WLAN standard. As specified in the *802.11a* WLAN standard, different modulation schemes are used to achieving various bit-rates. For lower data rates, BPSK and QPSK are used, while for higher data rates 16QAM and 64QAM are specified.

1. BPSK/QPSK Modulation

The *802.11a* receiver, optimized to operate when the signal is transmitted over a fading channel and in the presence of AWGN for BPSK modulation, is assumed to use the maximum likelihood detection criterion (MLDC) discussed in section III.A. One way of implementing the MLDC is by using the receiver modeled by the block diagram shown in Figure 12. The performance with QPSK is identical to that obtained for BPSK and will not be obtained separately.

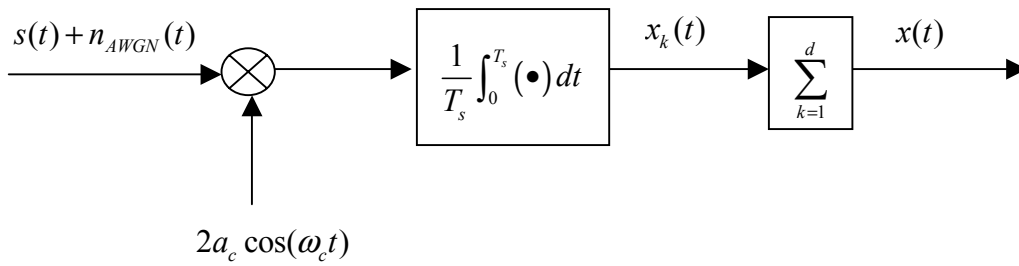


Figure 12. 802.11a receiver block diagram, optimized to operate with AWGN

At the input of the receiver, the desired BPSK signal can be represented as $s(t) = \sqrt{2}a_c d(t) \cos(\omega_c t)$, where a_c is the amplitude of the received signal, $d(t)$ is the

information waveform, T_s is the time duration of a symbol, and ω_c is the frequency of the sub-carrier signal. Since the signal $s(t)$ is assumed to have been transmitted over a flat, slowly-fading Nakagami channel, the amplitude of $s(t)$ is modeled as a Nakagami- m random variable with PDF

$$f_{A_c}(a_c) = \frac{2}{\Gamma(m)} \left(\frac{m}{\Omega} \right)^m a_c^{2m-1} e^{-\frac{mr^2}{\Omega}}, \quad (3.18)$$

which been discussed in Chapter II.

At the input of the receiver, the signal $s(t)$ arrives corrupted by the channel AWGN, denoted as $n_{AWGN}(t)$, with power spectral density (PSD) $N_o/2$.

At the local oscillator the corrupted signal, $s(t) + n_{AWGN}(t)$, is multiplied by $2a_c \cos(\omega_c t)$, where a_c is considered to be known since perfect side information is assumed. As a result of the existing multi-path environment, each bit of the transmitted code sequence may have been affected differently. Therefore, the transmitted signal $s(t)$ for every bit may arrive at the receiver with different amplitudes a_c . The signal $x_k(t)$ at the integrator output represents those sequence bits that have been affected in a random way by the channel. The signal $x_k(t)$ can be modeled as GRV [4] with mean

$$\overline{X_k} = \sqrt{2}a_c^2 \quad (3.19)$$

and variance

$$\sigma_{x_k}^2 = a_c^2 \sigma_k^2 \quad (3.20)$$

where $\sigma_{x_k}^2$ is the noise power at the integrator output that has corrupted the signal $s(t)$. Since the receiver is subjected only to AWGN, we can assume that the signal for each bit is corrupted by the same amount of noise power, $\sigma_o^2 = N_o/T_s$. Therefore, Equation (3.20) can be rewritten as

$$\sigma_{x_k}^2 = a_c^2 \sigma_o^2. \quad (3.21)$$

The overall received signal for a sequence of d bits can be expressed as the summation of independent, random signals

$$x(t) = \sum_{k=1}^d x_k(t). \quad (3.22)$$

Since the quantities $x_k(t)$ are modeled as GRVs, the signal $x(t)$ is also a GRV with mean

$$\overline{X} = \sqrt{2} \sum_{k=1}^d a_c^2 \quad (3.23)$$

and variance

$$\sigma_x^2 = \sum_{k=1}^d \sigma_k^2 a_c^2 = \sigma_o^2 \sum_{k=1}^d a_c^2. \quad (3.24)$$

As already discussed in Chapter II, the *802.11a* WLAN standard specifies the implementation of convolutional FEC in order to improve the receiver performance. When FEC is implemented, there is not an analytic formula expressing BER. However, an upper bound can be used, and it is given by [4]

$$P_b < \frac{1}{k} \sum_{d=d_{free}}^{\infty} B_d P_d \quad (3.25)$$

where d_{free} is the free distance of the convolutional code, B_d is the total number of information bit ones on all weight d paths, P_d is the probability of selecting a weight- d output sequence as the transmitted code sequence, and k is the number of information bits. The quantities B_d and d_{free} are parameters of the convolutional code, and the convolutional code is specified by the *802.11a* WLAN standard. The parameters of the code specified by the *802.11a* standard are listed in Table 2 in Chapter II. In Equation (3.25) the first five elements dominate the summation; therefore, it can be rewritten as

$$P_b < \frac{1}{k} \sum_{d=d_{free}}^{d_{free}+4} B_d P_d. \quad (3.26)$$

For the optimum receiver with BPSK or QPSK modulation and, without taking into account the existence of the multi-path environment, the probability P_d can be expressed as [4]

$$P_d = Q\left(\frac{\bar{X}}{\sigma_x}\right) = Q\left(\sqrt{\frac{\bar{X}^2}{\sigma_x^2}}\right), \quad (3.27)$$

where \bar{X} and σ_x^2 are given in Equations (3.23) and (3.24), respectively.

Substituting Equations (3.23) and (3.24) into (3.27), we get

$$\begin{aligned} P_d\left(\sum_{k=1}^d a_c^2\right) &= Q\left(\sqrt{\frac{2\left(\sum_{k=1}^d a_c^2\right)^2}{\sigma_o^2 \sum_{k=1}^d a_c^2}}\right) = Q\left(\sqrt{\frac{2\sum_{k=1}^d a_c^2}{\sigma_o^2}}\right) \\ &= Q\left(\sqrt{2\sum_{k=1}^d \frac{a_c^2}{\sigma_o^2}}\right). \end{aligned} \quad (3.28)$$

If we compare Equation (3.28) to (3.17), we find that both expressions are analogous. Thus, the receiver modeled in Figure 2 is indeed an optimum receiver. Moreover, as we can see from Equation (3.28), due to the multi-path environment, the resulting probability is conditional on the sum of d Nakagami- m squared random variables a_c^2 .

In order to obtain the average, unconditional probability of selecting a weight- d output sequence P_d , we need to calculate the integral

$$P_d = \int_0^\infty P_d(a_c) f_{A_c}(a_c) da_c, \quad (3.29)$$

where $f_{A_c}(a_c)$ is the Nakagami- m PDF given in Equation (3.18).

For notational purposes, Equation (3.28) can be rewritten

$$P_d(\gamma_b) = Q\left(\sqrt{2\gamma_b}\right) \quad (3.30)$$

where

$$\gamma_b = \sum_{k=1}^d \frac{a_c^2}{\sigma_o^2}, \quad (3.31)$$

is also a random variable, resulting from the summation of the squares of d independent Nakagami- m random variables.

The resulting probability P_d has been evaluated in [1] and is given by

$$P_d = \left[\sqrt{\frac{\frac{1}{m\gamma_b}}{1 + \frac{1}{m\gamma_b}}} \right] \left[\frac{\Gamma(md + 0.5)}{2\sqrt{\pi}\Gamma(md + 1) \left(1 + \frac{1}{m\gamma_b}\right)^{md}} \right] \left[\sum_{q=0}^{\infty} \frac{\prod_{n=0}^{q-1} (md + 0.5 + n)}{\prod_{n=0}^{q-1} (md + 1 + n)} \frac{1}{\left(1 + \frac{1}{m\gamma_b}\right)^q} \right] \quad (3.32)$$

where $\overline{\gamma_b} = \frac{1}{r E_b / N_o}$.

Finally, the general formula for the upper bound on the BER of the optimum 802.11a receiver when the signal is transmitted over a fading channel with AWGN and BPSK/QPSK is obtained by combining Equations (3.25) and (3.32) to get

$$P_b < \frac{1}{k} \sum_{d=d_{free}}^{d_{free}+4} B_d \times \left[\sqrt{\frac{\frac{1}{m\gamma_b}}{1 + \frac{1}{m\gamma_b}}} \right] \left[\frac{\Gamma(md + 0.5)}{2\sqrt{\pi}\Gamma(md + 1) \left(1 + \frac{1}{m\gamma_b}\right)^{md}} \right] \times \sum_{q=0}^{\infty} \frac{\prod_{n=0}^{q-1} (md + 0.5 + n)}{\prod_{n=0}^{q-1} (md + 1 + n)} \frac{1}{\left(1 + \frac{1}{m\gamma_b}\right)^q}. \quad (3.33)$$

Figures 13 and 14, showing the performance of an 802.11a optimum receiver when the signal is transmitted over a fading channel with AWGN and when BPSK/QPSK is used, can be found in [1]. They have computed to check the method of this thesis and are the same as they are in [1].

a. Data Rates of 6 and 12 Mbps

For bit rates of 6 and 12 Mbps, a code rate of $r=1/2$ and BPSK and QPSK are used, respectively. Therefore, substituting $k=1$ and $r=1/2$ into Equation (3.33) and using the values of B_d and d_{free} specified in Table 2, the BER is upper bounded and is plotted in Figure 13 [1] as a function of signal-to-noise ratio (SNR) at the receiver for different fading conditions. From Figure 13, it is clear that the receiver performance becomes poorer as the fading conditions worsen. Examining the two limiting cases for $m=0.5$ and $m \rightarrow \infty$, we conclude that, for a BER of 10^{-5} , approximately 7 dB more signal power is required for $m=0.5$ than for no fading.

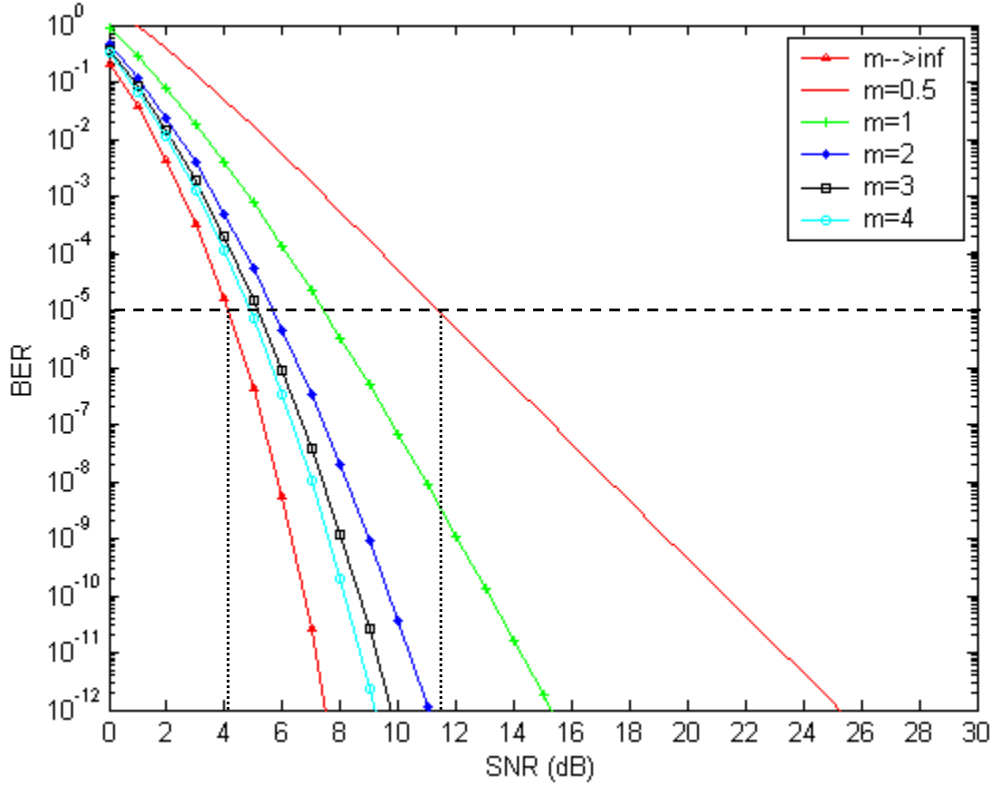


Figure 13. Optimum 802.11a receiver for a Nakagami fading channel with AWGN for bit rates of 6 and 12 Mbps.

b. Data Rates of 9 and 18 Mbps

For data rates of 9 and 18 Mbps, a code-rate of $r=3/4$ and BPSK and QPSK are used, respectively. In a manner analogous to the previous analysis but with

$k=3$ and $r=3/4$, the BER is computed and plotted in Figure 14 [1]. In this case also the receiver performance worsens as the fading conditions worsen. Again examining the two limiting cases for $m=0.5$ and $m \rightarrow \infty$, we conclude that for a BER of 10^{-5} , approximately 15.5 dB more signal power is required for $m=0.5$ than for no fading. It is obvious that in this case the effect of the fading environment on the receiver is more severe.

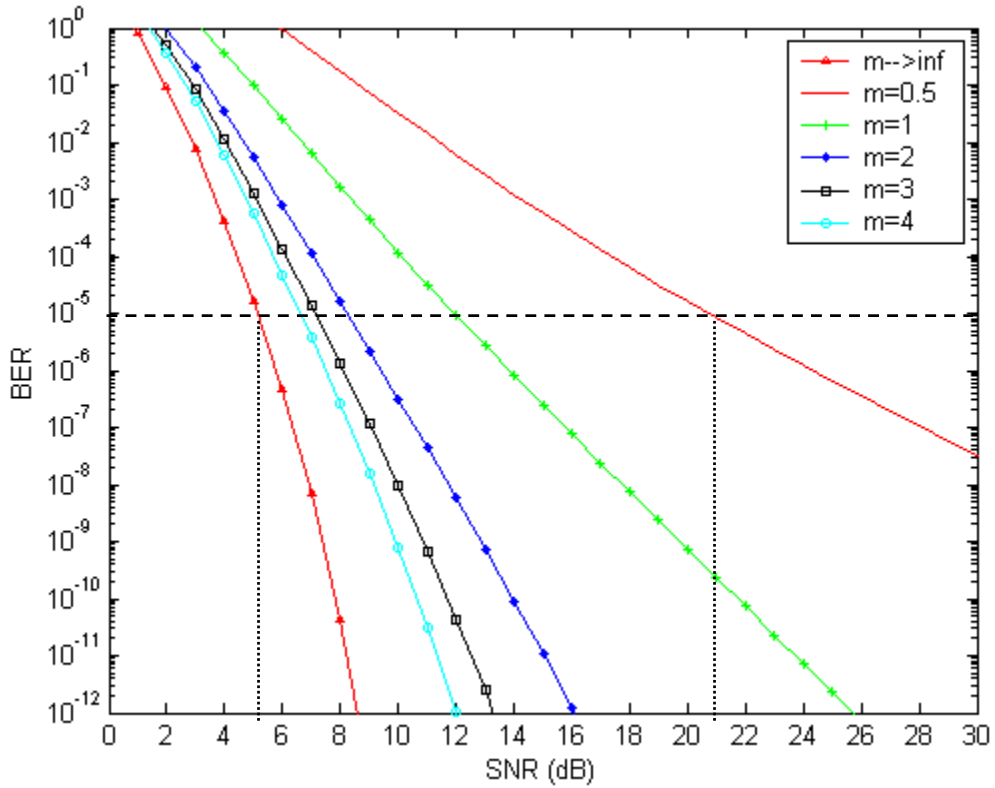


Figure 14. Optimum 802.11a receiver for a Nakagami fading channel with AWGN for bit rates of 9 and 18 Mbps.

2. Non-Binary Modulation

As previously discussed, higher bit rates require non-binary modulation, specifically 16QAM and 64QAM. In Chapter II, it was proven that the best approximation of the BER for MQAM operating in a non-fading environment is given by

$$P_b \simeq \frac{4}{q} Q \left(\sqrt{\frac{3q}{M-1} \frac{E_b}{N_o}} \right). \quad (3.34)$$

Following the same methodology we used in the binary case and keeping in mind the assumption made previously in Chapter II, that the information bits keep the “soft” information that the demodulated symbol that represented the bits had, we can see that the conditional probability of selecting a weight- d output sequence, $P_d(\gamma_b)$, is given by

$$P_d(\gamma_b) = \frac{4}{q} Q \left(\sqrt{\frac{3q}{M-1} \gamma_b} \right) \quad (3.35)$$

where γ_b is given by Equation (3.14), q is the number of information bits per symbol and M is the number of symbols. Consequently, the unconditional probability P_d can be obtained, by calculating the integral

$$P_d = \int_0^\infty P_d(\gamma_b) f_{\Gamma_b}(\gamma_b) d\gamma_b. \quad (3.36)$$

In order to evaluate this integral, we first need to obtain the PDF $f_{\Gamma_b}(\gamma_b)$ of the new random variable γ_b . This new random variable is rewritten as

$$\gamma_b = \sum_{k=1}^d \gamma_{b_k} \quad (3.37)$$

where $\gamma_{b_k} = a_c^2 / \sigma_o^2$ is defined as the second power of the Nakagami- m random variable a_c .

The PDF of the random variable γ_{b_k} is computed by using Equation (3.18) and performing the change of variables

$$f_{\Gamma_{b_k}}(\gamma_{b_k}) = \left| \frac{da_c}{d\gamma_{b_k}} \right| f_{A_c}(a_c^2) \Big|_{a_c = \sqrt{\gamma_{b_k} \sigma_o^2}} \quad (3.38)$$

where $f_{A_c}(a_c^2)$ represents the PDF of the second power of the Nakagami- m random variable a_c given by

$$f_{A_c}(a_c^2) = \frac{2}{\Gamma(m)} \left(\frac{m}{\Omega} \right)^m a_c^{2m-1} e^{-\frac{ma_c^2}{\Omega}}, \quad a_c \geq 0. \quad (3.39)$$

We have

$$\left| \frac{da_c}{d\gamma_{b_k}} \right| = \frac{\sigma_o}{2\sqrt{\gamma_{b_k}}}. \quad (3.40)$$

Substituting (3.39) and (3.40) into (3.38), we get the PDF

$$f_{\Gamma_{b_k}}(\gamma_{b_k}) = \frac{\sigma_o}{2\sqrt{\gamma_{b_k}}} \frac{2}{\Gamma(m)} \left(\frac{m}{\Omega} \right)^m \left(\sqrt{\gamma_{b_k} \sigma_o^2} \right)^{2m-1} e^{-\frac{m\gamma_{b_k} \sigma_o^2}{\Omega}}, \quad a_c \geq 0. \quad (3.41)$$

Setting $\Omega = E[a_c^2] = A_c^2$ and rearranging the terms, we get the resulting PDF

$$f_{\Gamma_{b_k}}(\gamma_{b_k}) = \frac{\left(\frac{m\sigma_o^2}{A_c^2} \right)^m}{\Gamma(m)} \gamma_{b_k}^{m-1} e^{-\left(\frac{m\sigma_o^2}{A_c^2} \right) \gamma_{b_k}}, \quad \gamma_{b_k} \geq 0, \quad (3.42)$$

or

$$f_{\Gamma_{b_k}}(\gamma_{b_k}) = \frac{\left(m\overline{\gamma_b} \right)^m}{\Gamma(m)} \gamma_{b_k}^{m-1} e^{-\left(m\overline{\gamma_b} \right) \gamma_{b_k}}, \quad \gamma_{b_k} \geq 0, \quad (3.43)$$

where

$$\begin{aligned} \overline{\gamma_b} &= \frac{\sigma_o^2}{A_c^2} = \frac{\frac{N_o}{T_s}}{A_c^2} = \frac{N_o}{rT_b A_c^2} \\ &= \frac{1}{r} \left(\frac{E_b}{N_o} \right)^{-1}. \end{aligned} \quad (3.44)$$

Having found the PDF of γ_{b_k} , we now find the PDF of γ_b since $\gamma_b = \sum_{k=1}^d \gamma_{b_k}$. It is shown in [10] that the PDF of the sum of d independent random variables is given by the d -fold convolution of the PDFs of the d random variables. Unfortunately, the evaluation of this PDF cannot be done analytically. However, the Laplace transform (LT) of the

convolution of d functions is $L\{x_1(t) \otimes x_2(t) \otimes \dots \otimes x_d(t)\} = L\{x_1\} \times L\{x_2\} \times \dots \times L\{x_d\}$ [10], where $L\{\bullet\}$ is the Laplace transform operator. Hence, we can obtain the desired PDF by evaluating the LT of the PDF $f_{\Gamma_{b_k}}(\gamma_{b_k})$, raise it to the d^{th} power, and finally evaluate the inverse Laplace transform (ILT) to obtain the desired PDF.

The LT of $f_{\Gamma_{b_k}}(\gamma_{b_k})$ [10] is defined by

$$F_{\Gamma_{b_k}}(s) = L\{f_{\Gamma_{b_k}}(\gamma_{b_k})\} = \int_0^\infty f_{\Gamma_{b_k}}(\gamma_{b_k}) e^{-s\gamma_{b_k}} d\gamma_{b_k}. \quad (3.45)$$

Substituting (3.43) into (3.45), we get

$$F_{\Gamma_{b_k}}(s) = \frac{(m\overline{\gamma_b})^m}{\Gamma(m)} \int_0^\infty \gamma_{b_k}^{m-1} e^{-(s+m\overline{\gamma_b})\gamma_{b_k}} d\gamma_{b_k}. \quad (3.46)$$

Using the identity $\int_0^\infty x^{y-1} e^{-zx} dx = \frac{1}{z^y} \Gamma(y)$ [11], we can evaluate Equation (3.46) to get

$$F_{\Gamma_{b_k}}(s) = \frac{(m\overline{\gamma_b})^m}{(s+m\overline{\gamma_b})^m}. \quad (3.47)$$

Since $F_{\Gamma_b}(s) = (F_{\Gamma_{b_k}}(s))^d$, the LT of the PDF of the random variable γ_b is

$$F_{\Gamma_b}(s) = \frac{(m\overline{\gamma_b})^{md}}{(s+m\overline{\gamma_b})^{md}}. \quad (3.48)$$

The last step is to evaluate the ILT of $F_{\Gamma_b}(s)$. Using the identity [10]

$$L^{-1}\left\{\frac{1}{(s+a)^b}\right\} = \frac{t^{b-1}}{\Gamma(b)} \exp(-at), \text{ the PDF of the random variable } f_{\Gamma_b}(\gamma_b) \text{ is given by}$$

$$f_{\Gamma_b}(\gamma_b) = (m\overline{\gamma_b})^{md} \frac{\gamma_b^{md-1}}{\Gamma(md)} e^{-(m\overline{\gamma_b})\gamma_b}. \quad (3.49)$$

Substituting (3.35) and (3.49) into (3.36), we obtain the unconditional probability P_d expressed by the integral form

$$P_d = \frac{4}{q} \frac{(m\overline{\gamma}_b)^{md}}{\Gamma(md)} \int_0^\infty Q\left(\sqrt{\frac{3q}{M-1}} \gamma_b\right) \gamma_b^{md-1} e^{-(m\overline{\gamma}_b)\gamma_b} d\gamma_b. \quad (3.50)$$

For computational purposes, we make a change in our notation and rewrite Equation (3.50) as

$$P_d = \frac{4}{q} \frac{a^b}{\Gamma(b)} \int_0^\infty Q(\sqrt{ct}) t^{b-1} e^{-at} dt \quad (3.51)$$

where

$$a = m\overline{\gamma}_b, \quad b = md, \quad c = \frac{3q}{M-1}, \quad \text{and} \quad t = \gamma_b. \quad (3.52)$$

We have the identity [11]

$$\begin{aligned} \frac{a^b}{\Gamma(b)} \int_0^\infty Q(\sqrt{ct}) t^{b-1} e^{-at} dt &= \sqrt{\frac{\Psi}{1+\Psi}} \frac{\Gamma(b+0.5)}{2\sqrt{\pi}\Gamma(b+1)(1+\Psi)^b} \\ &\times {}_2F_1\left(1, b+0.5; b+1; \frac{1}{1+\Psi}\right) \end{aligned} \quad (3.53)$$

where ${}_2F_1(1, b+0.5; b+1; z)$ is called Gauss' hypergeometric function and is defined as

$${}_2F_1(1, b+0.5; b+1; z) = \sum_{g=0}^{\infty} \frac{(b+0.5)_g}{(b+1)_g} z^g \quad (3.54)$$

with

$$\Psi = \frac{c}{2a} = \frac{3q}{2(M-1)} \frac{1}{m\overline{\gamma}_b} \quad (3.55)$$

and [11]

$$\begin{aligned} (b+0.5)_g &= \prod_{n=0}^{g-1} (b+0.5+n), \\ (b+1)_g &= \prod_{n=0}^{g-1} (b+1+n). \end{aligned} \quad (3.56)$$

Combining Equations (3.51) through (3.56), we obtain the probability P_d

$$P_d = \left[\frac{4}{q} \sqrt{\frac{\frac{3q}{2(M-1)} \frac{1}{m\gamma_b}}{1 + \frac{3q}{2(M-1)} \frac{1}{m\gamma_b}}} \right] \left[\frac{\Gamma(md + 0.5)}{2\sqrt{\pi}\Gamma(md + 1) \left(1 + \frac{3q}{2(M-1)} \frac{1}{m\gamma_b}\right)^{md}} \right] \quad (3.57)$$

$$\times \sum_{g=0}^{\infty} \frac{\prod_{n=0}^{g-1} (md + 0.5 + n)}{\prod_{n=0}^{g-1} (md + 1 + n)} \frac{1}{\left(1 + \frac{3q}{2(M-1)} \frac{1}{m\gamma_b}\right)^g}$$

Finally, the general formula for the upper bound on BER for the optimum 802.11a receiver operating over a fading channel with AWGN when MQAM is used is obtained by combining Equations (3.26) and (3.57):

$$P_b < \frac{1}{k} \sum_{d=d_{free}}^{d_{free}+4} B_d \times \left[\frac{4}{q} \sqrt{\frac{\frac{3q}{2(M-1)} \frac{1}{m\gamma_b}}{1 + \frac{3q}{2(M-1)} \frac{1}{m\gamma_b}}} \right] \left[\frac{\Gamma(md + 0.5)}{2\sqrt{\pi}\Gamma(md + 1) \left(1 + \frac{3q}{2(M-1)} \frac{1}{m\gamma_b}\right)^{md}} \right] \quad (3.58)$$

$$\times \sum_{g=0}^{\infty} \frac{\prod_{n=0}^{g-1} (md + 0.5 + n)}{\prod_{n=0}^{g-1} (md + 1 + n)} \frac{1}{\left(1 + \frac{3q}{2(M-1)} \frac{1}{m\gamma_b}\right)^g}.$$

a. Data Rate of 24 Mbps

The lowest data rate that is achieved using non-binary modulation is 24 Mbps. For this data rate 16QAM is used along with $r=1/2$ FEC. Substituting $M=16$, $q=4$ and $r=1/2$, along with the values of d_{free} and B_d specified in Table 2, into Equation (3.58), we get the upper bound on BER, plotted in Figure 15 with respect to SNR at the receiver and for different fading conditions. From Figure 15, it is clear that the receiver performance degrades as the fading conditions worsen. Examining the two limiting cases for $m=0.5$ and $m \rightarrow \infty$, we conclude that for a BER of 10^{-5} , approximately

7.5 dB more signal power is required when $m = 0.5$ than for no fading. Note that this is the same as for BPSK/QPSK with a rate $r = 1/2$ code, although the absolute performance is quite different.

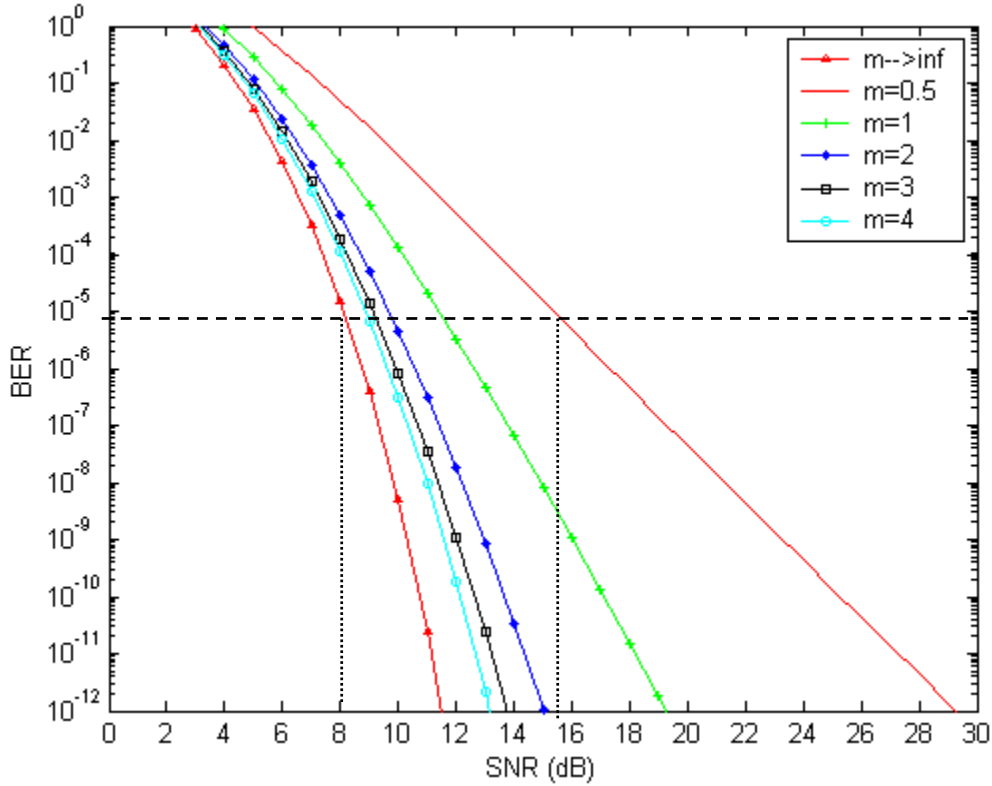


Figure 15. Optimum 802.11a receiver in a Nakagami fading channel with AWGN for bit rate of 24 Mbps ($r = 1/2$).

b. Data Rate of 36 Mbps

For a data rate of 36 Mbps, 16QAM is also used but with a higher code rate of $r = 3/4$. Substituting $M = 16$, $q = 4$, and $r = 3/4$, along with the values of d_{free} and B_d specified in Table 2, into Equation (3.58), we get the upper bound on BER, plotted in Figure 16 with respect to SNR at the receiver and for different fading conditions. The receiver performance for this data rate also degrades as the fading conditions worsen. Examining the two limiting cases for $m = 0.5$ and $m \rightarrow \infty$, we conclude that for achieving a BER of 10^{-5} , approximately 15 dB of more signal power is required when $m = 0.5$ than for no fading. As we can see, the performance of the receiver is affected signifi-

cantly more due to the fading environment than for the case of 24 Mbps. As for the 24-Mbps data rate, this is very similar to what was found for BPSK/QPSK with a rate $r = 3/4$ code; although, absolute performance is much worse. This is expected since the conditional P_b for BPSK/QPSK and MQAM is expressed in terms of the Q-function.

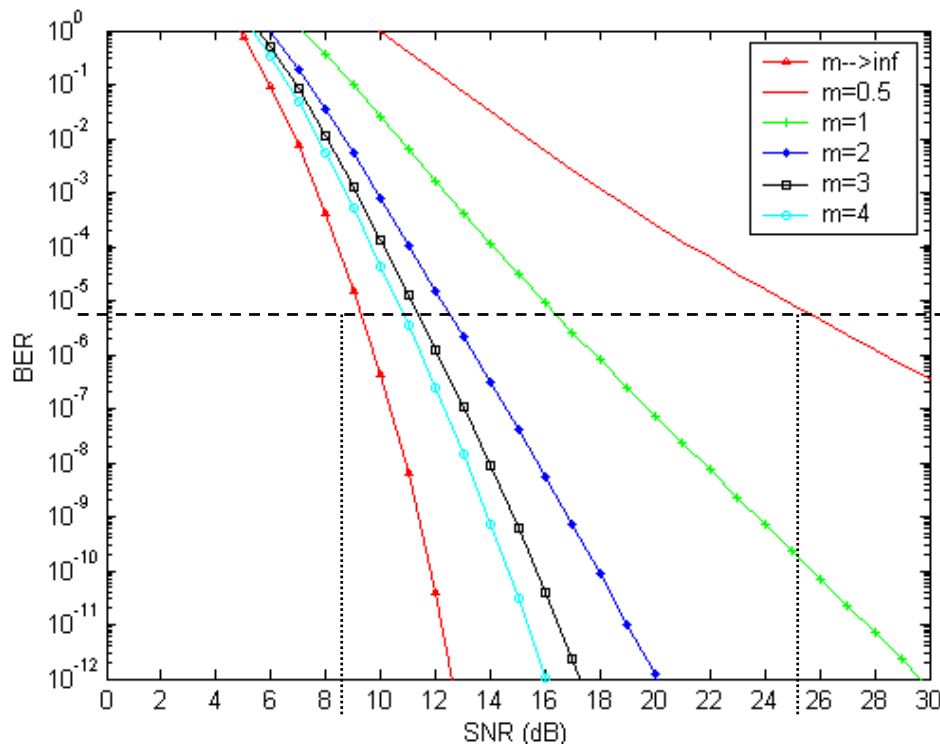


Figure 16. Optimum 802.11a receiver in a Nakagami fading channel with AWGN for bit rate of 36 Mbps ($r = 3/4$).

c. Data Rate of 48 Mbps

For a data rate of 48 Mbps, 64QAM is used with a code rate of $r = 2/3$. Substituting $M = 64$, $q = 6$, and, $r = 2/3$, along with the values of d_{free} and B_d specified in Table 2, into Equation (3.58), we get the upper bound on BER, plotted in Figure 17 with respect to SNR at the receiver and for different fading conditions. Examining the two limiting cases for $m = 0.5$ and $m \rightarrow \infty$, we conclude that for a BER of 10^{-5} , approximately 9 dB more signal power is required when $m = 0.5$ than for no fading. It

clear that the receiver performance is affected less than for the 36-Mbps case but more than the 24-Mbps case.

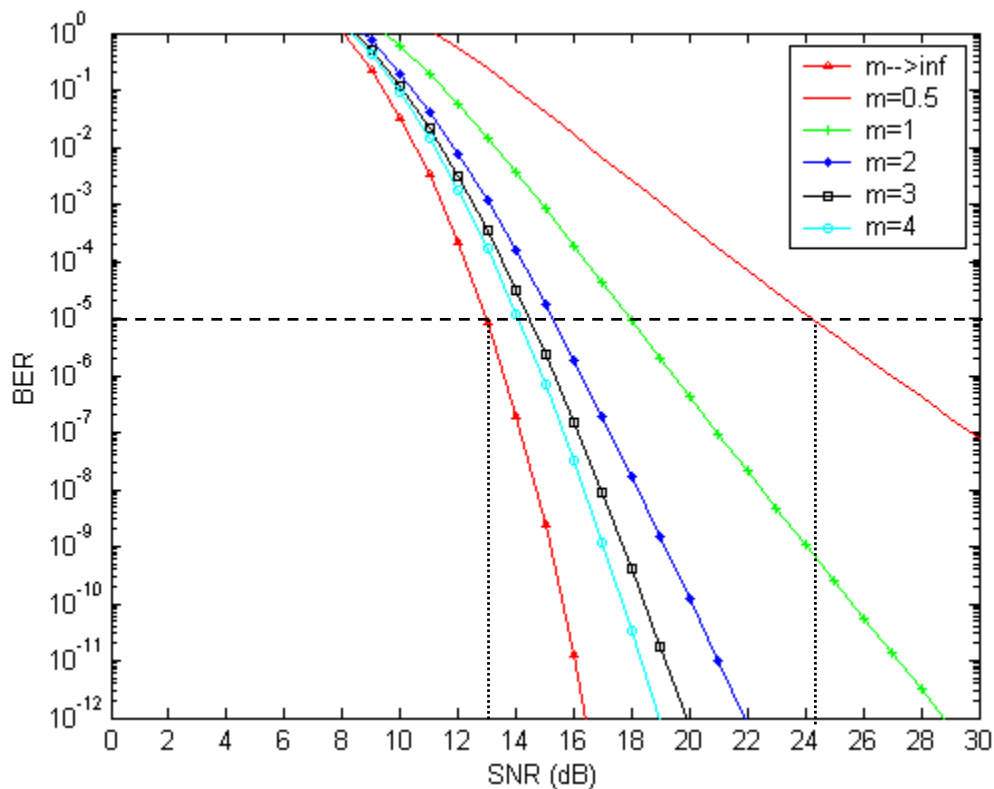


Figure 17. Optimum 802.11a receiver in a Nakagami fading channel with AWGN for bit rate of 48 Mbps ($r = 2/3$).

d. Data Rate of 54 Mbps

Finally, the highest data rate of 54 Mbps is achieved by using 64QAM and a FEC with $r = 3/4$. Substituting $M = 64$, $q = 6$, and $r = 3/4$, along with the values of d_{free} and B_d specified in Table 2, into Equation (3.58), we get the upper bound on BER, plotted in Figure 18 with respect to SNR at the receiver and for different fading conditions. Examining the two limiting cases for $m = 0.5$ and $m \rightarrow \infty$, we conclude that for a BER of 10^{-5} , approximately 15 dB more signal power is required when $m = 0.5$ than for no fading. This change in the required signal power is analogous to the change required in the 36-Mbps case. This stands to reason since both of the 54-Mbps and 36-Mbps cases use a rate $r = 3/4$ code. Clearly, what determines the relative effect of the fading channel

is the code rate, while absolute performance is determined by the combination of modulation and coding.

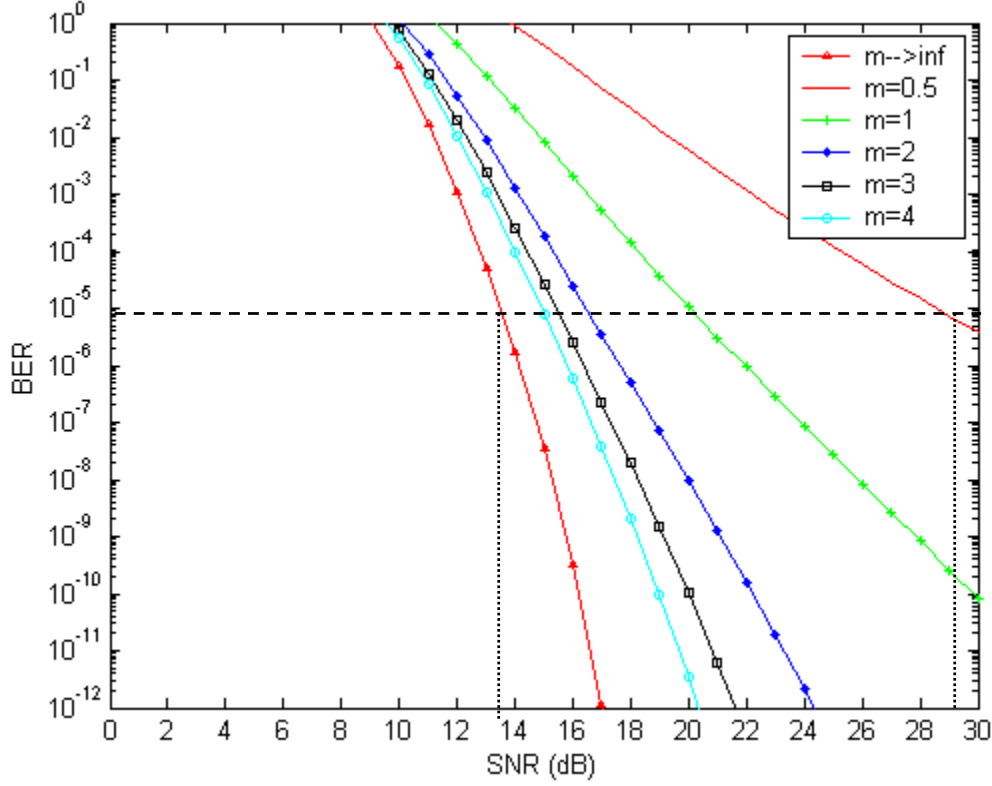


Figure 18. Optimum 802.11a receiver in a Nakagami fading channel with AWGN for bit rate of 54 Mbps ($r = 3/4$).

3. Conclusions on the Effect of AWGN on the 802.11a Optimum Receiver

Summarizing, the overall performance of the optimum receiver is discussed for all specified operational data rates when operating with AWGN.

The first comment we make regards the effect the fading environment has on the receiver performance. Studying Figures 13 through 18, we conclude that the effect of the fading environment depends on the code rate used. The fading environment affects the receiver less when lower code rates are used. When a code rate of $r = 1/2$ is used (data rates of 6, 12, and 24 Mbps), in order to achieve a $P_b = 10^{-5}$, the signal power difference between the severe fading condition $m = 0.5$ and the non-fading condition is on the order

of 7 dB. When a FEC with $r = 2/3$ is used (data rate of 48 Mbps), the additional signal power required to achieve $P_b = 10^{-5}$ is on the order of 9 dB. Finally, the receiver is affected the most when FEC with $r = 3/4$ is used (data rates of 9, 18, 36, and 54 Mbps). In this case the difference in the signal power is on the order of 15 dB. It is notable that the above quantities are independent of the modulation scheme used.

The receiver performance is also examined for different types of fading environments. First, the receiver is assumed to operate in an intense fading environment (i.e., fading figure $m = 1$), with $E_b/N_o = 15$ dB. The performance of the receiver in this case, in terms of BER, is plotted in Figure 19.

Second, the performance of the optimum receiver is examined when the fading environment is not severe (i.e., fading figure $m = 3$), $E_b/N_o = 15$ dB. The performance of the receiver when $m = 3$ is plotted in Figure 20.

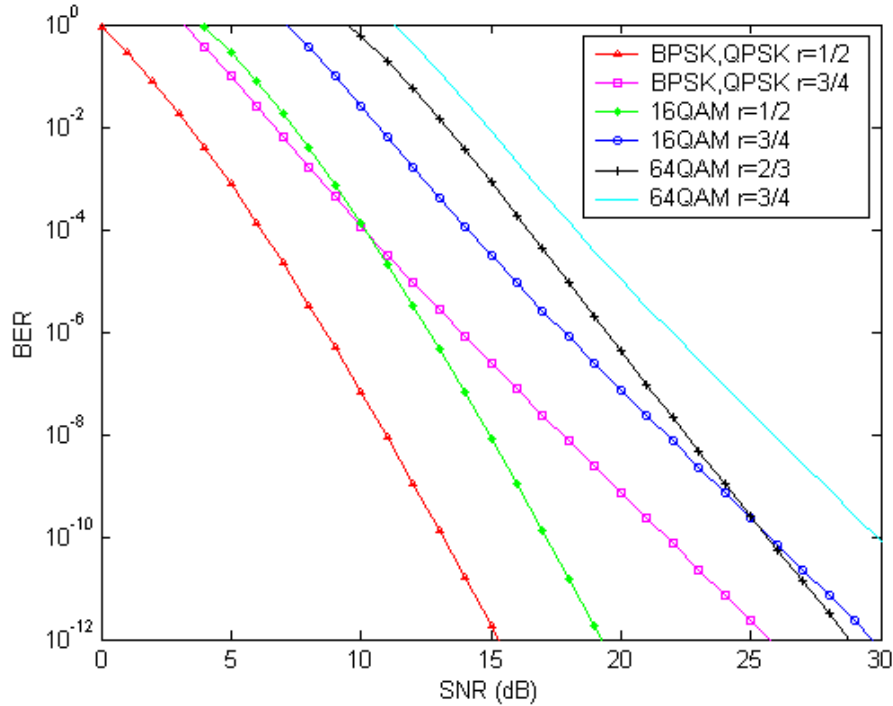


Figure 19. BER performance of the optimum 802.11a receiver in severe Nakagami fading channel ($m = 1$) with AWGN for all specified bit rates.

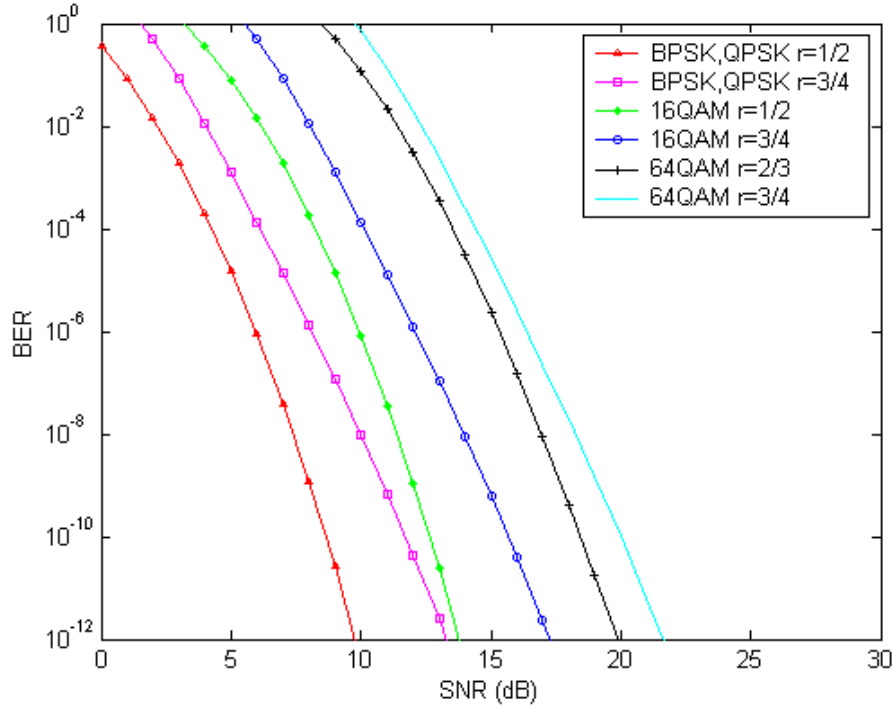


Figure 20. BER performance of the optimum *802.11a* receiver in a Nakagami fading channel ($m = 3$) with AWGN for all specified bit rates.

In Figure 19, when severe fading conditions exist, the receiver performance is affected by the code rate used. We can see that for larger signal power, the performance of the receiver for the 24-Mbps case (i.e., 16QAM with $r = 1/2$), is better than the 9 and 18-Mbps case (i.e., BPSK with $r = 3/4$). The same phenomenon occurs for the 36 and 48-Mbps data rates for large values of SNR.

From Figure 20, where the receiver performance in a non-severe fading environment is examined, we can see that the receiver performance degrades as the data rate increases. This occurs due to the use of non-binary modulation for the higher data rates, since in general non-binary modulation is known to have poorer performance.

C. PERFORMANCE ANALYSIS WITH A HOSTILE PULSED-NOISE JAMER

After studying the performance of the optimum receiver for fading channels with AWGN, the performance of the receiver affected by a pulsed-noise jammer (PNJ) is ex-

amined. The *802.11a* receiver is assumed to be optimized to operate in the presence of a PNJ. Additionally, perfect side information is assumed.

1. BPSK/QPSK Modulation

Initially, the performance of the receiver with either BPSK or QPSK is examined. The optimum receiver, equivalent to the MLR, can also be modeled by the block diagram shown in Figure 11.

The noise signal $n(t)$ that arrives at the receiver can no longer be assumed to be uniform. As a consequence, not all the received bits are affected by the same amount of noise power $\sigma_{x_k}^2$. Furthermore, since the jammer is considered to operate in a pulsed mode, a received bit may be corrupted either by AWGN only (i.e., the PNJ is not transmitting an interference signal) or by both AWGN and by the jammer signal (i.e., the jammer is transmitting an interference signal). The effect of the jammer signal is to increase the total noise power that corrupts each received bit when the jammer is on. So the noise power at the integrator output for each received bit can be expressed as

$$\sigma_{x_k}^2 = \begin{cases} \sigma_{x_j}^2 = \sigma_o^2 + \sigma_j^2 & \text{when PNJ is operational,} \\ \sigma_{x_o}^2 = \sigma_o^2 & \text{otherwise.} \end{cases} \quad (3.59)$$

where $\sigma_{x_j}^2$ is the noise power of a jammed bit, $\sigma_{x_o}^2$ is the noise power of a non-jammed bit, σ_o^2 is the AWGN noise power, and σ_j^2 is the jamming noise power. These quantities can be expressed as

$$\begin{aligned} \sigma_o^2 &= \frac{N_o}{T_s}, \\ \sigma_j^2 &= \frac{N'_I}{T_s}, \end{aligned} \quad (3.60)$$

where N_o and N'_I are the noise PSDs of the AWGN and the jamming signal, respectively. If we assume that the PNJ is operational a fraction of time ρ , where $0 < \rho \leq 1$, and that the average jamming noise power is the same for all ρ (i.e., $N'_I = N_I/\rho$, where N_I is the jammer PSD when $\rho = 1$ and is independent of ρ), we can write

$$\sigma_j^2 = \frac{N_I}{\rho T_s}. \quad (3.61)$$

Substituting Equation (3.60) and (3.61) into (3.59), we get

$$\sigma_{x_k}^2 = \begin{cases} \frac{N_I / \rho + N_o}{T_s} & \text{when PNJ is operational,} \\ \frac{N_o}{T_s} & \text{otherwise.} \end{cases} \quad (3.62)$$

As discussed previously and repeated here for convenience, the upper bound on the BER with FEC is

$$P_b < \frac{1}{k} \sum_{d=d_{free}}^{d_{free}+4} B_d P_d \quad (3.63)$$

where d_{free} is the free distance of the convolutional code, B_d is the total number of information bit ones on all weight- d paths, P_d is the probability of selecting a weight- d output sequence as the transmitted code sequence, and k is the number of information bits. Since the jammer is operating in a pulsed mode, we assume that of the d independently received bits, only i bits are assumed to be jammed, while the remaining $(d-i)$ bits are considered to be affected only by AWGN. Since we implicitly assume an ideal interleaver at the transmitter and an ideal de-interleaver at the receiver, every received bit can be assumed to be independent. In other words, the channel is modeled as a memoryless channel. Now the probability that i of the d received bits are jammed is given by

$$\Pr(\text{jammed} / i) = \rho^i (1 - \rho)^{d-i} \quad (3.64)$$

where for any bit there are $\binom{d}{i}$ different ways in which i of the d received bits can be jammed. Therefore, the probability P_d can be expressed

$$P_d = \sum_{i=0}^d \binom{d}{i} \Pr(\text{jammed} / i) P_{d_i} = \sum_{i=0}^d \binom{d}{i} \rho^i (1 - \rho)^{d-i} P_{d_i} \quad (3.65)$$

where P_{d_i} is the average independent probability of selecting a weight- d output sequence when i bits are jammed, while the remaining $(d-i)$ bits are affected only by AWGN. The quantity ρ denotes the fraction of time that the PNJ is operational and is, therefore, the probability that one bit will be jammed.

Keeping in mind that the receiver is optimized to operate with hostile PNJ and following an analysis analogous to the AWGN case, we obtain the average probability P_{d_i} as

$$P_{d_i} = \int_0^\infty P_{d_i}(\gamma_b) f_{\Gamma_b}(\gamma_b) d\gamma_b \quad (3.66)$$

where $P_{d_i}(\gamma_b)$ is the conditional probability of selecting a weight- d output sequence when only i bits are jammed. As discussed previously, the probability $P_{d_i}(\gamma_b)$ in the case of an optimum receiver is obtained in Equation (3.17) and is repeated here for convenience:

$$P_{d_i}(i) = Q\left(\sqrt{2\gamma_b}\right) \quad (3.67)$$

where the random variable γ_b is defined

$$\gamma_b = \sum_{k=1}^d \frac{a_c^2}{\sigma_{x_k}^2}. \quad (3.68)$$

Since only i bits are jammed, from Equations (3.59) and (3.68)

$$\gamma_b = \sum_{k=1}^i \frac{a_c^2}{\sigma_{x_j}^2} + \sum_{k=1}^{d-i} \frac{a_c^2}{\sigma_{x_o}^2} \quad (3.69)$$

or

$$\gamma_b = \gamma_{b_j} + \gamma_{b_o} \quad (3.70)$$

where

$$\begin{aligned}\gamma_{b_j} &= \sum_{k=1}^i \frac{a_c^2}{\sigma_{x_j}^2} = \sum_{k=1}^i \gamma_{b_{k_j}}, \\ \gamma_{b_o} &= \sum_{k=1}^{d-i} \frac{a_c^2}{\sigma_{x_o}^2} = \sum_{k=1}^{d-i} \gamma_{b_{k_o}}.\end{aligned}\tag{3.71}$$

The next step is to obtain the PDF of the random variable γ_b , $f_{\Gamma_b}(\gamma_b)$. Before doing that, we need to evaluate the PDF of the random variables γ_{b_j} and γ_{b_o} , which are defined as sums of the independent random variables $\gamma_{b_{k_j}}$ and $\gamma_{b_{k_o}}$, respectively.

The procedure followed to determine the PDFs of the random variables γ_{b_j} and γ_{b_o} is the same as was used in the AWGN case. Performing a change of variables

$$\begin{aligned}\gamma_{b_{k_j}} &= \frac{a_c^2}{\sigma_{x_j}^2}, \\ \gamma_{b_{k_o}} &= \frac{a_c^2}{\sigma_{x_o}^2}\end{aligned}\tag{3.72}$$

we first obtain the PDFs for $\gamma_{b_{k_j}}$ and $\gamma_{b_{k_o}}$. For the jammed bits the PDF of $\gamma_{b_{k_j}}$ is analogous to the PDF obtained in Equation (3.43) in the AWGN case and is given by

$$f_{\Gamma_{b_{k_j}}}(\gamma_{b_{k_j}}) = \frac{(m\overline{\gamma_{b_j}})^m}{\Gamma(m)} \gamma_{b_{k_j}}^{m-1} e^{-(m\overline{\gamma_{b_j}})\gamma_{b_{k_j}}}, \quad \gamma_{b_{k_j}} \geq 0\tag{3.73}$$

where

$$\overline{\gamma_{b_j}} = \frac{\sigma_{x_j}^2}{A_c^2} = \frac{\frac{N_I + N_o}{\rho}}{A_c^2} = \frac{\frac{N_I + N_o}{rT_b A_c^2}}{A_c^2} = \frac{1}{r} \left[\frac{1}{\rho} \left(\frac{E_b}{N_I} \right)^{-1} + \left(\frac{E_b}{N_o} \right)^{-1} \right].\tag{3.74}$$

By the same token, for the non-jammed bits, the PDF of $\gamma_{b_{k_o}}$ is given by

$$f_{\Gamma_{b_{k_o}}}(\gamma_{b_{k_j}}) = \frac{(m\overline{\gamma_{b_o}})^m}{\Gamma(m)} \gamma_{b_{k_o}}^{m-1} e^{-(m\overline{\gamma_{b_o}})\gamma_{b_{k_o}}}, \quad \gamma_{b_{k_o}} \geq 0 \quad (3.75)$$

where

$$\overline{\gamma_{b_o}} = \frac{\sigma_o^2}{A_c^2} = \frac{\frac{N_o}{T_s}}{A_c^2} = \frac{N_o}{rT_b A_c^2} = \frac{1}{r} \left(\frac{E_b}{N_o} \right)^{-1}. \quad (3.76)$$

Next we need to obtain the LT of the PDFs given in Equations (3.73) and (3.75). Following the same method described for the AWGN case, we get

$$F_{\Gamma_{b_{k_j}}}(s) = \frac{(m\overline{\gamma_{b_j}})^m}{(s + m\overline{\gamma_{b_j}})^m} \quad (3.77)$$

and

$$F_{\Gamma_{b_{k_o}}}(s) = \frac{(m\overline{\gamma_{b_o}})^m}{(s + m\overline{\gamma_{b_o}})^m}. \quad (3.78)$$

Consequently, the LT of the PDFs of the random variables γ_{b_j} and γ_{b_o} are given by

$$F_{\Gamma_{b_{k_j}}}(s) = \frac{(m\overline{\gamma_{b_j}})^{mi}}{(s + m\overline{\gamma_{b_j}})^{mi}} \quad (3.79)$$

and

$$F_{\Gamma_{b_{k_o}}}(s) = \frac{(m\overline{\gamma_{b_o}})^{m(d-i)}}{(s + m\overline{\gamma_{b_o}})^{m(d-i)}}. \quad (3.80)$$

Finally, the LT of the PDF of the random variable γ_b is

$$F_{\Gamma_b}(s) = \frac{(m\overline{\gamma_{b_j}})^{mi}}{(s + m\overline{\gamma_{b_j}})^{mi}} \times \frac{(m\overline{\gamma_{b_o}})^{m(d-i)}}{(s + m\overline{\gamma_{b_o}})^{m(d-i)}}. \quad (3.81)$$

The last step is to evaluate the ILT of $F_{\Gamma_b}(s)$. In general, the evaluation of the inverse LT of Equation (3.81) is very difficult. Therefore, $f_{\Gamma_b}(\gamma_b) = L^{-1}\{F_{\Gamma_b}(s)\}$ is evaluated numerically using the method described in the APPENDIX A. From the APPENDIX A, the PDF required is given by the numerical evaluation of

$$f_{\Gamma_b}(\gamma_b) = \frac{c \exp(c\gamma_b)}{\pi} \int_0^{\pi/2} [\operatorname{Re}\{F_{\Gamma_b}(c + jc \tan(\varphi))\} \cos(c\gamma_b \tan(\varphi)) - \operatorname{Im}\{F_{\Gamma_b}(c + jc \tan(\varphi))\} \sin(c\gamma_b \tan(\varphi))] \sec^2(\varphi) d\varphi \quad (3.82)$$

where c must be within the strip of convergence of $F_{\Gamma_b}(s)$.

The required PDF can be obtained analytically for the special case where the fading factor m is assumed to be an integer. Let

$$a = \overline{\gamma_{b_j}}, \quad b = mi, \quad c = \overline{\gamma_{b_o}}, \quad d = m(d-i). \quad (3.83)$$

Now Equation (3.81) can be written

$$F_{\Gamma_b}(s) = \left(\frac{a}{s+a} \right)^b \left(\frac{c}{s+c} \right)^d. \quad (3.84)$$

For $b > 0$ and $d > 0$ we can perform partial fraction expansion of Equation (3.84) to get

$$F_{\Gamma_b}(s) = a^b c^d \left[\sum_{k=1}^b C_j \frac{1}{(s+a)^k} + \sum_{k=1}^d C_o \frac{1}{(s+c)^k} \right], \quad b > 0, d > 0 \quad (3.85)$$

where

$$C_j = (-1)^{-1} \frac{(d+b-k-1)!}{(b-k)!(d-1)!} \frac{1}{(c-a)^{d+b-k}},$$

$$C_o = (-1)^{-1} \frac{(d+b-k-1)!}{(d-k)!(b-1)!} \frac{1}{(a-c)^{d+b-k}}. \quad (3.86)$$

Substituting Equation (3.83) into (3.86), we get

$$\begin{aligned} C_j &= (-1)^{-1} \frac{(md-k-1)!}{(mi-k)![m(d-i)-1]!} \frac{1}{\left(m\overline{\gamma_{b_o}} - m\overline{\gamma_{b_j}}\right)^{md-k}}, \\ C_o &= (-1)^{-1} \frac{(md-k-1)!}{[m(d-i)-k]!(mi-1)!} \frac{1}{\left(m\overline{\gamma_{b_j}} - m\overline{\gamma_{b_o}}\right)^{md-k}}. \end{aligned} \quad (3.87)$$

Using the identity [10] $L^{-1} \left\{ \frac{1}{(s+x)^y} \right\} = \frac{t^{y-1}}{\Gamma(y)} e^{-xt}$, and using Equation (3.83), we obtain

$$f_{\Gamma_b}(\gamma_b) = \left(m\overline{\gamma_{b_j}}\right)^{mi} \left(m\overline{\gamma_{b_o}}\right)^{m(d-i)} \left[\sum_{k=1}^{mi} C_j \frac{\gamma_b^{k-1}}{\Gamma(k)} e^{-(m\overline{\gamma_{b_j}})\gamma_b} + \sum_{k=1}^{m(d-i)} C_o \frac{\gamma_b^{k-1}}{\Gamma(k)} e^{-(m\overline{\gamma_{b_o}})\gamma_b} \right]. \quad (3.88)$$

Equation (3.88) is valid only when b and d are positive integers. This statement is equivalent to $i \neq 0$ and $i \neq d$. If $i = 0$, then it is assumed that no bits are affected by the jammer. In this case, all bits are subjected only to AWGN. This PDF was computed earlier in the Chapter III.A and is repeated for convenience:

$$f_{\Gamma_b}(\gamma_b) = \frac{\left(m\overline{\gamma_{b_o}}\right)^{md}}{\Gamma(md)} \gamma_b^{m-1} e^{-(m\overline{\gamma_{b_o}})\gamma_b}, \quad \gamma_b \geq 0. \quad (3.89)$$

By the same token, if $i = d$ then all received bits are affected by the jammer. This situation is also equivalent to the AWGN case since the noise power is the same for all bits (i.e., $\sigma_x^2 = \sigma_{x_j}^2$ for all bits). Therefore, the PDF $f_{\Gamma_b}(\gamma_b)$ is given by

$$f_{\Gamma_b}(\gamma_b) = \frac{\left(m\overline{\gamma_{b_j}}\right)^{md}}{\Gamma(md)} \gamma_b^{m-1} e^{-(m\overline{\gamma_{b_j}})\gamma_b}, \quad \gamma_b \geq 0. \quad (3.90)$$

Summarizing Equations (3.88), (3.89) and (3.90), we get

$$f_{\Gamma_b}(\gamma_b) = \begin{cases} \frac{(m\overline{\gamma_{b_o}})^{md}}{\Gamma(md)} \gamma_b^{m-1} e^{-(m\overline{\gamma_{b_o}})\gamma_b} & i = 0, \\ \frac{(m\overline{\gamma_{b_j}})^{md}}{\Gamma(md)} \gamma_b^{m-1} e^{-(m\overline{\gamma_{b_j}})\gamma_b} & i = d, \\ (m\overline{\gamma_{b_j}})^{mi} (m\overline{\gamma_{b_o}})^{m(d-i)} \left[\sum_{k=1}^{mi} C_j \frac{\gamma_b^{k-1}}{\Gamma(k)} e^{-(m\overline{\gamma_{b_j}})\gamma_b} + \sum_{k=1}^{m(d-i)} C_o \frac{\gamma_b^{k-1}}{\Gamma(k)} e^{-(m\overline{\gamma_{b_o}})\gamma_b} \right] & \text{else.} \end{cases} \quad (3.91)$$

Now that the PDF $f_{\Gamma_b}(\gamma_b)$ has been obtained, we can determine the average unconditional probability P_{d_i} of selecting a weight- d output sequence when only i bits are jammed. In the general case, when the PDF $f_{\Gamma_b}(\gamma_b)$ is determined numerically by Equation (3.82), we must numerically evaluate the integral in Equation (3.66).

However, in the special case when the fading factor is an integer, the PDF $f_{\Gamma_b}(\gamma_b)$ is given by Equation (3.91) and the integral in Equation (3.66) can be evaluated analytically. Using the mathematical identity given in Equation (3.53) and following the same steps previously discussed, we find the average unconditional probability

$$P_{d_i} = \begin{cases} \sqrt{\frac{1}{m\overline{\gamma_{b_o}}}} \frac{\Gamma(md + 0.5)}{2\sqrt{\pi}\Gamma(md + 1) \left(1 + \frac{1}{m\overline{\gamma_{b_o}}}\right)^{md}} \sum_{q=0}^{\infty} \frac{\prod_{n=0}^{q-1} (md + 0.5 + n)}{\prod_{n=0}^{q-1} (md + 1 + n)} \frac{1}{\left(1 + \frac{1}{m\overline{\gamma_{b_o}}}\right)^q} & i = 0, \\ \sqrt{\frac{1}{m\overline{\gamma_{b_j}}}} \frac{\Gamma(md + 0.5)}{2\sqrt{\pi}\Gamma(md + 1) \left(1 + \frac{1}{m\overline{\gamma_{b_j}}}\right)^{md}} \sum_{q=0}^{\infty} \frac{\prod_{n=0}^{q-1} (md + 0.5 + n)}{\prod_{n=0}^{q-1} (md + 1 + n)} \frac{1}{\left(1 + \frac{1}{m\overline{\gamma_{b_j}}}\right)^q} & i = d, \\ (m\overline{\gamma_{b_j}})^{mi} (m\overline{\gamma_{b_o}})^{m(d-i)} \left[\sum_{k=1}^{mi} C_j \frac{1}{(m\overline{\gamma_{b_j}})^k} P_J(k) + \sum_{k=1}^{m(d-i)} C_o \frac{1}{(m\overline{\gamma_{b_o}})^k} P_O(k) \right] & \text{else.} \end{cases} \quad (3.92)$$

where

$$P_J(k) = \sqrt{\frac{\frac{1}{m\gamma_{b_j}}}{1 + \frac{1}{m\gamma_{b_j}}}} \frac{\Gamma(k+0.5)}{2\sqrt{\pi}\Gamma(k+1) \left(1 + \frac{1}{m\gamma_{b_j}}\right)^k} \sum_{q=0}^{\infty} \frac{\prod_{n=0}^{q-1} (md+0.5+n)}{\prod_{n=0}^{q-1} (md+1+n)} \frac{1}{\left(1 + \frac{1}{m\gamma_{b_j}}\right)^q} \quad (3.93)$$

and

$$P_O(k) = \sqrt{\frac{\frac{1}{m\gamma_{b_o}}}{1 + \frac{1}{m\gamma_{b_o}}}} \frac{\Gamma(k+0.5)}{2\sqrt{\pi}\Gamma(k+1) \left(1 + \frac{1}{m\gamma_{b_o}}\right)^k} \sum_{q=0}^{\infty} \frac{\prod_{n=0}^{q-1} (md+0.5+n)}{\prod_{n=0}^{q-1} (md+1+n)} \frac{1}{\left(1 + \frac{1}{m\gamma_{b_o}}\right)^q}. \quad (3.94)$$

Finally, combining Equations (3.63) and (3.65), the performance of the 802.11a receiver, optimized to operate in hostile PNJ, is given by

$$P_b < \frac{1}{k} \sum_{d=d_{free}}^{\infty} B_d \times \sum_{i=0}^d \binom{d}{i} \rho^i (d-i)^{d-i} P_{d_i} \quad (3.95)$$

where the probability P_{d_i} can either be determined numerically by calculating the integral in Equation (3.66) or analytically from Equation (3.92) when m is an integer.

a. Data Rates of 6 and 12 Mbps

As previously discussed, for bit rates of 6 and 12 Mbps, a code rate of $r=1/2$ is implemented and BPSK and QPSK are used, respectively. Therefore, substituting $k=1$ and $r=1/2$ into Equation (3.95) and using the values of B_d and d_{free} specified in Table 2, the BER can be obtained analytically. In Figure 21 the BER is plotted with respect to signal-to-interference ratio (SIR) at the receiver and for different fading conditions. In order to validate the results obtained using the numerical technique described in the APPENDIX A, the BER is obtained both analytically and numerically. For these calculations, the SNR is assumed to be $E_b/N_o=15$ dB and the coefficient ρ that defines the fraction of time that the jammer is operational is $1/2$.

From Figure 21, it is clear that both methods give virtually identical results for all fading conditions. This is an indication that the numerical technique developed in the APPENDIX A is very accurate. Additionally, the numerical method is valid for all possible values of the coefficient m (integer or not). Moreover, the BER calculated analytically in Equation (3.95) introduces numerical errors either when smaller values of SNR are used or for larger values of coefficient m . Therefore, the numerical method developed in the APPENDIX A will be used exclusively in order to investigate the BER performance of the *802.11a* receiver.

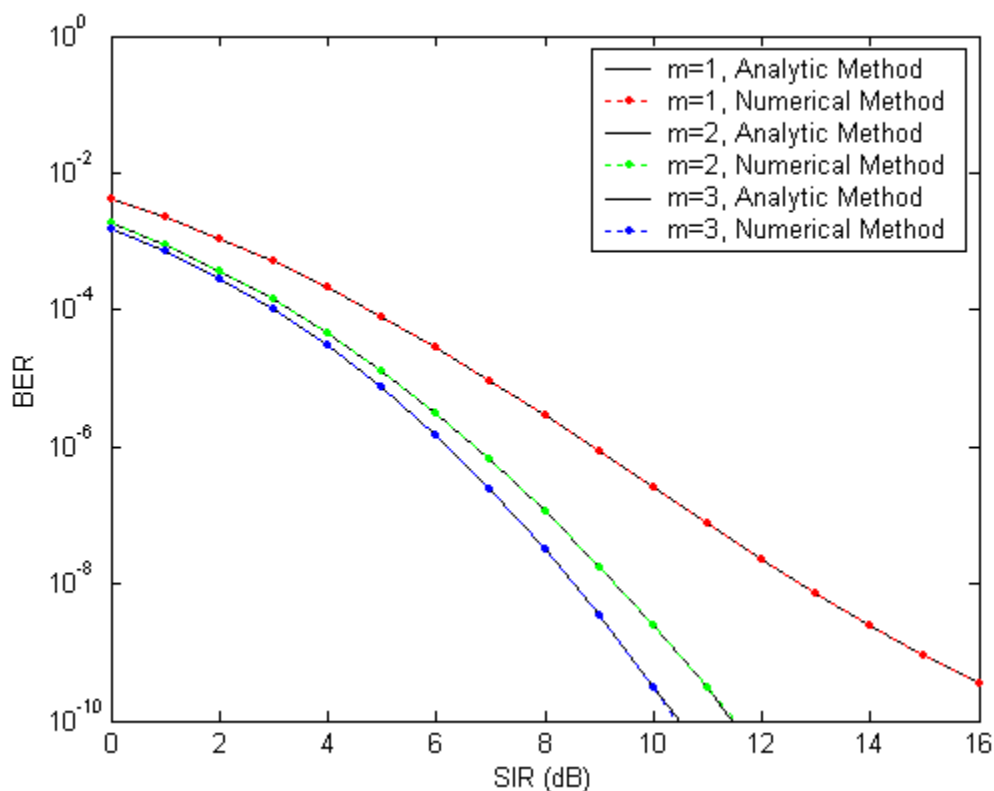


Figure 21. BER performance of *802.11a* receiver optimized to operate with PNJ, estimated both analytically and numerically, for data rates of 6 and 12 Mbps

Having proved the validity of our method, we can proceed to examine the performance of the *802.11a* receiver when operating in PNJ and in the mode of transferring data at 6 Mbps. In Figure 22 the BER performance is plotted for various fading conditions with $E_b/N_o = 15$ dB and $\rho = 0.5$. As expected, the performance of the receiver

rapidly improves as we move from severe fading conditions (i.e., $m=1/2$) to the non-fading condition (i.e., m approaches infinity asymptotically).

An other interesting observation is the fact that as the SIR increases, the performance is improved up to the point where the AWGN power dominates. As a result, for values of $E_b/N_f > 25$ dB, the performance of the receiver converges to a limit determined by AWGN.

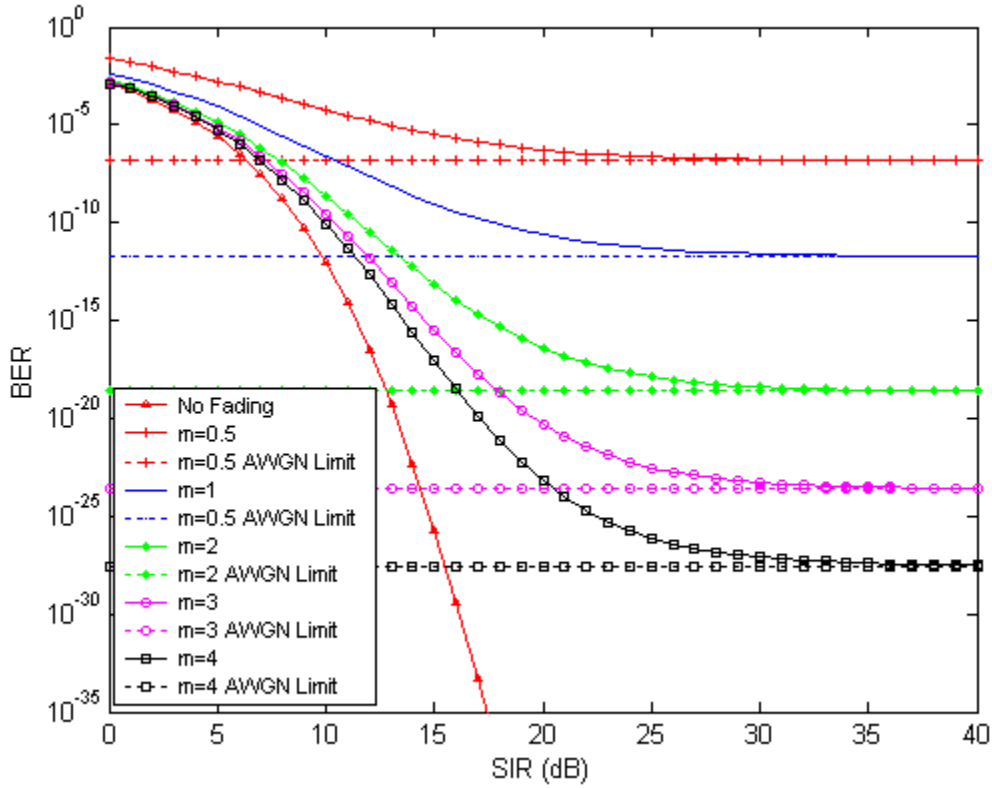


Figure 22. BER performance of 802.11a receiver optimized to operate with PNJ for various fading conditions and for data rates of 6 and 12 Mbps.

Next, we will investigate the effect that the coefficient ρ has on receiver performance. In Figure 23 we plot the BER of the receiver for different values of ρ , keeping in mind the limitation $0 < \rho \leq 1$, with $E_b/N_o = 15$ dB and $m=1$. It is clear that varying ρ affects the receiver performance significantly, especially when the SIR is small. It can be seen that the worst case PNJ against a receiver that is optimized to oper-

ate in PNJ is achieved when $\rho = 1$. Essentially, this means that the jammer is operational at all times and that the receiver is subjected to barrage jamming instead of pulsed jamming. Therefore, we conclude that a barrage noise jammer (BNJ) is more effective against an optimum receiver than a PNJ. Furthermore, we can see that as ρ approaches zero (i.e., for $\rho = 0$ the jammer is not operating), the receiver performance tends to be constant and approaches the AWGN limit.

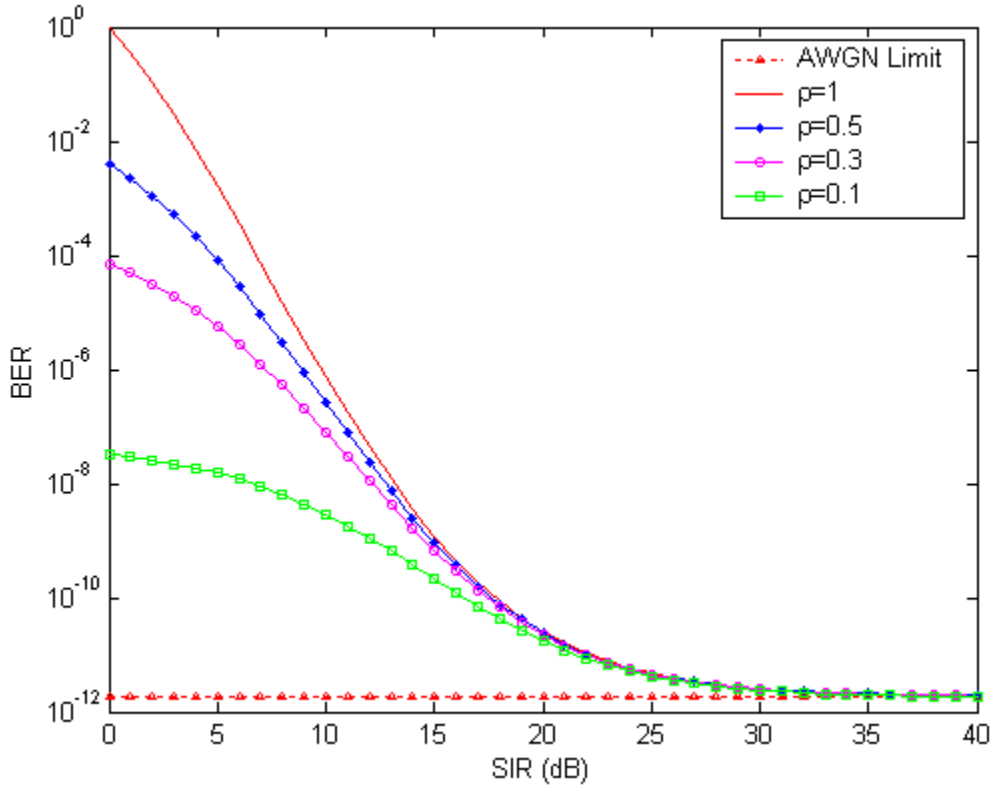


Figure 23. BER performance of 802.11a receiver optimized to operate with PNJ for different values of ρ ($0 < \rho \leq 1$) and for data rates of 6 and 12 Mbps.

This behavior is explained by the fact that the receiver is considered to be optimized to operate with hostile PNJ. In other words, from the receiver perspective, the worst jamming case is when the jamming power has been spread to all received bits. This forces the receiver to make a decision using all received, jammed bits. On the other hand, if the jamming power has been spread to only a number of the received bits, the receiver

is able to make the decision using primarily the nonjammed bits, resulting in better performance. Therefore, the larger the ρ , the poorer the receiver performance.

b. Data Rates of 9 and 18 Mbps

For bit rates of 9 and 18 Mbps, a code rate of $r = 3/4$ is implemented and BPSK and QPSK are used, respectively. Therefore, using the values $k = 1$ and $r = 3/4$ we can numerically determine the BER of the receiver. In Figure 24 the resulting BER is plotted with respect to SIR at the receiver and for different fading conditions. For these calculations, as before $E_b/N_o = 15$ dB and $\rho = 0.5$ are used. Examining Figure 24 we arrive at the same conclusions as before. The receiver performance is improved as fading conditions diminish (i.e., m approaches infinity asymptotically). Moreover, the receiver performance is also dictated by the power of the AWGN.

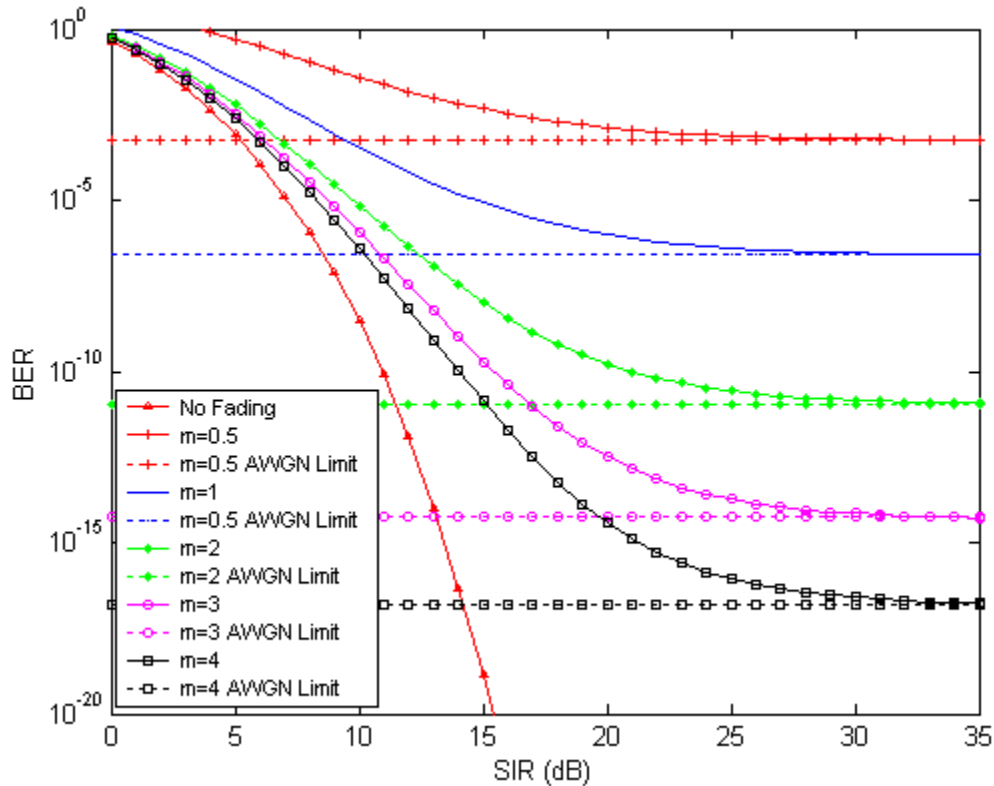


Figure 24. BER performance of 802.11a receiver optimized to operate with PNJ for data rates of 9 and 18 Mbps.

Finally, in Figure 25 we plot the BER of the receiver for different values of ρ , with $E_b/N_o = 15$ dB and $m = 1$. It is clear that the coefficient ρ has the same effect on the receiver performance as in the lower data rate case (6 or 12 Mbps). The larger the coefficient ρ , the poorer the receiver performance. So when the receiver is transferring data at a rate of 9 or 18 Mbps, a BNJ again is more effective. Also, for the limiting case $\rho \rightarrow 0$, the receiver performance tends to be constant and approaches the AWGN limit.

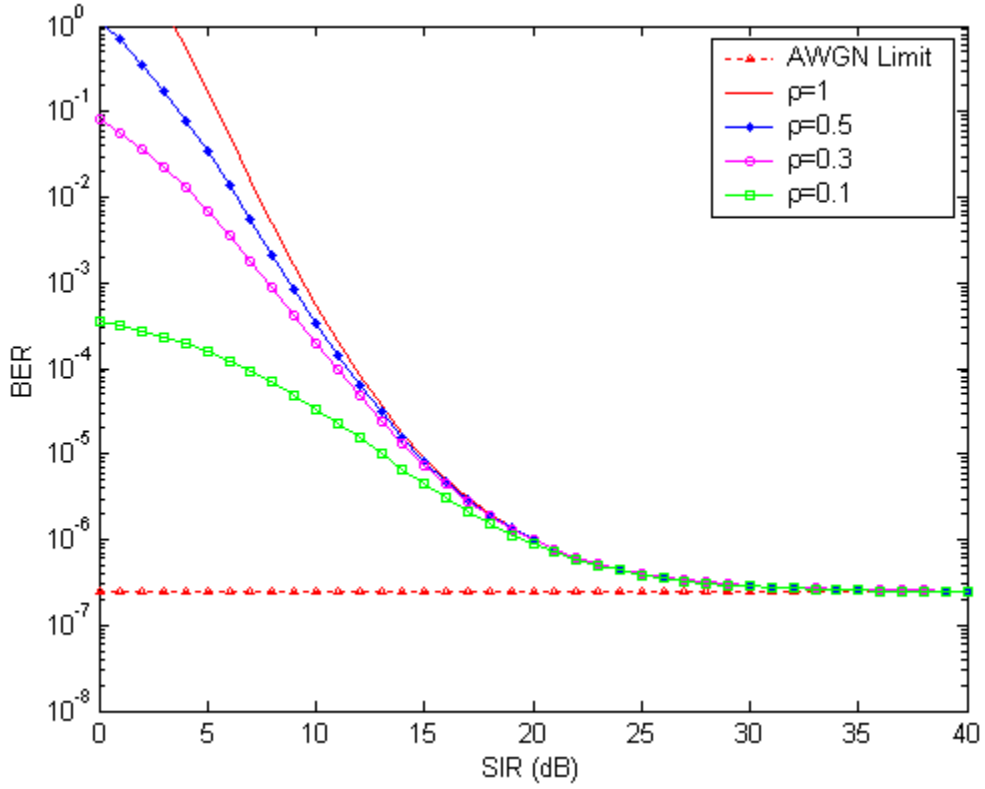


Figure 25. BER performance of 802.11a receiver, optimized to operate with PNJ for different values of ρ ($0 < \rho \leq 1$) and for data rates of 9 and 18 Mbps.

2. Non-Binary Modulation

Following the method discussed previously in section III.B.1, the BER of the optimum 802.11a receiver can be obtained when MQAM modulation is used. This method is briefly summarized here for convenience.

As already discussed, an upper bound on BER with FEC is given by Equation (3.63) [4]. In order to estimate the required upper bound, we need first to determine the probability P_d of selecting a weight- d output sequence as the actual code sequence. The evaluation of P_d was also discussed previously and is given by Equation (3.65). In order to evaluate P_d , we need to estimate the average independent probability P_{d_i} of selecting a weight- d output sequence when i bits are jammed, given by Equation (3.66).

In order to evaluate the integral in Equation (3.66), we need $f_{\Gamma_b}(\gamma_b)$ and $P_{d_i}(\gamma_b)$. The PDF $f_{\Gamma_b}(\gamma_b)$ is numerically evaluated by Equation (3.82). Furthermore, when MQAM is used the conditional probability $P_{d_i}(\gamma_b)$ has been analyzed and is repeated here for convenience:

$$P_{d_i}(\gamma_b) = \frac{4}{q} Q\left(\sqrt{\frac{3q}{M-1}} \gamma_b\right), \quad (3.96)$$

where q is the number of information bits per symbol and M is the number of symbols.

Finally, combining Equations (3.63), (3.65), (3.66), (3.82), and (3.96) the BER of 802.11a receiver optimized to operate with PNJ for higher data rates (i.e., when non-binary modulation is used) can be obtained.

a. Data Rate of 24 Mbps

The receiver performance when data are transferred with a rate of 24 Mbps is discussed in this sub-section. For this data rate 16QAM is specified along with $r=1/2$ FEC. Using the values $M=16$, $q=4$, and $r=1/2$, along with the values of d_{free} and B_d specified in Table 2 in the relevant equations, we get the upper bound on BER, plotted in Figure 26 with respect to SIR at the receiver and for different fading conditions. For these calculations, the SNR is assumed to be $E_b/N_o = 15$ dB and the coefficient ρ that defines the fraction of time that the jammer is operational is $1/2$.

As was found for the lower data rate cases, it is clear that the receiver performance significantly improves as the fading conditions improve. As the SIR increases,

the performance improves up to the point where the AWGN power dominates. As a result, for values of $E_b/N_I > 25$ dB the performance of the receiver converges to a limit determined by AWGN.

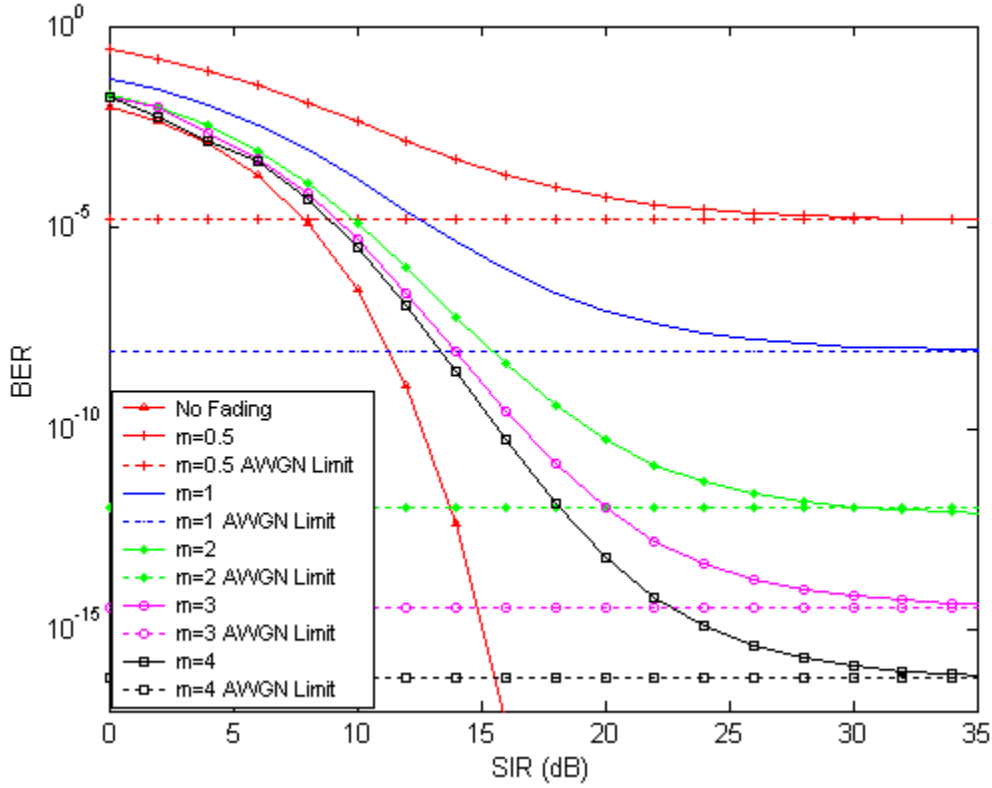


Figure 26. BER performance of 802.11a receiver optimized to operate with PNJ for data rate of 24 Mbps.

Next, in Figure 27 we plot the BER of the receiver for different values of ρ , keeping in mind the limitation $0 < \rho \leq 1$, with $E_b/N_o = 15$ dB and $m = 1$. It is clear that varying ρ affects the receiver performance significantly, especially when the SIR is small. As in the lower data rate cases, we conclude that BNJ is more effective against an optimum receiver than a PNJ. Furthermore, we can see that as ρ approaches zero (i.e., for $\rho = 0$ the jammer is not operating) the receiver performance tends to be constant and approaches the AWGN limit.

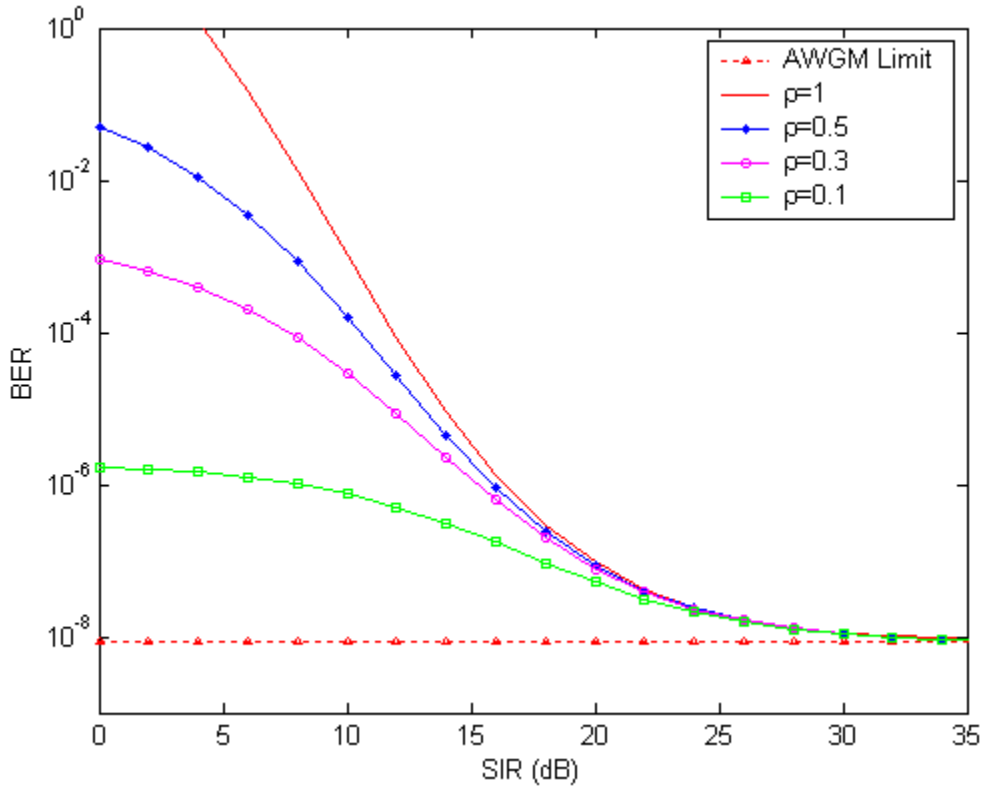


Figure 27. BER performance of 802.11a receiver optimized to operate with PNJ for different values of ρ ($0 < \rho \leq 1$) and for data rate of 24 Mbps.

b. Data Rate of 36 Mbps

Substituting $M = 16$, $q = 4$, and $r = 3/4$ into the relevant equations, we get the upper bound on BER of the optimum receiver for the 36 Mbps data rate. The estimated BER is plotted in Figure 28 with respect to SIR at the receiver and for different fading conditions. For these calculations, $E_b/N_o = 15$ dB and $\rho = 0.5$ was used. Examining Figure 28, we arrive at the same conclusions as before. The receiver performance is improved as fading conditions improve (i.e., m approaches infinity asymptotically). Moreover, the receiver performance is limited by the power of the AWGN (SNR).

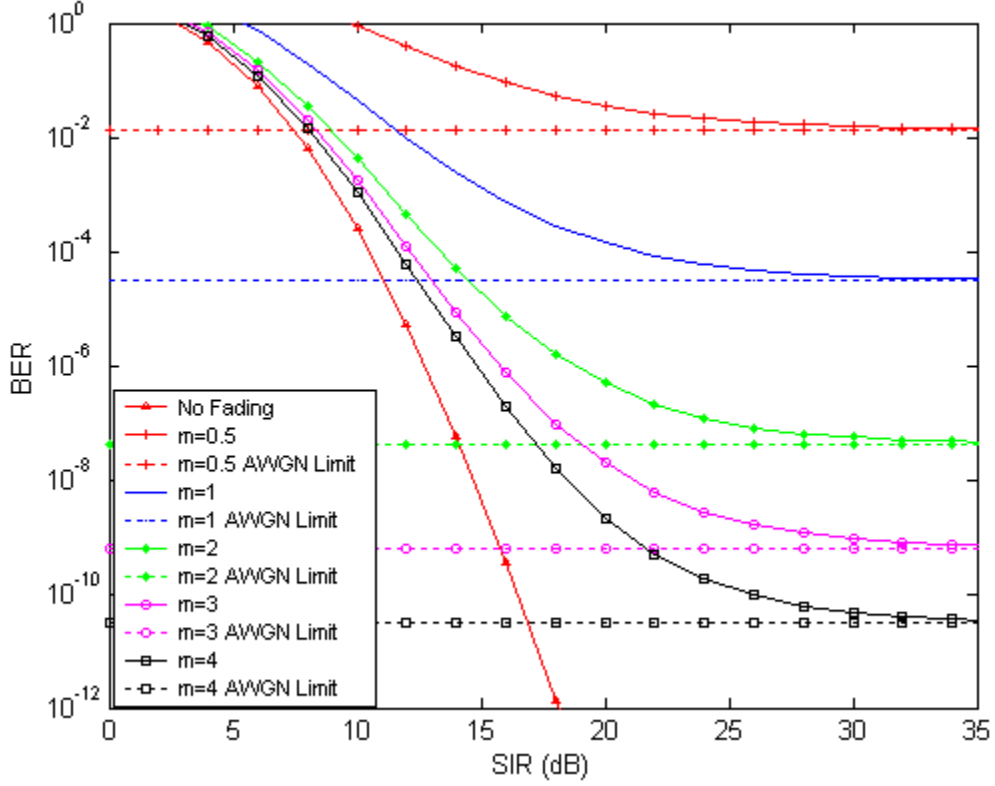


Figure 28. BER performance of 802.11a receiver optimized to operate with PNJ for data rate of 36 Mbps.

In Figure 29 we plot the BER of the receiver for different values of ρ , with $E_b/N_o = 15$ dB and $m = 1$. It is clear that the coefficient ρ has the same effect on the receiver performance as for the lower data rate cases. The larger the coefficient ρ , the poorer the receiver performance. When the receiver is transferring data at a rate of 36 Mbps, a BNJ again is more effective. Also, for the limiting case $\rho \rightarrow 0$, the receiver performance tends to be constant and approaches the AWGN limit.

c. Data Rate of 48 Mbps

For a data rate of 48 Mbps, 64QAM is used with a code rate of $r = 2/3$. Using $M = 64$, $q = 6$, and $r = 2/3$ in the relevant equations, we get the upper bound on BER, plotted in Figure 30 with respect to SIR at the receiver and for different fading

conditions. For these calculations, $E_b/N_o = 15$ dB and $\rho = 0.5$ was used. The same conclusion is derived here for the receiver performance with respect to the fading environment and the effect that the AWGN has on the receiver performance.

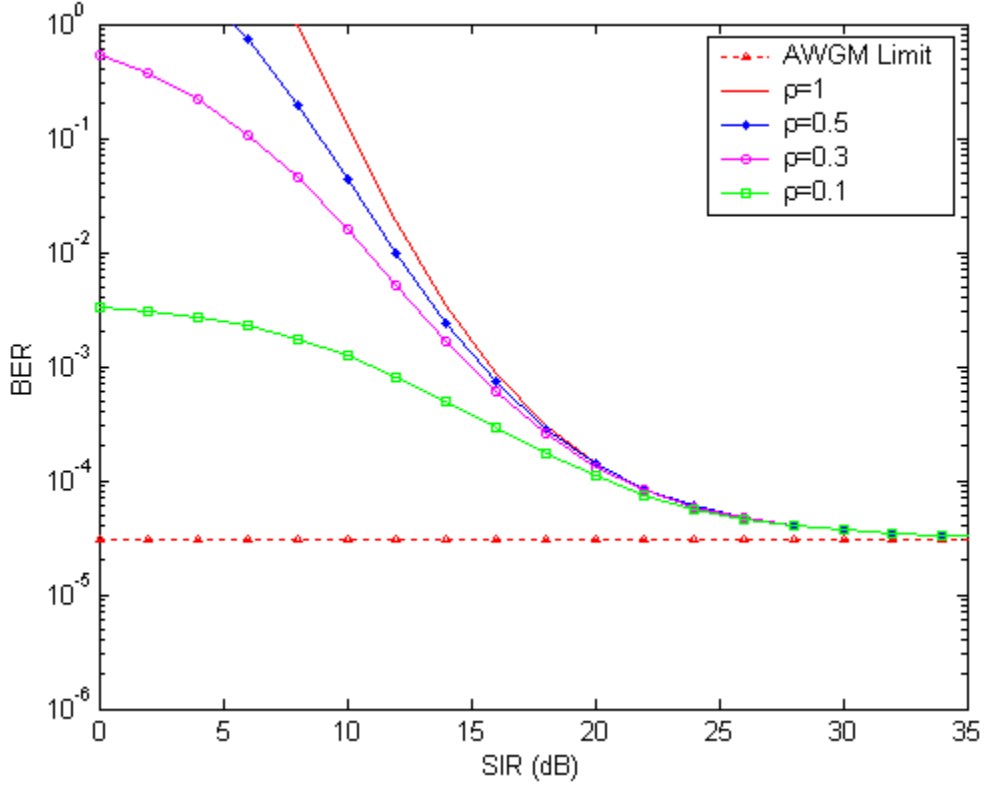


Figure 29. BER performance of 802.11a receiver optimized to operate with PNJ for different values of ρ ($0 < \rho \leq 1$) and for data rate of 36 Mbps.

In Figure 31 we plot the BER of the receiver for different values of ρ , with $E_b/N_o = 15$ dB and $m = 1$. Again, the larger the coefficient ρ , the poorer the receiver performance. Also, for the limiting case $\rho \rightarrow 0$, the receiver performance tends to be constant and approaches the AWGN limit.

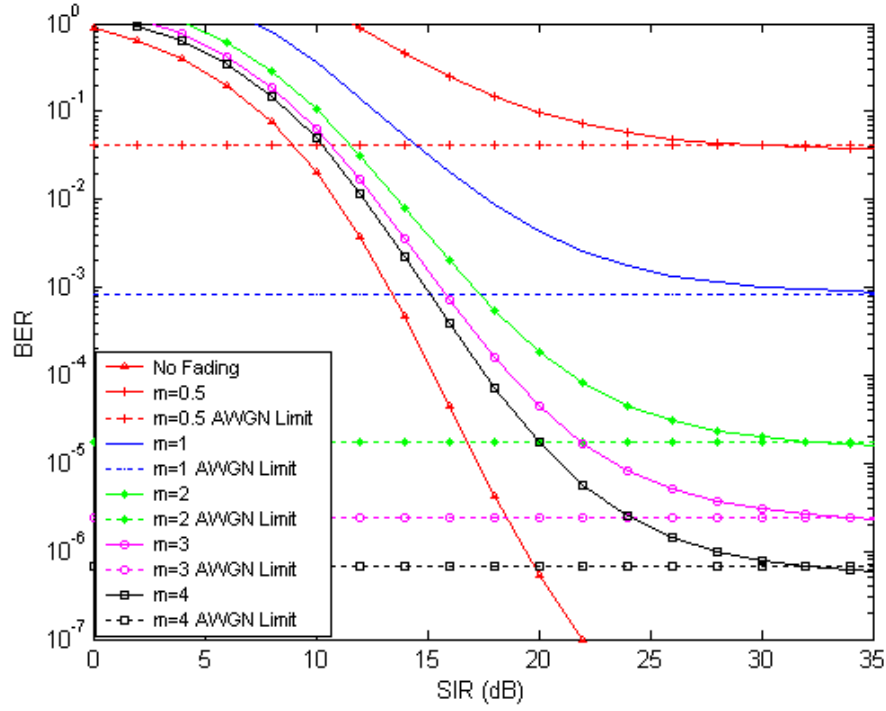


Figure 30. BER performance of 802.11a receiver optimized to operate with PNJ for data rate of 48 Mbps.

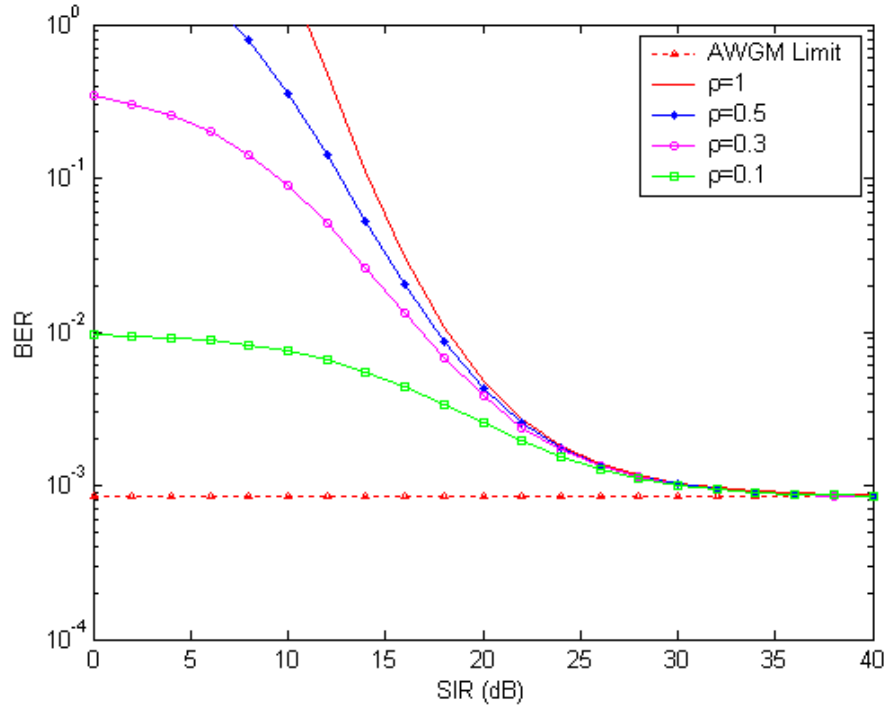


Figure 31. BER performance of 802.11a receiver optimized to operate under PNJ for different values of ρ ($0 < \rho \leq 1$) and for data rate of 48 Mbps.

d. Data Rate of 54 Mbps

Finally, the highest data rate of 54 Mbps is achieved by using 64QAM and a FEC with $r = 3/4$. Using $M = 64$, $q = 6$, and $r = 3/4$ in the relevant equations, we get the upper bound on BER, plotted in Figure 32 with respect to SIR at the receiver and for different fading conditions. For these calculations, $E_b/N_o = 15$ dB and $\rho = 0.5$ was used. The same conclusion as for lower data rates is reached here for the receiver performance with respect to the fading environment and the effect that AWGN has on receiver performance.

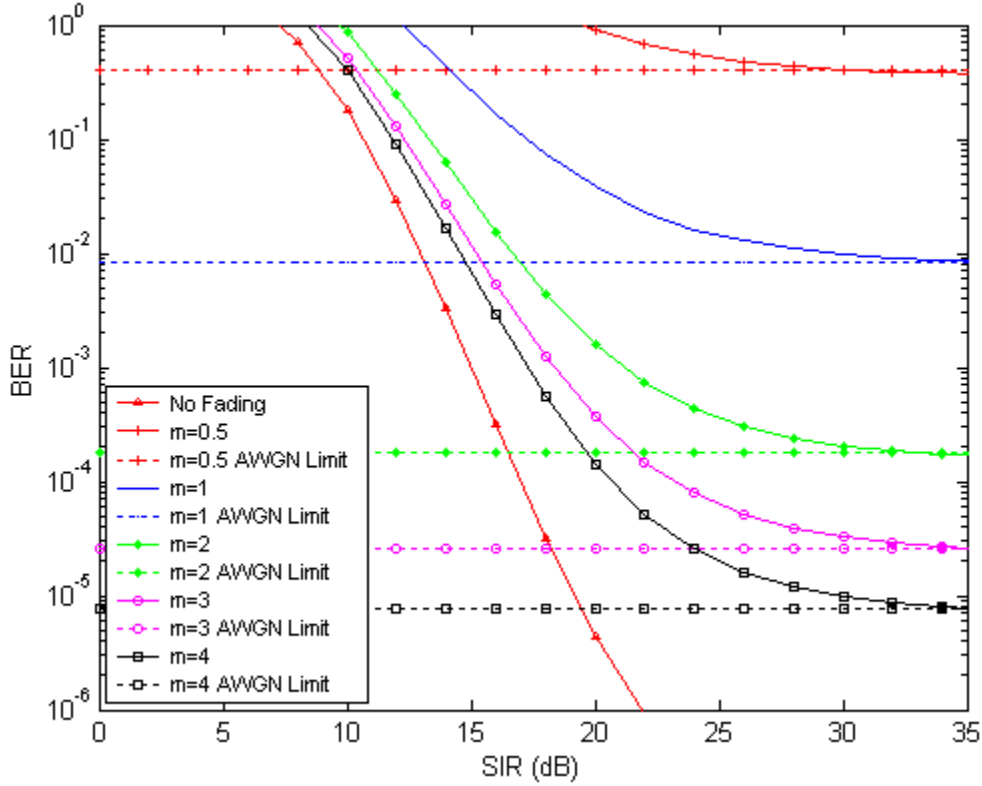


Figure 32. BER performance of 802.11a receiver optimized to operate with PNJ for data rate of 54 Mbps.

Finally, in Figure 33 we plot the BER of the receiver for different values of ρ , with $E_b/N_o = 15$ dB and $m = 1$. Again, the larger the coefficient ρ , the poorer the receiver performance. Also, for the limiting case $\rho \rightarrow 0$, the receiver performance tends to be constant and approaches the AWGN limit.

It is clear that for non-binary modulation with higher code rate FEC, the receiver performance degrades rapidly. This is a trade off between higher data rate and BER. The more information we try to process, the larger to the risk of making an error.

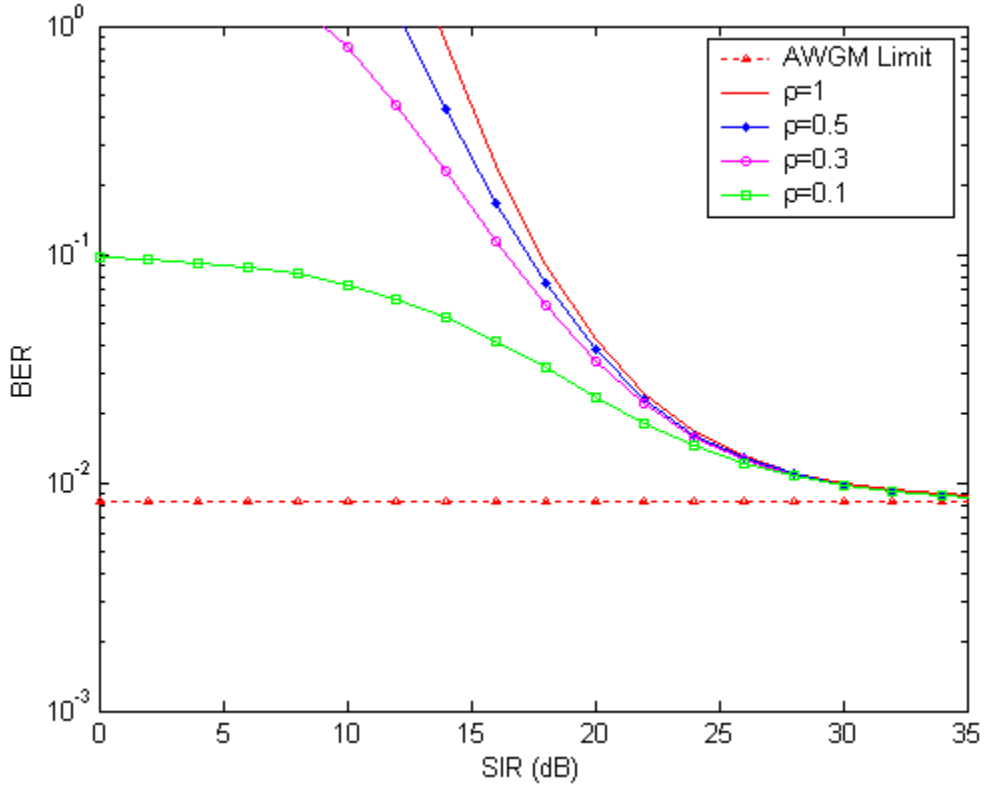


Figure 33. BER performance of 802.11a receiver optimized to operate with PNJ for different values of ρ ($0 < \rho \leq 1$) and for data rate of 54 Mbps.

3. Conclusions on the Effect of PNJ on the 802.11a Optimum Receiver

Summarizing, the overall performance of the optimum receiver was discussed for all specified operational data rates when operating under the effect of PNJ.

It is clear that the receiver performance in the presence of PNJ generally degrades as higher order modulation schemes are used. When binary modulation is used the receiver performance, for a constant $E_b/N_o = 15$ dB, remains acceptable for

$E_b/N_i \geq 10$ dB even when severe fading conditions are present (i.e., for $m = 0.5$ and

$E_b/N_i \geq 10$ dB, $P_b < 10^{-5}$). However, for higher data rates the performance is unaccept-

able, for the same SNR. Therefore, in order to be able to transfer data at an acceptable P_b for rates higher than 36 Mbps when $0.5 \leq m \leq 2$, $E_b/N_o \geq 15$ dB is required. Clearly, there is a trade off between data rate and BER when a receiver operates in the presence of a PNJ. The higher data rate we use, the more BER degrades for a given SNR, SIR and ρ . On the other hand, for non-severe fading conditions (i.e., $m \geq 3$), $E_b/N_o = 15$ dB is adequate since for all data rates since the BER is less than 10^{-5} for $E_b/N_o \geq 10$ dB.

Next, the receiver performance is examined for different types of fading environments. For that reason the receiver BER is plotted for different fading environments and for all specified data rates.

First, in Figure 34 the receiver is assumed to operate in an intense fading environment (i.e., fading figure $m=1$) with $E_b/N_o = 15$ dB while the PNJ is assumed to operate half the time (i.e., $\rho = 0.5$).

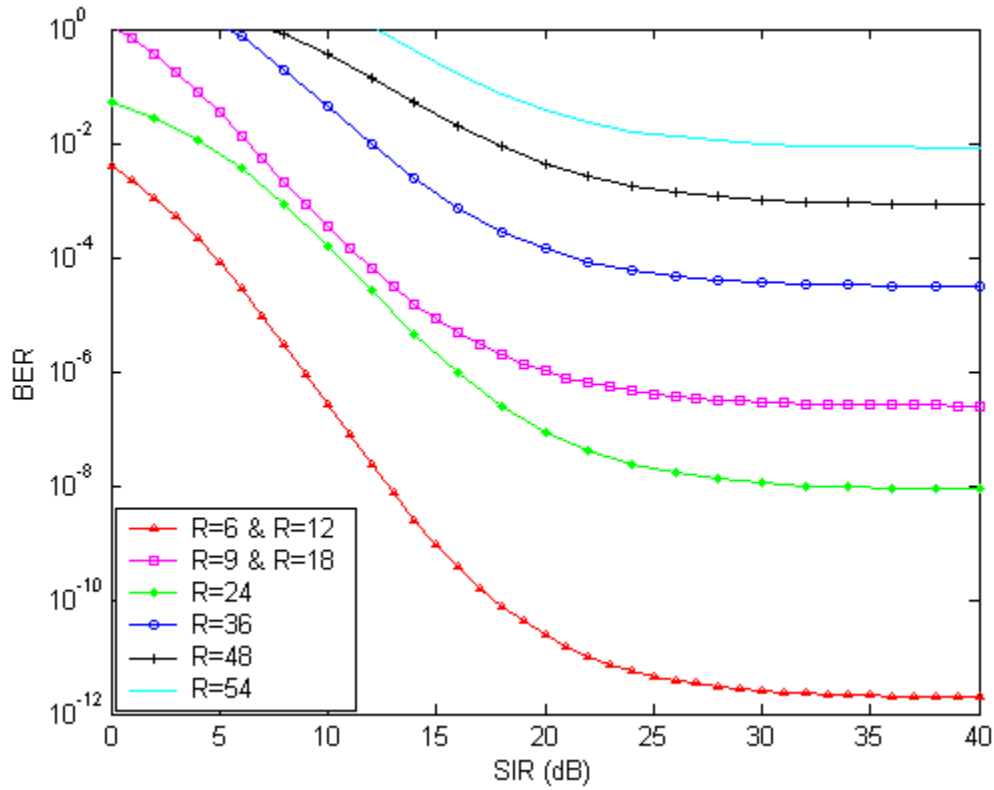


Figure 34. BER performance of the optimum 802.11a receiver for a severe Nakagami fading channel ($m=1$) with PNJ and $\rho=0.5$ for all specified bit rates.

Second, in Figure 35 the performance of the optimum receiver is examined when the fading environment is not severe (i.e., fading figure $m=3$) with $E_b/N_o = 15$ dB while the PNJ is assumed to operate half the time (i.e., $\rho = 0.5$).

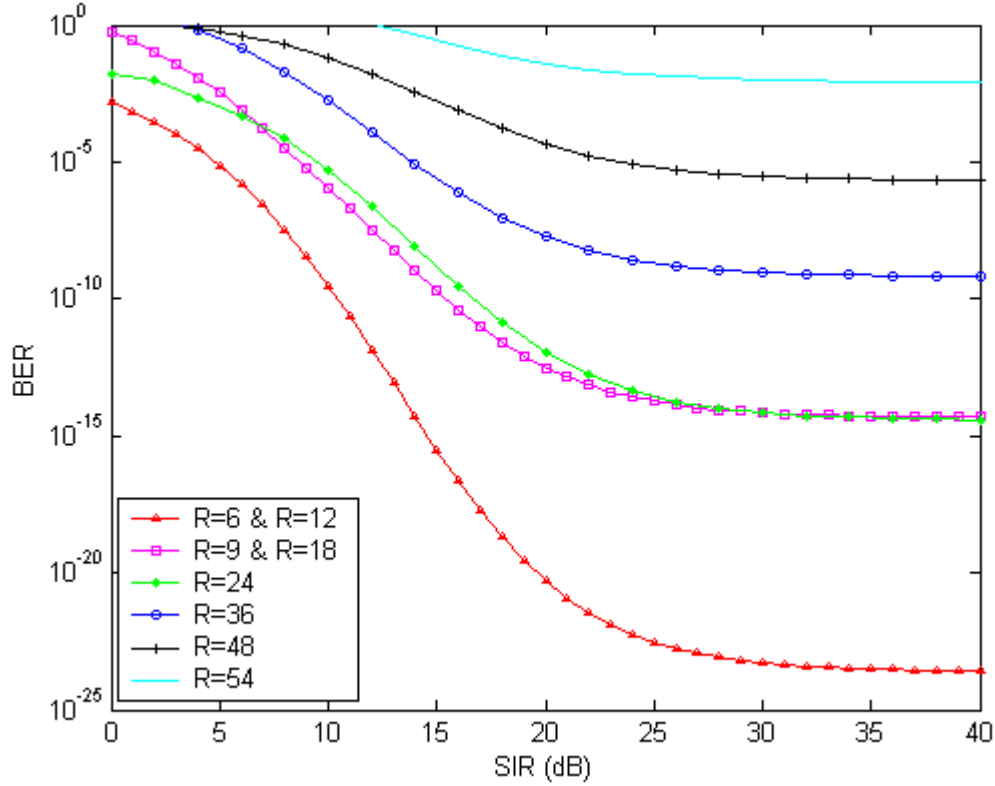


Figure 35. BER performance of the optimum 802.11a receiver for non-severe Nakagami fading channel ($m=3$) with PNJ and for all specified bit rates.

Studying Figures 34 and 35, we arrive at the same conclusions we did for the AWGN case. When severe fading conditions exist, the receiver performance is affected by the code rate used. We can see that for larger signal power, the performance of the receiver for the 24 Mbps case (i.e., 16QAM with $r=1/2$), is better than the 9 and 18 Mbps case (i.e., BPSK with $r=3/4$).

Moreover, in non-severe conditions the code rate also affects the BER. As we can see, the performance of the receiver for 9, 18 and, 24 Mbps are similar even if 16QAM is used in the 24-Mbps case.

Having examined the performance of the theoretical optimum receiver in this Chapter, we continue our analysis in Chapter IV examining a more practical receiver, the sub-optimum receiver. For the sub-optimum receiver no side-information is necessary.

THIS PAGE INTENTIONALLY LEFT BLANK

IV. PERFORMANCE ANALYSIS OF THE IEEE 802.11A SUB-OPTIMUM RECEIVER

In Chapter III, the performance of the *802.11a* optimum receiver was examined, both when operating in an AWGN channel with fading and when PNJ is also present. This type of receiver is ideal since it applies the MLDC, expressed in Equation (3.7), and receiver performance is the best that can be achieved. However, the optimum receiver is theoretical and cannot be realized in real life applications since the perfect side information that is assumed is not available in practice.

This being the case, in Chapter IV a more practical type of receiver is examined. This receiver can be realized in practice since no side information is assumed. The performance this receiver, referred as the sub-optimum receiver, is examined when the signal is transmitted over a Nakagami fading channel. The performance of the receiver, in terms of BER, is analyzed both when operating in an AWGN channel with fading and when PNJ is also present.

A. THE IEEE 802.11A SUB-OPTIMUM RECEIVER

The *IEEE 802.11a* sub-optimum receiver examined in this chapter is designed to operate without the need for side information. In other words, the amplitude of the received signal and the noise power that corrupts every received bit are not known. Instead a liner combination is utilized.

The model of the sub-optimum receiver, when BPSK modulation is used, is presented in Figure 36.

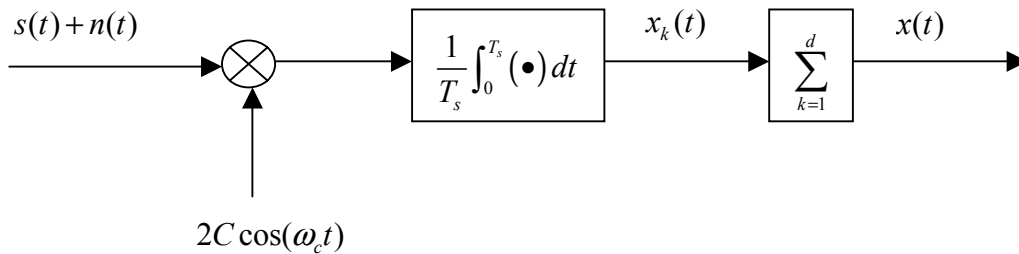


Figure 36. The *IEEE 802.11a* sub-optimum receiver

If we compare the receiver in Figure 36 to the optimum receiver examined in Chapter III, we will see that the two receiver models are analogous. At the input to the receiver, the desired BPSK signal can be represented as $s(t) = \sqrt{2}a_c d(t) \cos(\omega_c t)$, where a_c is the amplitude of the received signal, $d(t)$ is the information waveform, T_s is the time duration of a symbol, and ω_c is the frequency of the sub-carrier signal. Since the signal $s(t)$ representing one of the 48 sub-carriers is assumed to have been transmitted over a flat, slowly-fading Nakagami channel, the amplitude a_c is modeled as a Nakagami- m random variable. At the input of the receiver, the signal $s(t)$ arrives corrupted by the channel noise, denoted as $n(t)$. However, at the local oscillator the corrupted signal $s(t) + n(t)$ is not multiplied by the received amplitude a_c , since it is not considered to be known. Instead, it is multiplied by a quantity C that remains constant for all received bits.

The signal $x_k(t)$ at the integrator output represents those sequence bits that have been affected in a random way by the channel. The signal $x_k(t)$ can be modeled as a GRV. This GRV has a mean

$$\overline{X_k} = \sqrt{2}Ca_c \quad (4.1)$$

and variance

$$\sigma_{x_k}^2 = C^2 \sigma_k^2, \quad (4.2)$$

where $\sigma_{x_k}^2$ is the noise power at the integrator output that has corrupted the signal $s(t)$.

The overall received signal for a sequence of d bits can be expressed as the summation of independent, random signals

$$x(t) = \sum_{k=1}^d x_k(t). \quad (4.3)$$

Since the quantities $x_k(t)$ are modeled as GRVs, the signal $x(t)$ is also a GRV with mean

$$\bar{X} = \sqrt{2}C \sum_{k=1}^d a_c \quad (4.4)$$

and variance

$$\sigma_x^2 = C^2 \sum_{k=1}^d \sigma_k^2. \quad (4.5)$$

For the BPSK receiver, the probability of making an incorrect detection P_b when the decision statistic is modeled as GRV can be expressed as [4]

$$P_b = Q\left(\frac{\bar{X}}{\sigma_x}\right), \quad (4.6)$$

where \bar{X} and σ_x^2 are the mean and variance of the random variable given in Equations (4.4) and (4.5), respectively.

Finally, substituting Equations (4.4) and (4.5) into (4.6), we obtain the probability of making an incorrect detection P_b for the *IEEE 802.11a* sub-optimum receiver as

$$P_b = Q\left(\frac{\sqrt{2}C \sum_{k=1}^d a_c}{\sqrt{C^2 \sum_{k=1}^d \sigma_k^2}}\right) = Q\left(\frac{\sqrt{2} \sum_{k=1}^d a_c}{\sqrt{\sum_{k=1}^d \sigma_k^2}}\right). \quad (4.7)$$

B. PERFORMANCE ANALYSIS IN A FADING CHANNEL WITH AWGN

The performance of the sub-optimum receiver operating in a fading channel with AWGN is examined here for all possible sub-carrier modulations as specified in the *802.11a* WLAN standard. As specified in the *802.11a* WLAN standard, different modulation schemes are used to achieve various bit-rates. For lower data rates, BPSK and QPSK are used, while for higher data rates, 16QAM and 64QAM are specified.

1. BPSK/QPSK Modulation

For data rates of 6, 9, 12, and 18 Mbps, BPSK and QPSK modulations are specified. The performance with QPSK is identical to that obtained for BPSK and will not be obtained separately. The model of the sub-optimum receiver, when BPSK modulation is used, is the one presented in Figure 36.

As discussed previously and repeated here for convenience, the upper bound on the BER with FEC is

$$P_b < \frac{1}{k} \sum_{d=d_{free}}^{d_{free}+4} B_d P_d \quad (4.8)$$

where d_{free} is the free distance of the convolutional code, B_d is the total number of information bit ones on all weight d paths, P_d is the average unconditional probability of selecting a weight- d output sequence as the transmitted code sequence, and k is the number of information bits.

The average probability P_d can be obtained by calculating the integral in Equation (3.29). Before doing so, the conditional probability $P_d(a_c)$ must be evaluated first. As discussed earlier, the conditional probability is equivalent to P_b for the receiver shown in Figure 36. Hence, from Equation (4.7), P_d can be written

$$P_d \left(\sum_{k=1}^d a_c \right) = Q \left(\frac{\sqrt{2} \sum_{k=1}^d a_c}{\sqrt{\sum_{k=1}^d \sigma_k^2}} \right). \quad (4.9)$$

At the input to the receiver shown in Figure 36, the signal $s(t)$ arrives corrupted by the channel AWGN with PSD $N_o/2$. Since the receiver is subjected only to AWGN, we can assume that the signal for each bit is corrupted by the same amount of noise power, $\sigma_k^2 = \sigma_o^2 = N_o/T_s$. Therefore, Equation (4.9) can be rewritten

$$\begin{aligned}
P_d \left(\sum_{k=1}^d a_c \right) &= Q \left(\frac{\sqrt{2} \sum_{k=1}^d a_c}{\sqrt{\sum_{k=1}^d \sigma_o^2}} \right) = Q \left(\frac{\sqrt{2} \sum_{k=1}^d a_c}{\sqrt{d \sigma_o^2}} \right) = Q \left(\frac{\sqrt{2} \sum_{k=1}^d a_c}{\sigma_o \sqrt{d}} \right) \\
&= Q \left(\sqrt{\frac{2}{d}} \sum_{k=1}^d \frac{a_c}{\sigma_o} \right).
\end{aligned} \tag{4.10}$$

For notational purposes, Equation (4.10) can be rewritten

$$P_d(\gamma_b) = Q \left(\sqrt{\frac{2}{d}} \gamma_b \right) \tag{4.11}$$

where

$$\gamma_b = \sum_{k=1}^d \frac{a_c}{\sigma_o} = \sum_{k=1}^d \gamma_{b_k} \tag{4.12}$$

is also a random variable, resulting from the summation of d independent, Nakagami- m random variables γ_{b_k} , and

$$\gamma_{b_k} = \frac{a_c}{\sigma_o}. \tag{4.13}$$

Using Equations (3.29) and (4.11) and following the new notation, we get the integral that must to be evaluated in order to obtain P_d as

$$P_d = \int_0^\infty Q \left(\sqrt{\frac{2}{d}} \gamma_b \right) f_{\Gamma_b}(\gamma_b) d\gamma_b, \tag{4.14}$$

where $f_{\Gamma_b}(\gamma_b)$ is the PDF of the random variable γ_b , defined in Equation (4.12).

Before we evaluate $f_{\Gamma_b}(\gamma_b)$, we need to determine $f_{\Gamma_{b_k}}(\gamma_{b_k})$, the PDF of γ_{b_k} . This PDF is obtained by performing the change of variables

$$f_{\Gamma_{b_k}}(\gamma_{b_k}) = \left| \frac{da_c}{d\gamma_{b_k}} \right| f_{A_c}(a_c) \Big|_{a_c=\gamma_{b_k} \sigma_o} \tag{4.15}$$

where $f_{A_c}(a_c)$ is the Nakagami- m PDF discussed in Chapter II and

$$\frac{da_c}{d\gamma_{b_k}} = \sigma_o. \quad (4.16)$$

Substituting Equations (2.2) and (4.16) into (4.15), we get

$$f_{\Gamma_{b_k}}(\gamma_{b_k}) = \frac{2}{\Gamma(m)} \left(m \overline{\gamma_{b_k}} \right)^m \gamma_{b_k}^{2m-1} e^{-(m \overline{\gamma_{b_k}}) \gamma_{b_k}^2}, \quad \gamma_{b_k} \geq 0 \quad (4.17)$$

where

$$\overline{\gamma_{b_k}} = \frac{1}{r} \left(\frac{E_b}{N_o} \right)^{-1}. \quad (4.18)$$

Having found the PDF of γ_{b_k} , we now find the PDF of γ_b since $\gamma_b = \sum_{k=1}^d \gamma_{b_k}$. As discussed earlier, the sum of d independent random variables is given by the d -fold convolution of the PDFs of the d random variables. Since the evaluation of this PDF cannot be done directly, we determine the LT of $f_{\Gamma_{b_k}}(\gamma_{b_k})$, raise it to the d^{th} power, and finally evaluate the ILT of the result.

The LT of $f_{\Gamma_{b_k}}(\gamma_{b_k})$ [10] is defined by

$$F_{\Gamma_{b_k}}(s) = L\{f_{\Gamma_{b_k}}(\gamma_{b_k})\} = \int_0^\infty f_{\Gamma_{b_k}}(\gamma_{b_k}) e^{-s\gamma_{b_k}} d\gamma_{b_k} \quad (4.19)$$

Substituting (4.17) into (3.45), we get

$$F_{\Gamma_{b_k}}(s) = \frac{2 \left(m \overline{\gamma_{b_k}} \right)^m}{\Gamma(m)} \int_0^\infty \gamma_{b_k}^{2m-1} e^{-[(m \overline{\gamma_{b_k}}) \gamma_{b_k}^2 + s \gamma_{b_k}]} d\gamma_{b_k}. \quad (4.20)$$

Unfortunately, there is not a closed form solution for this integral. Therefore, Equation (3.46) is calculated numerically. The resulting LT of the PDF of the random variable γ_b

is then obtained from $F_{\Gamma_b}(s) = \left(F_{\Gamma_{b_k}}(s) \right)^d$ or

$$F_{\Gamma_b}(s) = \left[\frac{2(m\overline{\gamma_{b_k}})^m}{\Gamma(m)} \int_0^\infty \gamma_{b_k}^{2m-1} e^{-[(m\overline{\gamma_{b_k}})\gamma_{b_k}^2 + s\gamma_{b_k}]} d\gamma_{b_k} \right]^d. \quad (4.21)$$

The PDF $f_{\Gamma_b}(\gamma_b)$ of the random variable γ_b is obtained by computing the ILT of $F_{\Gamma_b}(s)$. The evaluation of $f_{\Gamma_b}(\gamma_b) = L^{-1}\{F_{\Gamma_b}(s)\}$ is done numerically using the method described in the APPENDIX A. From the APPENDIX A, the PDF required is given by the numerical evaluation of

$$f_{\Gamma_b}(\gamma_b) = \frac{c \exp(c\gamma_b)}{\pi} \int_0^{\pi/2} [\operatorname{Re}\{F_{\Gamma_b}(c + jc \tan(\varphi))\} \cos(c\gamma_b \tan(\varphi)) - \operatorname{Im}\{F_{\Gamma_b}(c + jc \tan(\varphi))\} \sin(c\gamma_b \tan(\varphi))] \sec^2(\varphi) d\varphi \quad (4.22)$$

where c must be within the strip of convergence of $F_{\Gamma_b}(s)$.

Now that the PDF $f_{\Gamma_b}(\gamma_b)$ has been obtained, we can determine the unconditional probability P_d by numerically evaluating Equation (4.14).

Finally, combining Equations (4.8) and (4.14), we obtain the performance of the 802.11a sub-optimum receiver operating with AWGN. The method followed to determine the BER of the sub-optimum receiver is analogous to the method used to determine the BER of the optimum receiver. However, the presence of the fading environment affects the two receivers differently, resulting in a different BER for the two receivers.

It can be shown that for a non-fading environment both receivers perform the same. We recall from Chapter III that the BER for the optimum receiver when binary modulation is used is given by Equation (3.25). In Equation (3.25) the unconditional probability P_d of selecting a weight- d output sequence is given by

$$P_d^{opt} = Q\left(\sqrt{2 \sum_{k=1}^d \frac{a_c^2}{\sigma_o^2}}\right). \quad (4.23)$$

In the non-fading case, the amplitude of the received signal is constant, noted as A_c . Therefore, substituting a_c with A_c we get

$$P_d^{opt} = Q\left(\sqrt{2\sum_{k=1}^d \frac{A_c^2}{\sigma_o^2}}\right) = Q\left(\sqrt{2d \frac{A_c^2}{\sigma_o^2}}\right). \quad (4.24)$$

For the sub-optimum receiver, the BER with binary modulation is also given by Equation (4.8) (which is identical to Equation (3.25)). For the sub-optimum receiver scenario, the probability P_d is different and is expressed by

$$P_d^{subopt} = Q\left(\sqrt{\frac{2}{d} \sum_{k=1}^d \frac{a_c}{\sigma_o}}\right). \quad (4.25)$$

In the non-fading case Equation (4.25) can be rewritten as

$$P_d^{subopt} = Q\left(\sqrt{\frac{2}{d} \sum_{k=1}^d \frac{A_c}{\sigma_o}}\right) = Q\left(\sqrt{\frac{2}{d} d \frac{A_c}{\sigma_o}}\right) = Q\left(\sqrt{2d \frac{A_c}{\sigma_o}}\right) \quad (4.26)$$

which is identical to Equation (4.24). Clearly, in the non-fading situation since $P_d^{opt} = P_d^{subopt}$, the resulting BERs are identical. Clearly, as the fading conditions improve, the performance of the sub-optimum receiver approaches the performance of the optimum receiver. Therefore, our analysis is focused on determining the performance of the sub-optimum receiver for severe to moderate fading conditions (i.e., $0.5 \leq m \leq 2$). For those fading conditions, significant differences in the two receivers' performance are expected.

a. Data Rates of 6 and 12 Mbps

For bit rates of 6 and 12 Mbps, a code rate of $r=1/2$ is specified and modulations BPSK and QPSK are used, respectively. Using $k=1$ and $r=1/2$ in the previous analysis and using the values of B_d and d_{free} specified in Table 2, we get the BER upper bound which is plotted in Figure 37 as a function of SNR at the receiver. In order to gain some perspective on the performance of the sub-optimum receiver, the BER per-

formance curves for the optimum receiver obtained in Chapter III for the same fading conditions are also plotted.

From Figure 37, it is clear that the sub-optimum receiver performance is poorer than the optimum receiver, especially when the fading environment is severe. For severe fading conditions ($m = 0.5$) with AWGN and in order to maintain $P_b \leq 10^{-5}$, the sub-optimum receiver requires about 2 dB more signal power. However, as the fading conditions improve and for AWGN, the performance of the sub-optimum receiver improves with respect to the performance of the optimum receiver. Particularly, in moderate fading conditions ($m = 2$), in order to maintain the same level of BER, about 0.5 dB more signal power is required. Therefore, the assumption made previously that when m approaches infinity (i.e., non-fading environment) both receivers perform the same is seen to be confirmed. The same phenomenon is observed for the remaining data rates.

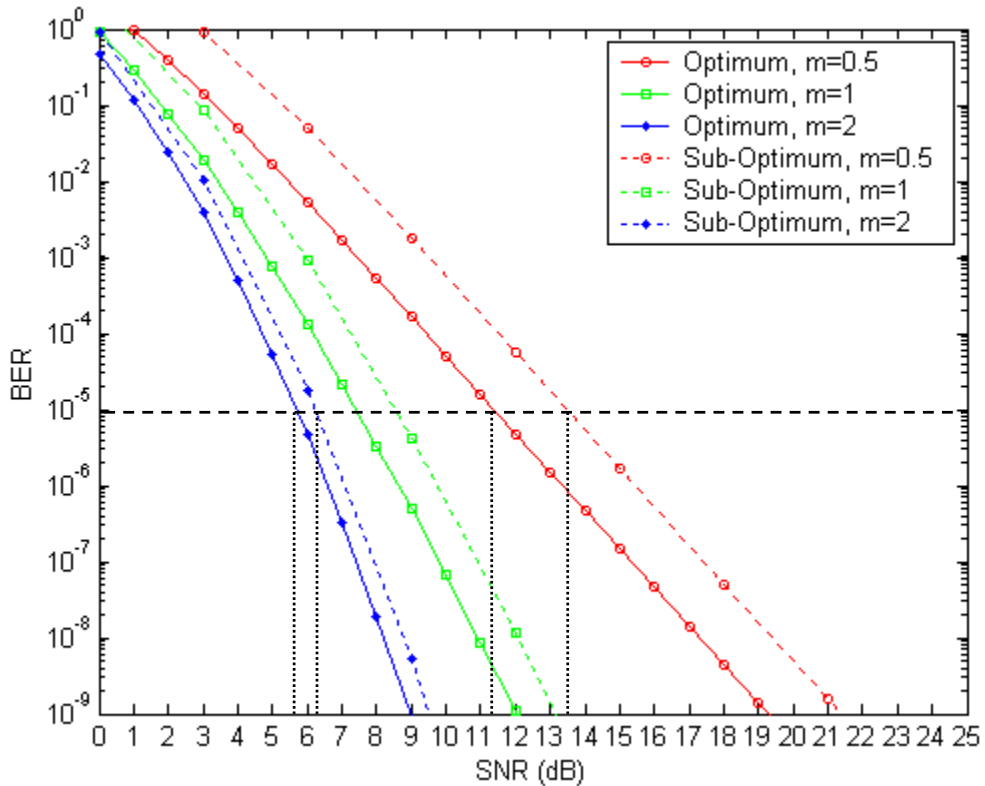


Figure 37. Sub-optimum *IEEE 802.11a* receiver performance for a Nakagami fading channel with AWGN for bit rates of 6 and 12 Mbps.

b. Data Rates of 9 and 18 Mbps

For data rates of 9 and 18 Mbps, a code-rate of $r = 3/4$ is utilized and BPSK and QPSK modulations are used, respectively. Following the previous analysis and using $k = 3$ and $r = 3/4$, we compute the BER, which is plotted in Figure 38. From Figure 38, we can see that the sub-optimum receiver performance follows the same pattern as in the previous case. Summarizing, the sub-optimum receiver performance is poorer than that of the optimum receiver and as the fading conditions improve, the sub-optimum receiver performance also improves with respect to the optimum receiver. It is also important to note that as in the 6-Mbps and 12-Mbps data rates case, the additional signal power required to achieve $P_b = 10^{-5}$ is the same for the 9-Mbps and 18-Mbps data rates case, regardless of the code rate used.

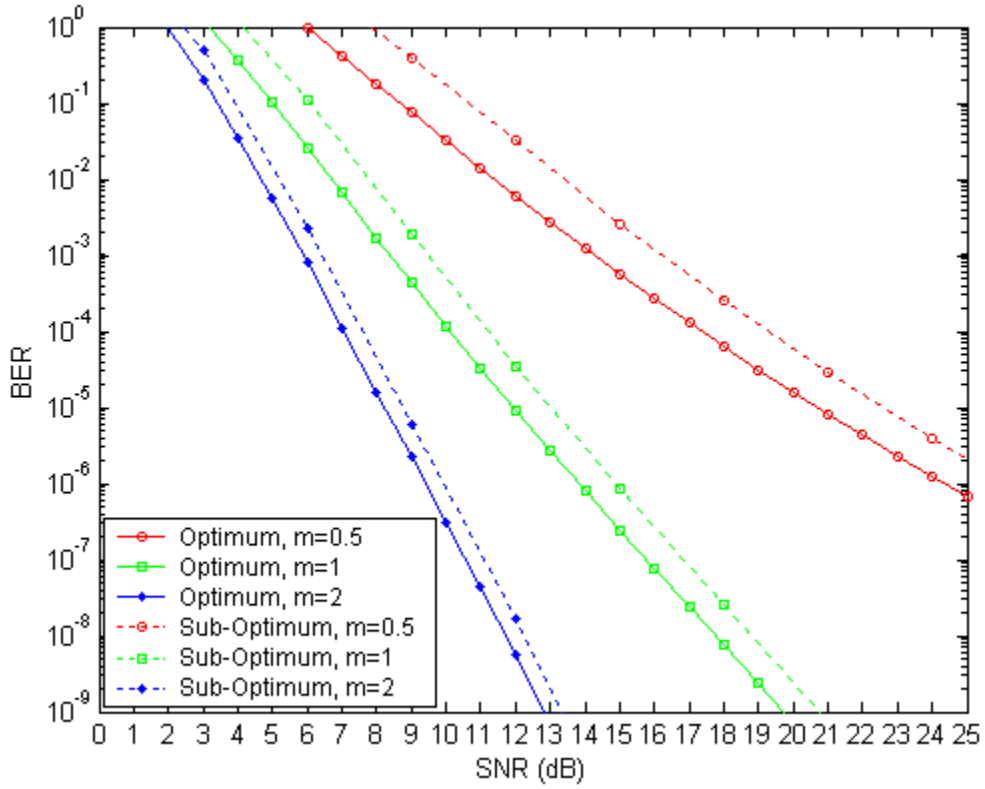


Figure 38. Sub-optimum *IEEE 802.11a* receiver performance for a Nakagami fading channel with AWGN for bit rates of 6 and 12 Mbps.

2. Non-Binary Modulation

As previously discussed, higher bit rates require non-binary modulation, specifically 16QAM and 64QAM. The BER of the sub-optimum receiver when non-binary modulation is used can also be upper bounded with Equation (4.8). As in the binary case, the probability P_d is obtained by calculating the integral

$$P_d = \int_0^\infty P_d(\gamma_b) f_{\gamma_b}(\gamma_b) d\gamma_b \quad (4.27)$$

where, as noted previously, $f_{\gamma_b}(\gamma_b)$ is the PDF of the random variable γ_b defined in Equation (4.12), and $P_d(\gamma_b)$ is the conditional probability of selecting a weight- d output sequence.

The PDF $f_{\gamma_b}(\gamma_b)$ is calculated numerically as discussed previously for the binary case via Equations (4.21) and (3.82). However, the conditional probability $P_d(\gamma_b)$ can no longer be obtained using Equation (4.11). When MQAM modulation is used, following the same methodology we used in section IV.B.2 and keeping in mind the assumption made previously in Chapter II (that the information bits keep the “soft” information that the demodulated symbol that represented the bits had), we see that the conditional probability of selecting a weight- d output sequence $P_d(\gamma_b)$ is given by

$$P_d(\gamma_b) = \frac{4}{q} Q\left(\sqrt{\frac{3q}{d(M-1)}} \gamma_b\right) \quad (4.28)$$

where q is the number of information bits per symbol and M is the number of symbols.

Substituting Equation (4.28) into (4.27), we get

$$P_d = \frac{4}{q} \int_0^\infty Q\left(\sqrt{\frac{3q}{d(M-1)}} \gamma_b\right) f_{\gamma_b}(\gamma_b) d\gamma_b. \quad (4.29)$$

Finally, substituting the estimated probability P_d into Equation (4.8), we get the BER of the sub-optimum receiver when non-binary modulation is used.

a. Data Rate of 24 Mbps

The lowest data rate that is achieved using non-binary modulation is 24 Mbps. For this data rate, 16QAM is used along with $r = 1/2$ FEC. Using $M = 16$, $q = 4$, and $r = 1/2$, along with the values of d_{free} and B_d specified in Table 2, we get the upper bound on BER, plotted in Figure 39 with respect to SNR at the receiver for severe and moderate fading conditions. In general, the two receivers performance follows the same pattern as in the binary modulation cases. For severe fading conditions ($m = 0.5$) and for AWGN, the performances relative difference is notable (on the order of 2 dB in order to maintain $P_b = 10^{-5}$). However, this difference gets smaller as $m \rightarrow \infty$. Particularly, for $m = 2$ and in order to maintain $P_b = 10^{-5}$, 0.5 dB more signal power is required. It is important to note that additional signal power required for the various fading conditions in the 24-Mbps case is the same as that obtained for binary and quaternary modulation (6, 9, 12, and 18 Mbps), regardless of the modulation and code rate used.

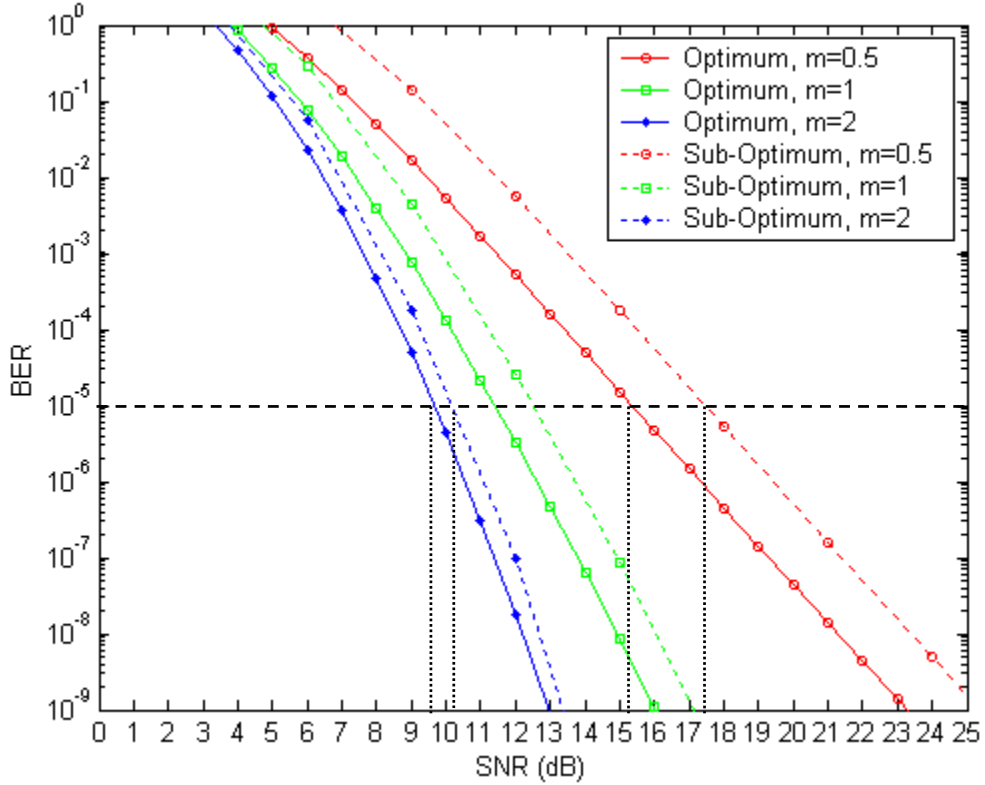


Figure 39. Sub-optimum *IEEE 802.11a* receiver performance for a Nakagami fading channel with AWGN for bit rate of 24 Mbps.

b. Data Rate of 36 Mbps

For a data rate of 36 Mbps, 16QAM is also used but with a higher code rate of $r=3/4$. Using $M=16$, $q=4$, and $r=3/4$, we get the upper bound on BER, plotted in Figure 40 with respect to SNR at the receiver. As in the binary cases and in the 24-Mbps case, the sub-optimum receiver performance is generally worse than the optimum receiver performance. Additionally, the sub-optimum receiver performance approaches the optimum receiver performance as fading conditions improve when AWGN is present.

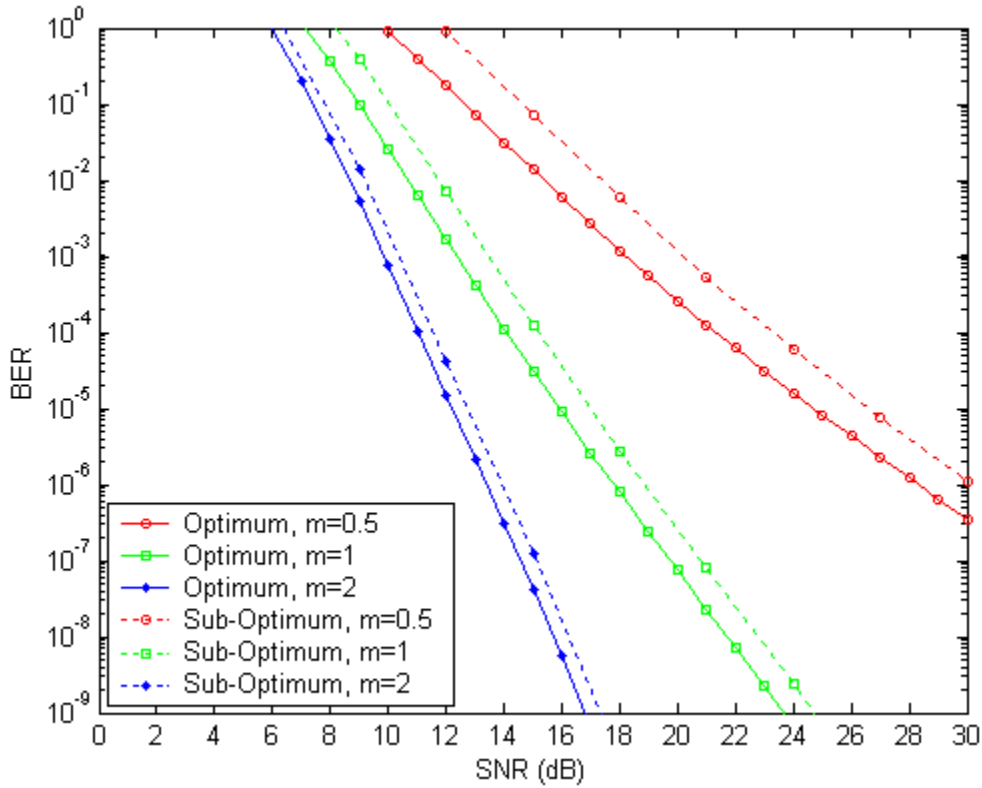


Figure 40. Sub-optimum *IEEE 802.11a* receiver performance for a Nakagami fading channel with AWGN for bit rate of 36 Mbps.

c. Data Rate of 48 Mbps

For a data rate of 48 Mbps, 64QAM is used with a code rate of $r=2/3$. Using $M=64$, $q=6$, and $r=2/3$, we get the upper bound on BER, plotted in Figure 41

with respect to SNR at the receiver. Similar conclusions as for the previous data rates are found for the 48-Mbps case. The performance pattern remains unaffected by the modulation scheme and code rate used.

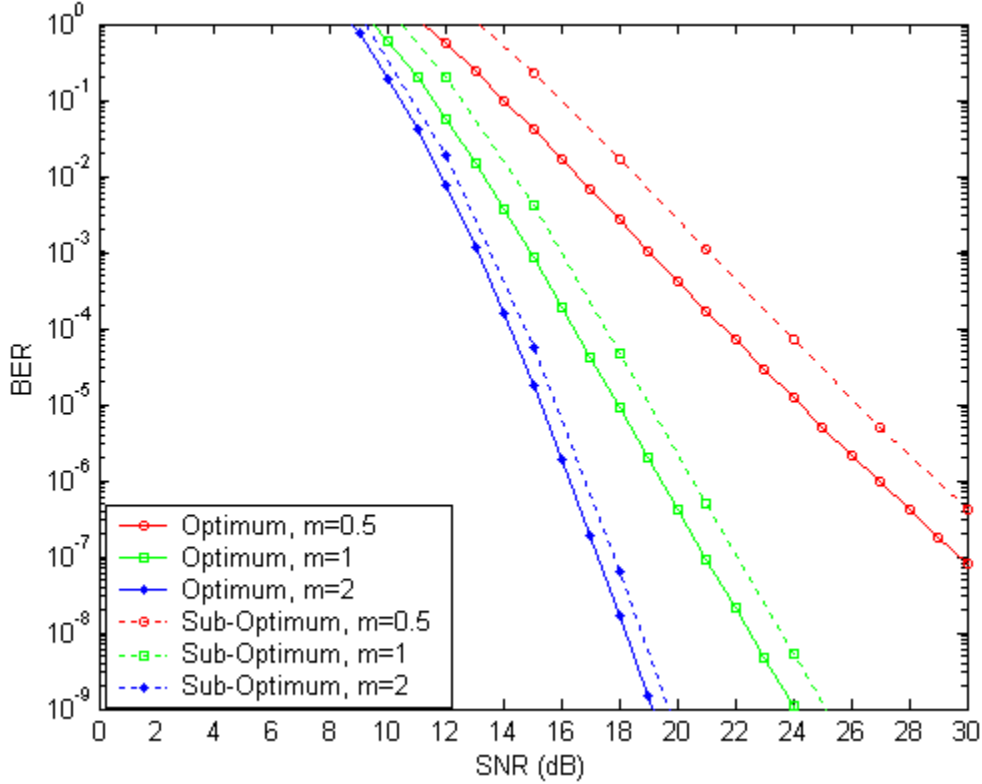


Figure 41. Sub-optimum *IEEE 802.11a* receiver performance for a Nakagami fading channel with AWGN for bit rate of 48 Mbps.

d. Data Rate of 54 Mbps

Finally, the highest data rate of 54 Mbps is achieved by using 64QAM and a FEC with $r = 3/4$. Using $M = 64$, $q = 6$, and $r = 3/4$, along with the values of d_{free} and B_d specified in Table 2, we get the upper bound on BER plotted in Figure 42 with respect to SNR at the receiver. As in all previous cases, it is seen that even when the receiver is operating at the highest data rate where the receiver has the worst performance, the sub-optimum receiver performance is not significantly poorer than the optimum receiver when the fading conditions are not severe. Actually, the difference between the

performances of the two receivers studied remains the same regardless the code rate or the modulation scheme used.

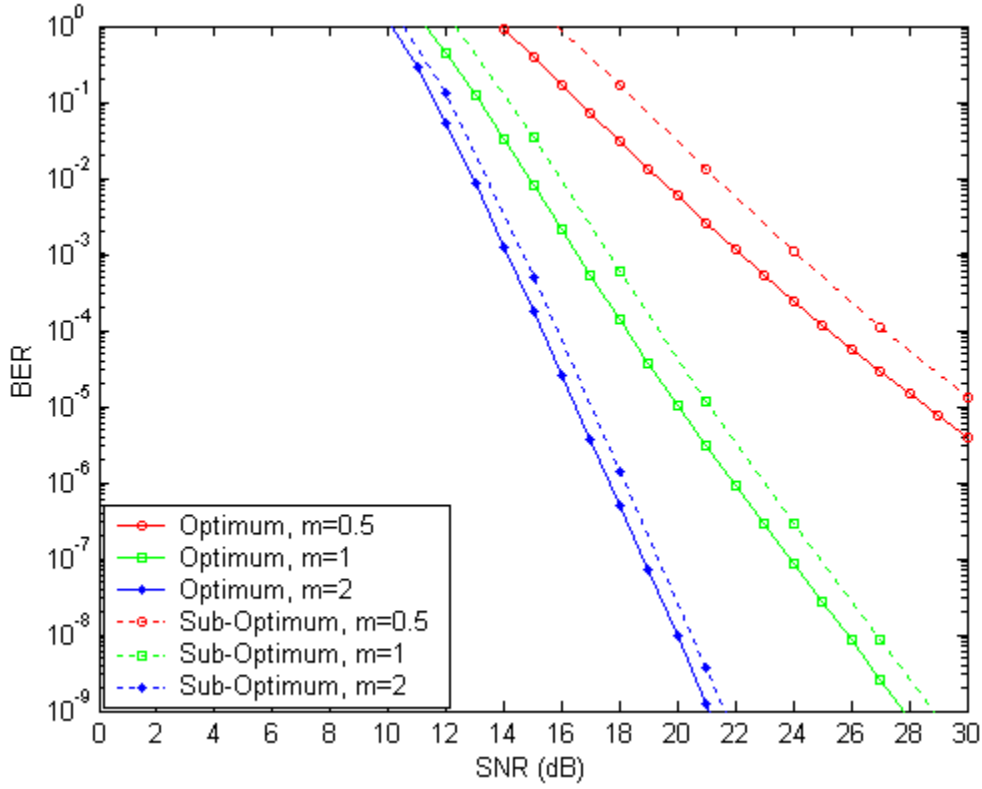


Figure 42. Sub-optimum *IEEE 802.11a* receiver performance for a Nakagami fading channel with AWGN for bit rate of 54 Mbps.

3. Conclusions on the Effect of AWGN on the 802.11a Sub-Optimum Receiver

Summarizing, the overall performance of the sub-optimum receiver was discussed for all specified operational data rates when operating with AWGN.

In general, the optimum receiver outperforms the sub-optimum receiver as expected. However, when only AWGN is present, that difference is not so significant. When operating in severe fading conditions and for AWGN, the sub-optimum receiver performance is the worst (the additional signal power required to maintain $P_b = 10^{-5}$ is on the order of 2 dB). Additionally, the performance of these two receivers tends to con-

verge as the fading conditions improve (i.e., m gets larger). In the limiting case as $m \rightarrow \infty$, it was proven that the two receivers have the same BER.

It is important to note that the relative difference between the performances of the two receivers in any given fading environment is not affected by the modulation scheme used or the code rate implemented. For severe fading conditions (i.e., $m = 0.5$) 2 dB more power is required to maintain $P_b = 10^{-5}$ for all data rates specified, regardless, the modulation and code rate used. In a more moderate fading environment (i.e., $m = 2$) a constant 0.5 dB more signal power is required to maintain BER at the same level for all specified operational data rates.

Finally, since the BER of the sub-optimum receiver follows a pattern similar to the optimum receiver BER regardless of the modulation or the code rate used, the conclusions drawn for the optimum receiver with AWGN made in section III.B.3 apply to the sub-optimum detector. Summarizing, the fading environment affects the receiver less when lower code rates are used. Additionally, for severe fading conditions, the sub-optimum receiver performance is mainly affected by the code rate used, while in less intense fading conditions, the receiver performance is mainly affected by the modulation utilized.

C. PERFORMANCE ANALYSIS WITH A HOSTILE PULSED NOISE JAMMER

After studying the performance of the sub-optimum receiver for fading channels with AWGN, the performance of the sub-optimum receiver affected by AWGN and PNJ is examined.

1. BPSK/QPSK Modulation

Initially, the performance of the sub-optimum receiver with either BPSK or QPSK is examined. The analysis following is analogous to the analysis made for the optimum receiver in section III.C.1, and it is done only for BPSK modulation since the receiver performance with QPSK is identical to the one obtained for BPSK.

As mentioned earlier, in the presence of a PNJ the noise power at the integrator output is not uniform for each received bit and is expressed as

$$\sigma_{x_k}^2 = \begin{cases} \sigma_{x_j}^2 = \sigma_j^2 + \sigma_o^2 = \frac{N_I/\rho + N_o}{T_s} & \text{when PNJ is operational,} \\ \sigma_{x_o}^2 = \sigma_o^2 = \frac{N_o}{T_s} & \text{otherwise.} \end{cases} \quad (4.30)$$

where $\sigma_{x_j}^2$ is the noise power of a jammed bit, $\sigma_{x_o}^2$ is the noise power of a non-jammed bit, σ_o^2 is the AWGN noise power, σ_j^2 is the jamming noise power, N_o and N_I are the noise PSDs of the AWGN and the jamming signal, respectively, and ρ is the fraction of time that the PNJ is operational.

The BER of the sub-optimum receiver is obtained from Equation (4.8) where the average probability P_d can be obtained from Equation (3.65), repeated here for convenience

$$P_d = \sum_{i=0}^d \binom{d}{i} \rho^i (1-\rho)^{d-i} P_{d_i} \quad (4.31)$$

where P_{d_i} is the average probability of selecting a weight- d output sequence when i bits are jammed, while the remaining $(d-i)$ bits are affected only by AWGN. The quantity ρ denotes the fraction of time that the PNJ is operational and is, therefore, the probability that a bit will be jammed.

The unconditional probability P_{d_i} is obtained as before by averaging for all values of the Nakagami- m random variable a_c

$$P_{d_i} = \int_0^\infty P_{d_i}(a_c) f_{\Gamma_b}(a_c) da_c \quad (4.32)$$

where $P_{d_i}(\gamma_b)$ is the conditional probability of selecting a weight- d output sequence when only i bits are jammed. Following an analysis analogous to the AWGN case and keeping in mind that the noise power is no longer uniform, we obtain the probability $P_{d_i}(\gamma_b)$ from

$$P_d \left(\sum_{k=1}^d a_c \right) = Q \left(\frac{\sqrt{2} \sum_{k=1}^d a_c}{\sqrt{\sum_{k=1}^d \sigma_{x_k}^2}} \right). \quad (4.33)$$

Substituting Equation (4.30) into (4.33), we get

$$P_{d_i} \left(\sum_{k=1}^d a_c \right) = Q \left(\frac{\sqrt{2} \sum_{k=1}^d a_c}{\sqrt{\sum_{k=1}^i \sigma_{x_k}^2 + \sum_{k=1}^{d-i} \sigma_{x_o}^2}} \right) = Q \left(\frac{\sqrt{2} \sum_{k=1}^d a_c}{\sqrt{i \sigma_j^2 + (d-i) \sigma_o^2}} \right). \quad (4.34)$$

Factoring out the quantity σ_j^2 , we write

$$\begin{aligned} P_{d_i} \left(\sum_{k=1}^d a_c \right) &= Q \left(\frac{\sqrt{2} \sum_{k=1}^d a_c}{\sigma_j \sqrt{i + (d-i) \frac{\sigma_o^2}{\sigma_j^2}}} \right) = Q \left(\frac{\sqrt{2} \sum_{k=1}^d a_c}{\sqrt{i + (d-i) \frac{\sigma_o^2}{\sigma_j^2}}} \right) \\ &= Q \left(\frac{\sqrt{2} \sum_{k=1}^d a_c}{\sqrt{i + (d-i) \frac{\sigma_o^2}{\sigma_j^2}}} \gamma_b \right) \end{aligned} \quad (4.35)$$

where

$$\gamma_b = \sum_{k=1}^d \frac{a_c}{\sigma_j} = \sum_{k=1}^d \gamma_{b_k} \quad (4.36)$$

is also a random variable resulting from the summation of d independent Nakagami- m random variables γ_{b_k} and

$$\gamma_{b_k} = \frac{a_c}{\sigma_j}. \quad (4.37)$$

Moreover, the ratio of the noise powers in the Equation (4.35) denominator can be rewritten using Equation (4.30) as

$$\begin{aligned} \frac{\sigma_o^2}{\sigma_j^2} &= R \left(\frac{E_b}{N_o}, \frac{E_b}{N_I} \right) = \frac{\frac{N_I + N_o}{\rho}}{\frac{T_s}{N_o}} = \frac{N_I + N_o}{\rho N_o} = \frac{N_I + N_o}{N_o} \frac{a_c^2}{a_c^2} \\ &= \frac{\left(\frac{E_b}{N_o} \right)^{-1}}{\left(\frac{E_b}{N_o} \right)^{-1} + \frac{1}{\rho} \left(\frac{E_b}{N_I} \right)^{-1}}. \end{aligned} \quad (4.38)$$

So, Equation (4.35) can be written

$$P_{d_i}(\gamma_b) = Q \left(\sqrt{\frac{2}{i + (d-i)R \left(\frac{E_b}{N_o}, \frac{E_b}{N_I} \right)}} \gamma_b \right) \quad (4.39)$$

Combining Equations (4.32) and (4.39), we get the integral

$$P_{d_i} = \int_0^\infty Q \left(\sqrt{\frac{2}{i + (d-i)R \left(\frac{E_b}{N_o}, \frac{E_b}{N_I} \right)}} \gamma_b \right) f_{\Gamma_b}(\gamma_b) d\gamma_b, \quad (4.40)$$

where $f_{\Gamma_b}(\gamma_b)$ is the PDF of the random variable γ_b .

Performing the change of variables

$$f_{\Gamma_{b_k}}(\gamma_{b_k}) = \left| \frac{da_c}{d\gamma_{b_k}} \right| f_{A_c}(a_c) \Big|_{a_c = \gamma_{b_k} \sigma_j} \quad (4.41)$$

where $f_{A_c}(a_c)$ is the Nakagami- m PDF discussed in Chapter II and

$$\frac{da_c}{d\gamma_{b_k}} = \sigma_j \quad (4.42)$$

we obtain $f_{\Gamma_{b_k}}(\gamma_{b_k})$, the PDF of the random variable γ_{b_k}

$$f_{\Gamma_{b_k}}(\gamma_{b_k}) = \frac{2}{\Gamma(m)} \left(m \overline{\gamma_{b_j}} \right)^m \gamma_{b_k}^{2m-1} e^{-\left(m \overline{\gamma_{b_j}} \right) \gamma_{b_k}^2}, \quad \gamma_{b_k} \geq 0 \quad (4.43)$$

where

$$\overline{\gamma_{b_j}} = \frac{1}{r} \left[\left(\frac{E_b}{N_o} \right)^{-1} + \frac{1}{\rho} \left(\frac{E_b}{N_I} \right)^{-1} \right]. \quad (4.44)$$

Having found the PDF of γ_{b_k} , we can now find the PDF of γ_b since $\gamma_b = \sum_{k=1}^d \gamma_{b_k}$.

The evaluation of $f_{\Gamma_b}(\gamma_b)$ is accomplished by the same method described for the AWGN case. The LT of $F_{\Gamma_b}(s)$ is obtained using Equation (4.21), replacing $\overline{\gamma_{b_k}}$ by $\overline{\gamma_{b_j}}$ given in Equation (4.44). Next, the ILT of $F_{\Gamma_b}(s)$ is calculated numerically with Equation (4.22).

Finally, combining Equations (4.8), (4.31), (4.40) and inserting the numerically obtained PDF $f_{\Gamma_b}(\gamma_b)$, we get the performance of the *802.11a* sub-optimum receiver operating with PNJ when BPSK/QPSK modulation is used.

The special case for no fading conditions is examined next for both receivers. As we recall from Chapter III, the BER of the optimum receiver when binary modulation is used is given by Equations (3.63), (3.65), and (3.66), where $P_{d_i}(a_c)$ is the conditional probability of selecting a weight- d output sequence when i bits are jammed while the remaining $(d-i)$ bits are affected only by AWGN and is given by

$$P_{d_i}^{opt}(a_c) = Q \left(\sqrt{2 \left(\sum_{k=1}^i \frac{a_c^2}{\sigma_{x_j}^2} + \sum_{k=1}^{d-i} \frac{a_c^2}{\sigma_{x_o}^2} \right)} \right). \quad (4.45)$$

In the non-fading case, the amplitude of the received signal is constant, noted as A_c . Therefore, substituting a_c with A_c , we see that the probability $P_{d_i}^{opt}$ is unconditional and the BER of the optimum receiver is obtained from Equations (3.63) and (3.65). The unconditional probability $P_{d_i}^{opt}$ for the non-fading scenario is given by

$$P_{d_i}^{opt} = Q \left(\sqrt{2 \left(\sum_{k=1}^i \frac{A_c^2}{\sigma_{x_j}^2} + \sum_{k=1}^{d-i} \frac{A_c^2}{\sigma_{x_o}^2} \right)} \right) = Q \left(\sqrt{2 \left(i \frac{A_c^2}{\sigma_j^2} + (d-i) \frac{A_c^2}{\sigma_o^2} \right)} \right) \quad (4.46)$$

or

$$P_{d_i}^{opt} = Q \left(\sqrt{2r \left(i \overline{\gamma_{b_j}} + (d-i) \overline{\gamma_{b_o}} \right)} \right) \quad (4.47)$$

where $\overline{\gamma_{b_j}}$ and $\overline{\gamma_{b_o}}$ are given by Equations (3.74) and (3.76), respectively.

By the same token, the BER of the sub-optimum receiver with binary modulation is given by Equations (4.8), (4.31), and (4.32) (these equations are identical to Equations (3.63), (3.65), and (3.66)), where $P_{d_i}(a_c)$ is the conditional probability of selecting a weight- d output sequence when i bits are jammed, given by

$$P_{d_i}^{subopt}(a_c) = Q \left(\frac{\sqrt{2} \sum_{k=1}^d a_c}{\sqrt{i \sigma_j^2 + (d-i) \sigma_o^2}} \right). \quad (4.48)$$

In the non-fading case, Equation (4.48) can be rewritten as

$$\begin{aligned} P_{d_i}^{subopt} &= Q \left(\frac{\sqrt{2} \sum_{k=1}^d A_c}{\sqrt{i \sigma_j^2 + (d-i) \sigma_o^2}} \right) = Q \left(\frac{\sqrt{2} d A_c}{\sqrt{i \sigma_j^2 + (d-i) \sigma_o^2}} \right) = Q \left(\sqrt{\frac{2d^2 A_c^2}{i \sigma_j^2 + (d-i) \sigma_o^2}} \right) \\ &= Q \left(\sqrt{\frac{2d^2}{i \frac{\sigma_j^2}{A_c^2} + (d-i) \frac{\sigma_o^2}{A_c^2}}} \right) \end{aligned} \quad (4.49)$$

or

$$P_{d_i}^{subopt} = Q \left(\sqrt{\frac{2rd^2}{\frac{i}{\overline{\gamma_{b_j}}} + \frac{(d-i)}{\overline{\gamma_{b_o}}}}} \right) \quad (4.50)$$

where $\overline{\gamma_{b_j}}$ and $\overline{\gamma_{b_o}}$ are given by Equations (3.74) and (3.76), respectively.

Clearly, for the non-fading scenario with PNJ, the two receivers' performances are not the same as was the case when only AWGN was present.

a. Data Rates of 6 and 12 Mbps

As previously discussed, for bit rates of 6 and 12 Mbps, a code rate of $r=1/2$ is implemented and BPSK and QPSK are used, respectively. Therefore, using $k=1$ and $r=1/2$ in the method described in the previous sub-section and using the values of B_d and d_{free} specified in Table 2, the BER of the sub-optimum receiver is obtained numerically. In Figure 43 the BER is plotted with respect to SIR at the receiver and for severe to moderate fading conditions (i.e., $0.5 \leq m \leq 2$). The BERs for non fading conditions is also plotted.

For these calculations, the SNR is assumed to be $E_b/N_o = 15$ dB and the coefficient ρ that defines the fraction of time that the jammer is operational is $1/2$. In order to gain some perspective for the performance of the sub-optimum receiver, the BER performance curves of the optimum receiver obtained in Chapter III for the same fading conditions are also plotted.

Generally, the performance of the sub-optimum receiver improves as we move from severe fading conditions to moderate fading conditions to no fading, following the same pattern as the optimum receiver.

However, comparing the two receivers, we find that the sub-optimum receiver performance is generally worse. Especially for low SIR (i.e., large jamming power), the sub-optimum receiver performance is significantly poorer. For a BER of 10^{-4} , the sub-optimum receiver requires approximately 1.5 dB more signal power than the optimum receiver for $m=2$, 2 dB more power for $m=1$, and 2.5 dB more signal power is required for severe fading condition with $m=0.5$. In other words, in order to achieve a reliable communication link with the sub-optimum receiver in a fading environment, more signal power is required than is required by the optimum receiver. More-

over, the additional signal power required is greater when the fading environment is more intense. For large SIR, the BERs of both receivers converge to a limit determined by the AWGN, resulting in a smaller difference between the two BERs. It is important to note that even for the no fading scenario, the sub-optimum receiver performance remains worse as we described above. However, as the SIR increases, the two receivers' performances converge. This is expected since, as was already discussed, both receivers have identical BERs when operating with AWGN only.

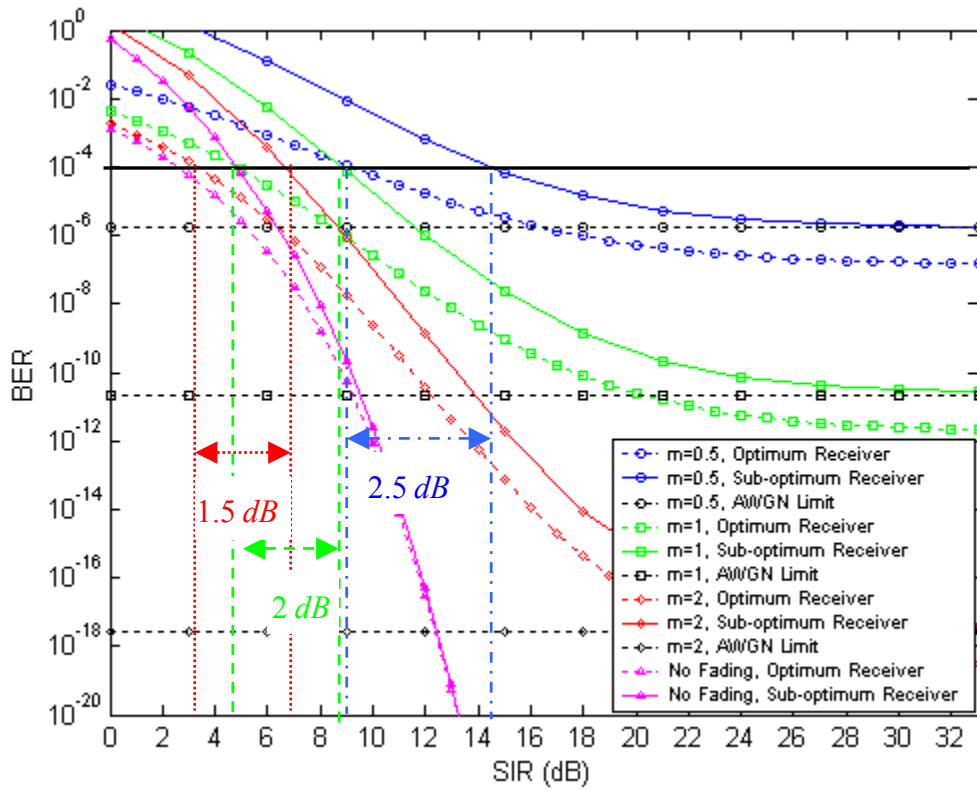


Figure 43. BER performance of *IEEE 802.11a* sub-optimum receiver with PNJ for various fading conditions and for data rates of 6 and 12 Mbps.

Next, we investigate the effect that the coefficient ρ has on receiver performance. In Figure 44 we plot the BER of the receiver for different values of ρ , keeping in mind the limitation $0 < \rho \leq 1$, with $E_b/N_o = 15$ dB and $m = 1$.

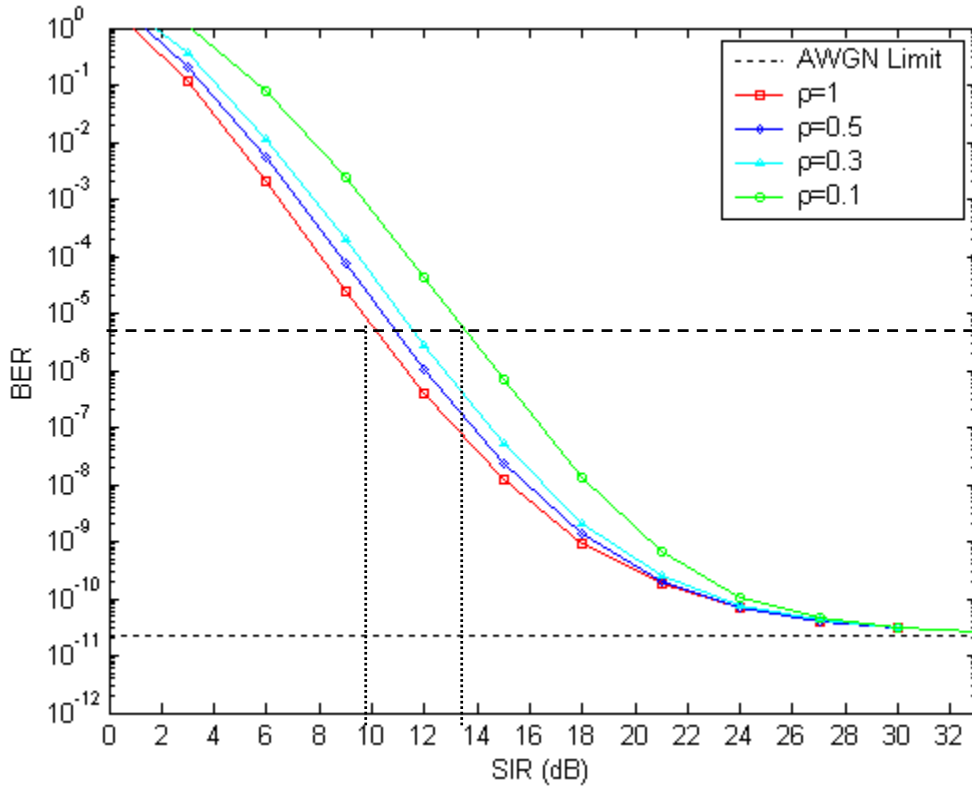


Figure 44. BER performance of *IEEE 802.11a* sub-optimum receiver with PNJ for various fading conditions and for data rates of 6 and 12 Mbps.

It can be seen that, from the receiver perspective, the worst case PNJ against a sub-optimum receiver is achieved when $\rho = 0.1$, while the jammer is less effective when $\rho = 1$. It is also clear that varying ρ does not affect receiver performance as significantly as in the optimum receiver jamming scenario. To be more specific, to achieve a BER of 10^{-5} , approximately 1.5 dB more signal power is required by the sub-optimum receiver when $\rho = 0.1$ than when $\rho = 1$. Therefore, we can assume that the worst case jamming scenario occurs for $\rho \rightarrow 0$. However, there are limitations on how small ρ can be. The jammer, due to hardware limitations, may not be able to transmit the peak power N_I/ρ or may not be able to transmit for as short a duration as called for when ρ becomes very small. In our analysis we assume that the minimum value of ρ that can be achieved by the jammer hardware is $\rho = 0.1$.

This behavior is explained by the fact that the receiver is not optimized to operate under hostile PNJ. In other words, from the receiver perspective, the worst jamming case is when the jamming power has been spread on only a percentage of the received bits. In this scenario, the bits that are affected are heavily jammed and are very unlikely to be demodulated correctly. So, the fact that about 10% of the received bits (i.e., for $\rho = 0.1$) are received incorrectly forces the receiver to make a decision error. On the other hand, if the jamming power has been spread over all received bits (i.e., $\rho = 1$), each received bit is no longer heavily jammed, and the receiver is more likely to make a correct decision, resulting in better performance. However, this improvement is not that significant, since all bits are still somehow affected even by lower jamming power. Therefore, the smaller the ρ , the poorer the receiver performance.

Another interesting observation is the fact that as the SIR increases, the performance is improved up to the point where the AWGN power dominates. As a result, for values of $E_b/N_f > 25$ dB, the performance of the sub-optimum receiver converges to a limit determined by AWGN.

Since the sub-optimum receiver BER follows a pattern analogous to the optimum receiver BER, as in the AWGN scenario, our analysis was focused on determining the performance of the sub-optimum receiver for severe to moderate fading conditions (i.e., $0.5 \leq m \leq 2$).

b. Data Rates of 9 and 18 Mbps

For bit rates of 9 and 18 Mbps, a code rate of $r = 3/4$ is implemented and BPSK and QPSK are used, respectively. Therefore, using the values $k = 1$ and $r = 3/4$, we can numerically determine the BER of the sub-optimum receiver. In Figure 45 the resulting BER is plotted with respect to SIR at the receiver for different fading conditions. For these calculations, as before $E_b/N_o = 15$ dB and $\rho = 0.5$ are used, while the BER performance curves of the optimum receiver obtained in Chapter III for the same fading conditions are also plotted.

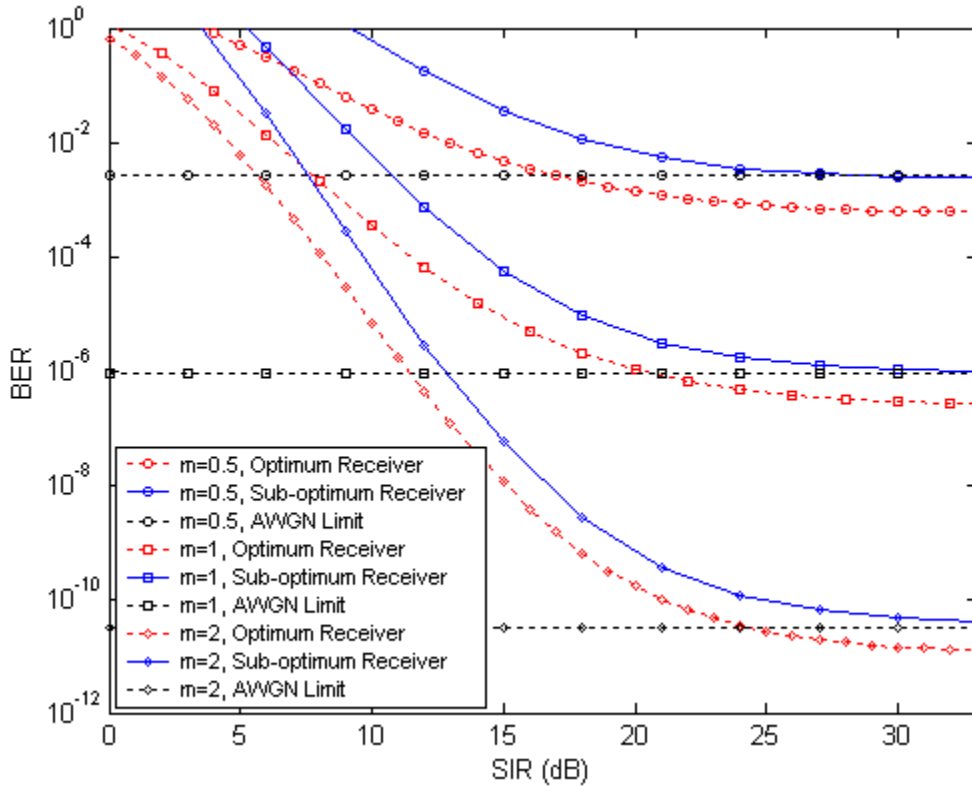


Figure 45. BER performance of *IEEE 802.11a* sub-optimum receiver with PNJ for data rates of 9 and 18 Mbps.

Examining Figure 45, we arrive at the same conclusions as in the 6-Mbps and 12-Mbps case. The receiver performance is improved as fading conditions diminish, while for large SIR the receiver performance is dictated by the power of the AWGN. The sub-optimum receiver performance is worse than the optimum receiver and requires more signal power to operate efficiently than the optimum receiver. The additional power required increases as fading conditions become more severe.

Finally, in Figure 46 we plot the BER of the receiver for different values of ρ , with $E_b/N_o = 15$ dB and $m = 1$. It is clear that the coefficient ρ has the same effect on the receiver performance as in the lower data rate case (6 or 12 Mbps). The smaller the coefficient ρ , the poorer the sub-optimum receiver performance. Moreover, the additional signal power required for the worst jamming scenario remains at the same order of 1.5 dB as for the lower data rate cases of 6 and 12 Mbps.

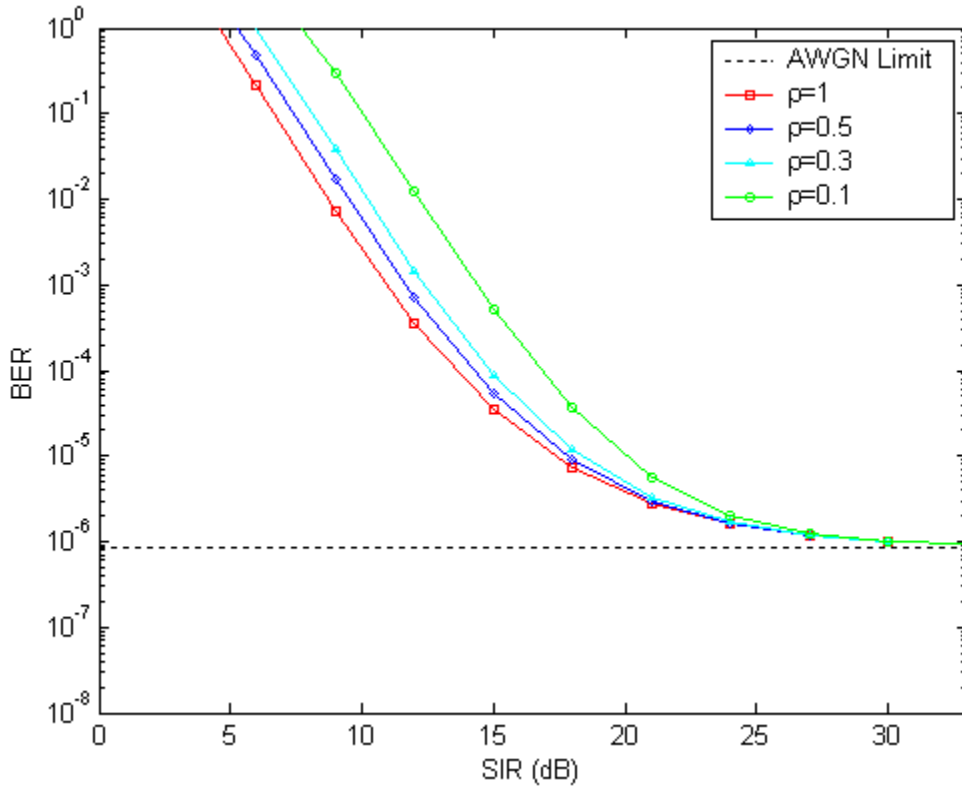


Figure 46. BER performance of *IEEE 802.11a* sub-optimum receiver with PNJ for various fading conditions and for data rates of 9 and 18 Mbps.

2. Non-binary Modulation

Following the method discussed previously, the BER of the sub-optimum *IEEE 802.11a* receiver can be obtained when MQAM modulation is used. Combining Equations (4.8), (4.31), (4.40) and inserting the numerically obtained PDF $f_{\Gamma_b}(\gamma_b)$, the BER of the *IEEE 802.11a* sub-optimum receiver operating with PNJ is obtained when MQAM modulation is used.

The only difference in our analysis is that the conditional probability $P_d(\gamma_b)$ is no longer given by Equation (4.39). When non-binary modulation is used and keeping in mind the assumption made previously in Chapter II that the information bits keep the “soft” information that the demodulated symbol that represented the bits had, we can see that the conditional probability of selecting a weight- d output sequence $P_d(\gamma_b)$ is given by

$$P_{d_i}(\gamma_b) = \frac{4}{q} Q \left(\sqrt{\frac{3q}{(M-1) \left[i + (d-i) R\left(\frac{E_b}{N_o}, \frac{E_b}{N_I}\right) \right]}} \gamma_b \right) \quad (4.51)$$

where q is the number of information bits per symbol, M is the number of symbols, and the ratio term $R\left(\frac{E_b}{N_o}, \frac{E_b}{N_I}\right)$ is given by Equation (4.38).

Next, the performance of the sub-optimum receiver in terms of BER is examined with PNJ and all higher data rates specified by the *IEEE 802.11a* standard and for severe to moderate fading conditions. Also, the BER performance curves of the optimum receiver obtained in Chapter III for the same fading conditions and the same data rates are plotted.

a. Data Rate of 24 Mbps

The receiver performance when data are transferred with a rate of 24 Mbps is discussed in this sub-section. For this data rate, 16QAM is specified along with $r=1/2$ FEC. Using the values $M=16$, $q=4$, and $r=1/2$ along with the values of d_{free} and B_d specified in Table 2 in the relevant equations, we get the upper bound on BER, plotted in Figure 47 with respect to SIR at the receiver and for different fading conditions. For these calculations, the SNR is assumed to be $E_b/N_o=15$ dB and the coefficient ρ that defines the fraction of time that the jammer is operational is $1/2$.

As was found for the lower data rate cases when binary modulation was utilized, it is clear that the receiver performance significantly improves as the fading conditions improve. As the SIR increases, the performance improves up to the point where the AWGN power dominates. Generally, the sub-optimum receiver performance is significantly poorer than optimum receiver performance, especially for low SIR.

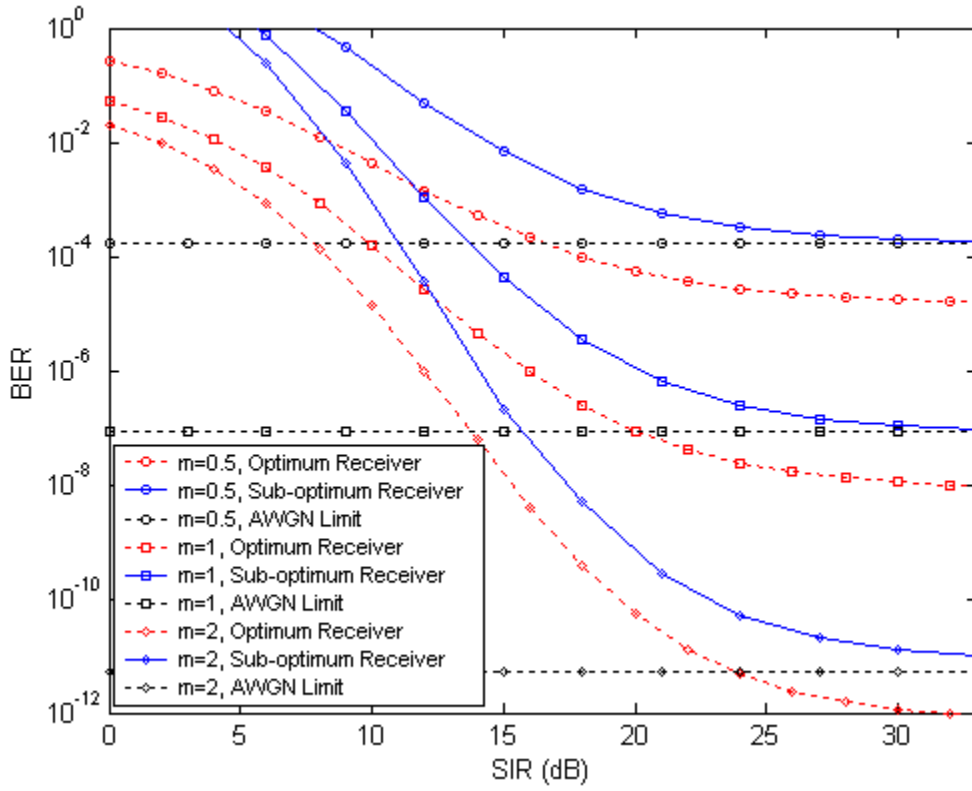


Figure 47. BER performance of *IEEE 802.11a* sub-optimum receiver with PNJ for a data rate of 24 Mbps.

Next, in Figure 48 we plot the BER of the receiver for different values of ρ , keeping in mind the limitation $0 < \rho \leq 1$, with $E_b/N_o = 15$ dB and $m = 1$. It is clear that varying ρ does not affect the receiver performance significantly. As in the binary modulation cases, the additional signal power required for the best ($\rho = 1$) and the worst case jamming ($\rho = 0.1$) remains on the order of 1.5 dB, regardless of the code rate used or the modulation scheme utilized.

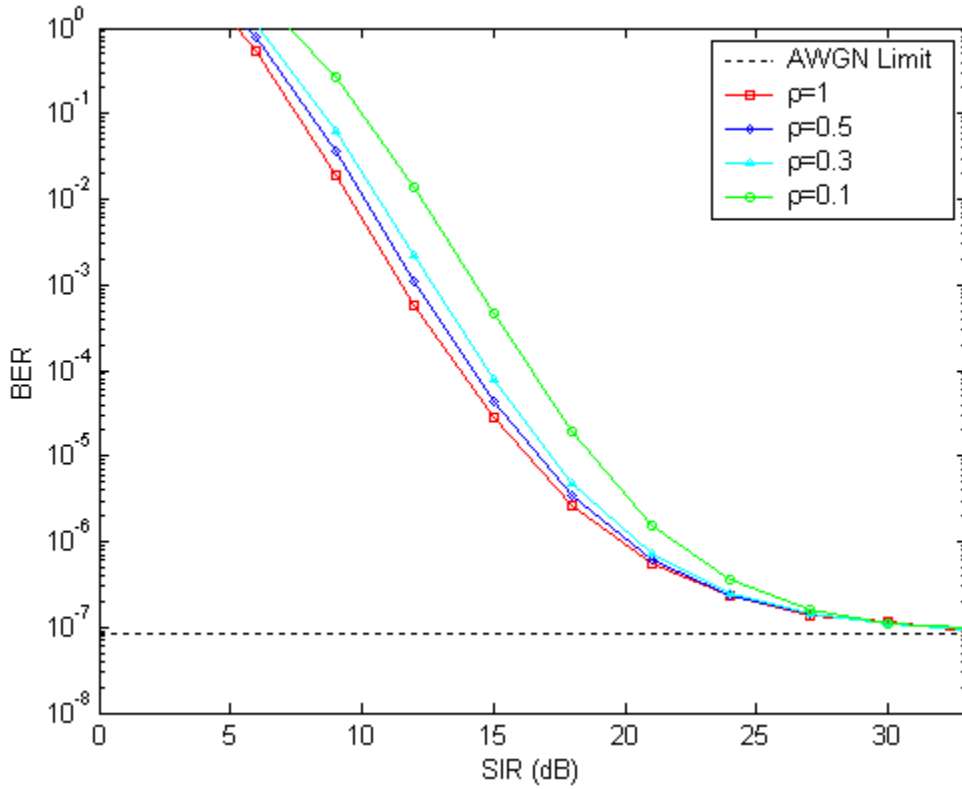


Figure 48. BER performance of *IEEE 802.11a* sub-optimum receiver with PNJ for different values of ρ ($0 < \rho \leq 1$) and for a data rate of 24 Mbps..

b. Data Rate of 36 Mbps

Substituting $M = 16$, $q = 4$, and $r = 3/4$ into the relevant equations, we get the upper bound on BER of the optimum receiver for the 36-Mbps data rate. The estimated BER is plotted in Figure 49 with respect to SIR at the receiver and for different fading conditions. Examining Figure 49, we arrive at the same conclusions as before. The receiver performance is worse as compared to the optimum receiver for low SIR, while for larger SIR the receiver performance is limited by the power of the AWGN (SNR).

In Figure 50 we plot the BER of the receiver for different values of ρ , with $E_b/N_o = 15$ dB and $m = 1$. The coefficient ρ has the same effect on the receiver performance as in the lower data rate cases. The smaller the coefficient ρ , the poorer the receiver performance except in the limit of large SIR.

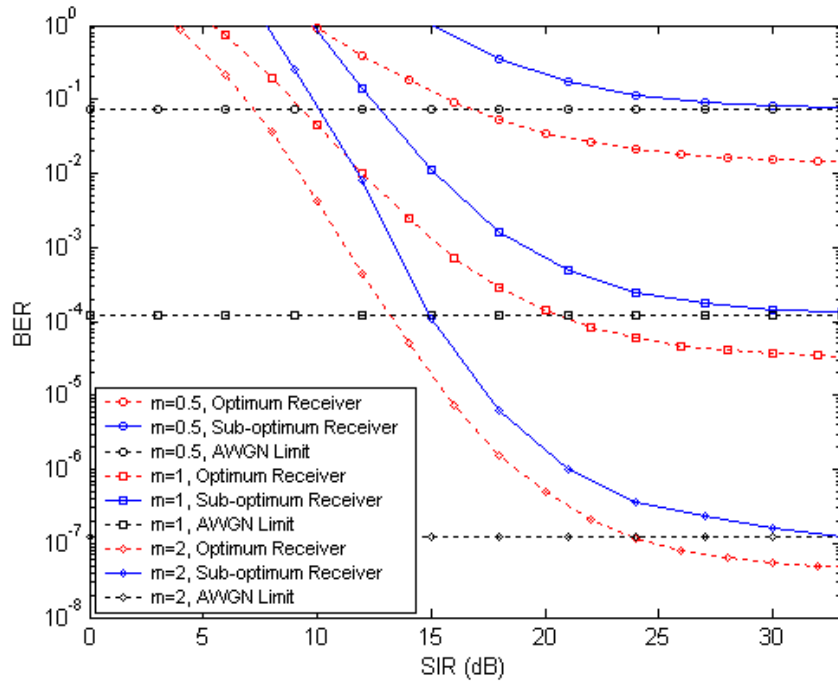


Figure 49. BER performance of *IEEE 802.11a* sub-optimum receiver with PNJ for a data rate of 36 Mbps.

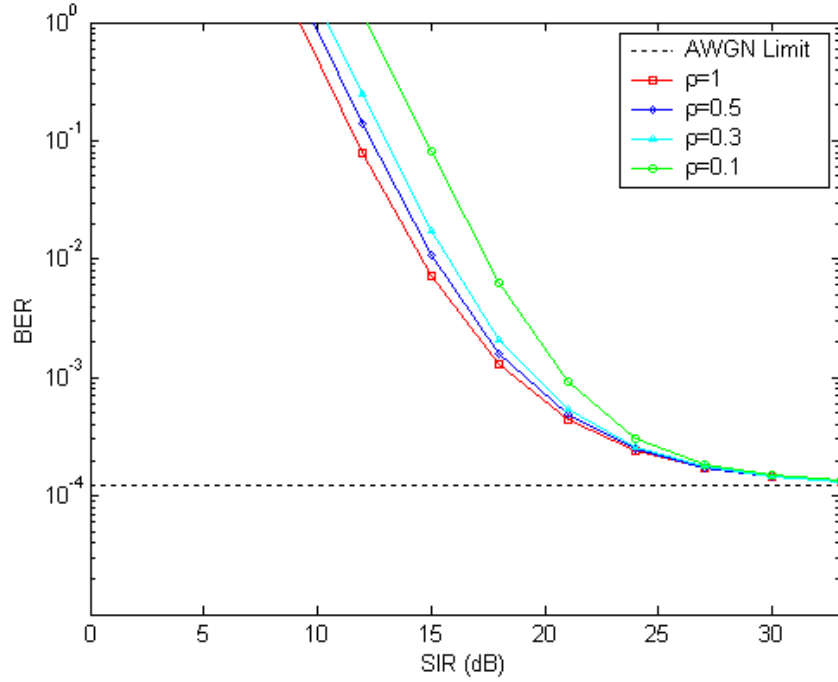


Figure 50. BER performance of *IEEE 802.11a* sub-optimum receiver with PNJ for different values of ρ ($0 < \rho \leq 1$) and for a data rate of 36 Mbps.

c. Data Rate of 48 Mbps

For a data rate of 48 Mbps, 64QAM is used with a code rate of $r = 2/3$. Using $M = 64$, $q = 6$, and $r = 2/3$ in the relevant equations, we get the upper bound on BER, plotted in Figure 51 with respect to SIR at the receiver and for different fading conditions. The same conclusion is obtained here for the sub-optimum receiver performance with respect to the fading environment and the optimum receiver performance.

It is obvious that no reliable transfer of data at this high rate is possible for $E_b/N_o = 15$ dB since for all m , $P_b > 10^{-5}$. In order to achieve an acceptable BER more signal power is required.

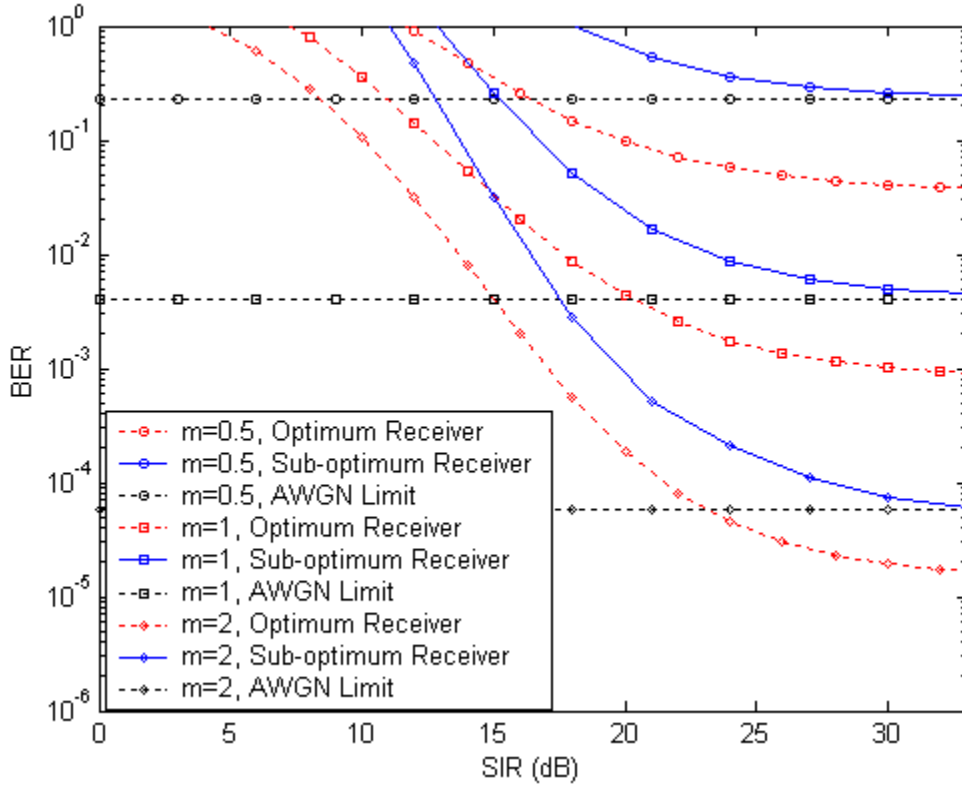


Figure 51. BER performance of *IEEE 802.11a* sub-optimum receiver with PNJ, for data rate of 48 Mbps.

In Figure 52 we plot the BER of the receiver for different values of ρ , with $E_b/N_o = 15$ dB and $m = 1$. Again, the smaller the coefficient ρ , the poorer the receiver performance. The effect of various ρ on the receiver performance is not significant.

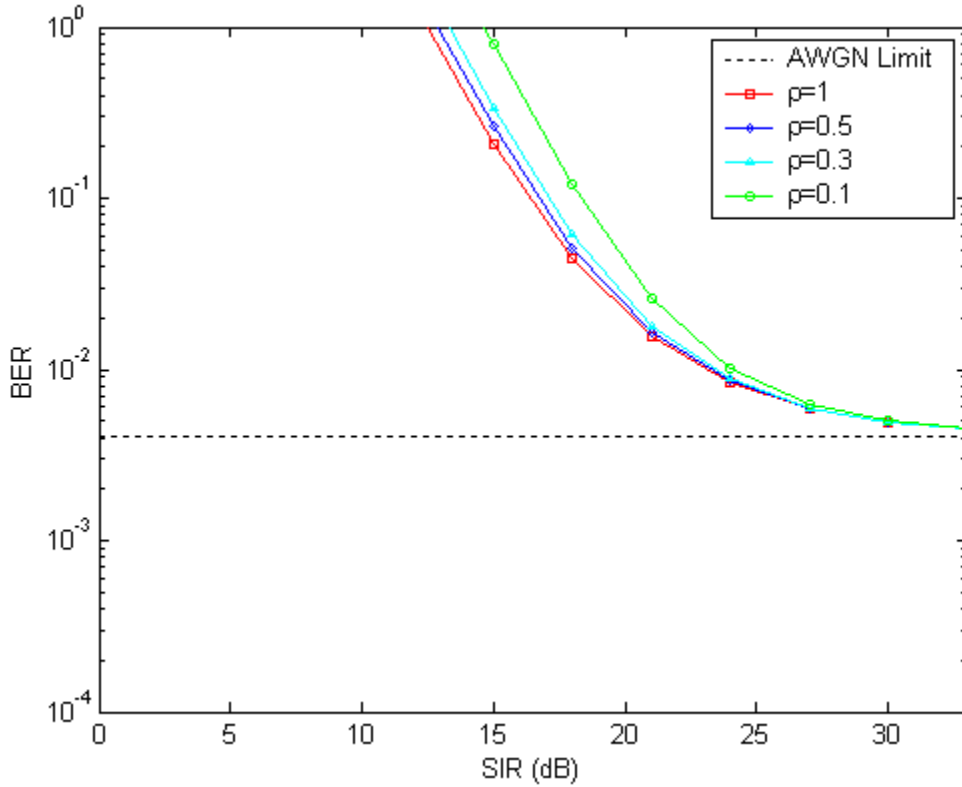


Figure 52. BER performance of *IEEE 802.11a* sub-optimum receiver with PNJ for different values of ρ ($0 < \rho \leq 1$) and for a data rate of 48 Mbps.

d. Data Rate of 54 Mbps

Finally, the highest data rate of 54 Mbps is achieved by using 64QAM and FEC with $r = 3/4$. Using $M = 64$, $q = 6$, and $r = 3/4$ in the relevant equations, we get the upper bound on BER, plotted in Figure 53 with respect to SNR at the receiver for severe to moderate fading conditions. The same conclusion as for the lower data rates is reached here for the receiver performance.

The sub-optimum receiver performance is significantly degraded. It is obvious that no reliable transfer of data at this high rate is possible for $E_b/N_o = 15$ dB since for all m , $P_b > 10^{-5}$. In order to achieve an acceptable BER, more signal power is required. We note that the sub-optimum receiver performance for $m = 0.5$ is not plotted here since the BER was found to be very large even for larger values of SIR.

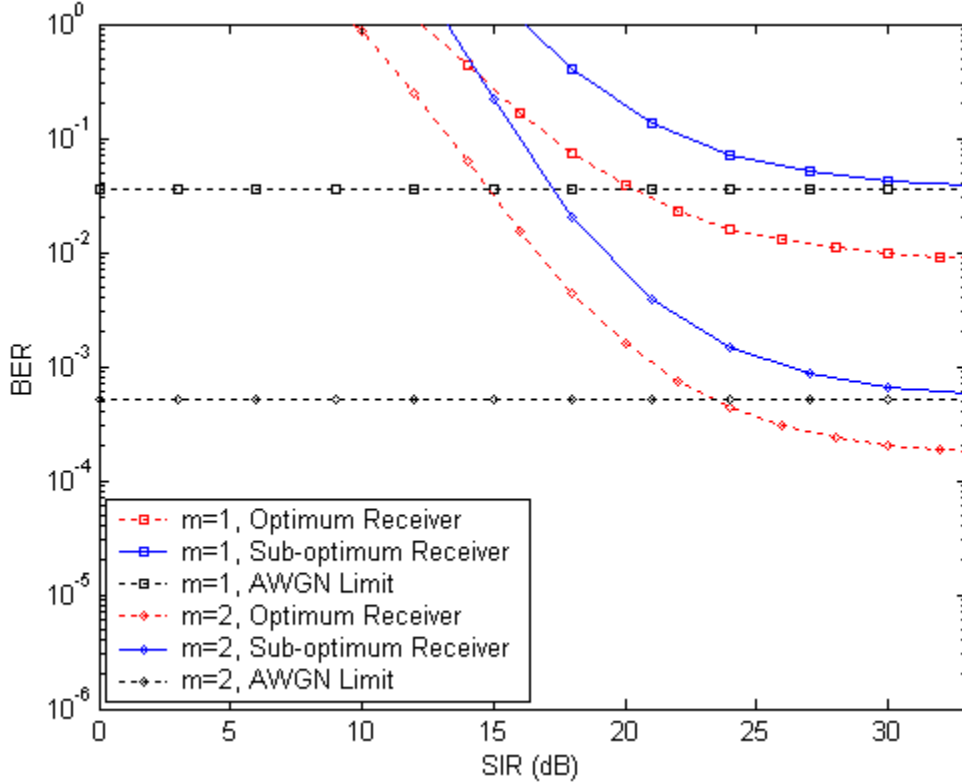


Figure 53. BER performance of *IEEE 802.11a* sub-optimum receiver with PNJ for a data rate of 54 Mbps.

It is clear that, for higher data rates, the receiver performance degrades rapidly. This is a trade-off between higher data rate and BER. The more information we try to process, the larger the risk of making an error. This trade off is more obvious in the sub-optimum receiver case since a larger signal power is required than for the optimum receiver case.

Finally, in Figure 54 we plot the BER of the receiver for different values of ρ , with $E_b/N_o = 15$ dB and $m = 1$. Again, the smaller the coefficient ρ , the poorer the receiver performance. However, the effect that different values of ρ have on the sub-optimum receiver performance has not been changed much by the code rate or the modulation used.

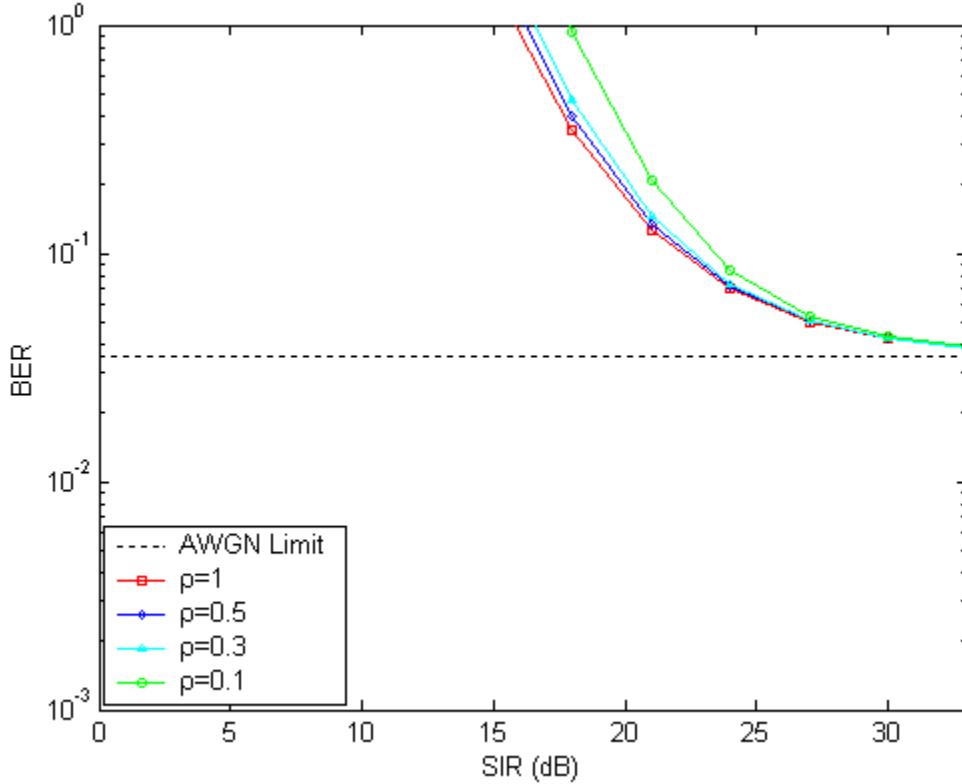


Figure 54. BER performance of *IEEE 802.11a* sub-optimum receiver with PNJ for different values of ρ ($0 < \rho \leq 1$) and for a data rate of 54 Mbps.

3. Conclusions on the Effect of PNJ on the 802.11a Sub-optimum Receiver

Summarizing, the overall performance of the sub-optimum receiver was discussed for all specified operational data rates when operating under the effect of PNJ.

Generally, the performance of the sub-optimum receiver improves as we move from severe fading conditions to moderate fading conditions, following the same pattern as the optimum receiver.

Comparing the two receivers, we found that the sub-optimum receiver performance is generally worse than that of the optimum receiver. Particularly, the sub-optimum receiver performance is significantly degraded for low SIR. As SIR gets larger, the difference between the two receivers' BER is reduced since they both converge to a limit determined by AWGN limit (i.e., SNR). For the no fading scenario, the two receivers' BERs converge for large SIR.

Since the sub-optimum receiver performance is worse, additional signal power is required by the receiver in order to achieve a reliable communication link. The additional signal power required is greater when the fading environment is more severe. Moreover, the use of excessive signal power is especially necessary for higher data rates. It was found that $E_b/N_o = 15$ dB is not adequate to achieve data rates higher than 36 Mbps, since for all SIR the receiver BER was greater than 10^{-5} for severe to moderate fading conditions. In the most severe fading condition when $m = 0.5$, we can transfer data reliably only with rates of 6 and 12 Mbps.

It is also found that from the receiver perspective, the worst case PNJ against a sub-optimum receiver is achieved when $\rho = 0.1$, while the jammer is less effective when $\rho = 1$. Therefore, the worst case jamming scenario occurs for $\rho \rightarrow 0$. It is also found that varying ρ does not affect the receiver performance significantly, as in the optimum receiver jamming scenario. In other words, to achieve a certain level of BER, approximately 1.5 dB more signal power is required by the sub-optimum receiver when $\rho = 0.1$ than when $\rho = 1$, regardless the modulation or the code rate used.

Finally, since the BER of the sub-optimum receiver operating under the effect of a PNJ follows a pattern similar to the optimum receiver BER regardless the modulation or the code rate used, the conclusions made for the optimum receiver with AWGN made in section III.C.3 apply here also. When severe to moderate fading conditions exist, the receiver performance is affected mainly by the code rate used, while the fading environment affects the receiver less when lower code rates are used.

In this chapter, the performance of the sub-optimum receiver was examined. Next in Chapter V the performance of the same receiver is examined when noise-normalization is utilized.

THIS PAGE INTENTIONALLY LEFT BLANK

V. PERFORMANCE ANALYSIS OF THE IEEE 802.11A SUB-OPTIMUM RECEIVER WITH NOISE-NORMALIZATION

In Chapters III and IV, the performance of the *IEEE 802.11a* optimum receiver and sub-optimum receiver was examined, respectively. From this analysis it was found that the performance of the sub-optimum receiver in AWGN is not significantly affected when only AWGN is present. On the other hand, when PNJ is present, the sub-optimum receiver performance is significantly poorer, especially when the transmitted signal power is low (i.e., $E_b/N_o < 15$ dB).

In Chapter V the performance of the sub-optimum receiver was examined when noise-normalization is utilized. To implement noise-normalization, a form of side information is assumed, in this case the assumption that the noise power that corrupts every received bit is either known or can be accurately measured. The performance of this receiver, named here the noise-normalized sub-optimum receiver, was examined only when a hostile PNJ is present. The AWGN case was not analyzed since with AWGN the noise-normalized receiver performance is identical to that of the sub-optimum receiver examined in Chapter IV. When AWGN is present, the noise power is uniform for all received bits and the noise-normalization has no effect.

The performance of an *IEEE 802.11a* noise-normalized sub-optimum receiver is examined when the signal is transmitted over a fading channel with PNJ and for all data rates specified by *IEEE 802.11a* standard.

A. THE IEEE 802.11A NOISE-NORMALIZED SUB-OPTIMUM RECEIVER

The *IEEE 802.11a* noise-normalized sub-optimum receiver examined is designed to operate given that the noise power for every received bit is known. In other words, at every instance it is known whether a bit is jammed or not, and the noise power in every bit can accurately be determined. This noise power is then used to normalize the received signal prior to combining each signal to obtain the decision statistics. By this technique the jammed bits are de-emphasized with respect to unjammed bits. As a result, the effect of the jammed bits on the overall decision statistic is minimized.

The model of the noise-normalized sub-optimum receiver when BPSK modulation is used is illustrated in Figure 55.

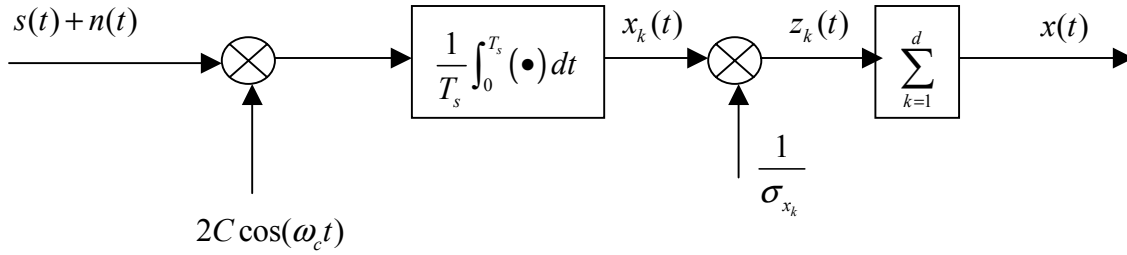


Figure 55. The *IEEE 802.11a* noise normalized sub-optimum receiver.

The signal $x_k(t)$ at the integrator output represents those sequence bits that have been affected in a random way by the channel. The signal $x_k(t)$ can be modeled as a GRV. The GRV, omitting the higher frequency terms, has a mean

$$\overline{X_k} = \sqrt{2}Ca_c \quad (5.1)$$

and variance

$$\sigma_{x_k}^2 = C^2 \sigma_k^2, \quad (5.2)$$

where $\sigma_{x_k}^2$ is the noise power at the integrator output that has corrupted the signal $s(t)$.

The quantity σ_{x_k} is then used to normalize the signal $x_k(t)$ at the integrator output. The resulting signal $z_k(t)$ after normalization, since all operations are linear, can be modeled as a GRV with mean

$$\overline{Z_k} = \frac{\sqrt{2}Ca_c}{\sigma_{x_k}} \quad (5.3)$$

and variance

$$\sigma_{z_k}^2 = \frac{C^2 \sigma_{x_k}^2}{\sigma_{x_k}^2} = C^2. \quad (5.4)$$

Since the quantities $z_k(t)$ are modeled as GRVs, the signal $x(t)$ is also a GRV with mean

$$\overline{X} = \sqrt{2}C \sum_{k=1}^d \frac{a_c}{\sigma_{x_k}} \quad (5.5)$$

and variance

$$\sigma_x^2 = \sum_{k=1}^d C^2 = dC^2. \quad (5.6)$$

As previously discussed, for the BPSK receiver the probability of making an incorrect detection P_d can be expressed as [4]

$$P_d = Q\left(\frac{\overline{X}}{\sigma_x}\right). \quad (5.7)$$

Substituting Equations (5.5) and (5.6) into (5.7), we get

$$P_d = Q\left(\sqrt{\frac{2}{d}} \sum_{k=1}^d \frac{a_c}{\sigma_{x_k}}\right). \quad (5.8)$$

B. PERFORMANCE ANALYSIS IN A FADING CHANNEL WITH HOSTILE PNJ

Next, the performance analysis of the noise-normalized sub-optimum receiver is examined in terms of BER when the receiver is subjected to PNJ for both binary and non-binary modulation.

1. BPSK/QPSK Modulation

For data rates of 6, 9, 12, and 18 Mbps, the use of BPSK and QPSK is specified. The performance with QPSK is identical to that obtained for BPSK and will not be obtained separately. The following analysis is analogous to the analysis made for the sub-optimum receiver in Section IV.C.1. The model of the sub-optimum receiver when BPSK

modulation is used is the one presented in Figure 55, while the noise power in each received bit is given by Equation (4.30).

Following the same steps as in the sub-optimum case in Chapter IV, we obtain the BER of the sub-optimum receiver from Equation (4.8) while the average probability P_d is obtained by Equation (4.31) and the unconditional probability P_{d_i} from Equation (4.32).

The conditional probability $P_{d_i}(\gamma_b)$ of selecting a weight- d output sequence when only i bits are jammed is obtained using Equation (3.8) and, using the proper notation, is expressed as

$$P_d(\sum_{k=1}^d a_c) = Q\left(\sqrt{\frac{2}{d}} \sum_{k=1}^d \frac{a_c}{\sigma_{x_k}}\right) \quad (5.9)$$

or

$$P_d(\gamma_b) = Q\left(\sqrt{\frac{2}{d}} \gamma_b\right) \quad (5.10)$$

where

$$\gamma_b = \sum_{k=1}^d \frac{a_c}{\sigma_{x_k}}. \quad (5.11)$$

Since only i bits are jammed, the PDF γ_b is written

$$\gamma_b = \sum_{k=1}^i \frac{a_c}{\sigma_{x_j}} + \sum_{k=1}^{d-i} \frac{a_c}{\sigma_{x_o}} \quad (5.12)$$

or

$$\gamma_b = \gamma_{b_j} + \gamma_{b_o} \quad (5.13)$$

where

$$\gamma_{b_j} = \sum_{k=1}^i \frac{a_c}{\sigma_{x_j}} = \sum_{k=1}^i \gamma_{b_{k_j}} \quad (5.14)$$

and

$$\gamma_{b_o} = \sum_{k=1}^{d-i} \frac{a_c}{\sigma_{x_o}} = \sum_{k=1}^{d-i} \gamma_{b_{k_o}}. \quad (5.15)$$

The random variables

$$\gamma_{b_{k_j}} = \frac{a_c}{\sigma_{x_j}} \quad (5.16)$$

and

$$\gamma_{b_{k_o}} = \frac{a_c}{\sigma_{x_o}} \quad (5.17)$$

are proportional to the first power of the Nakagami- m random variable a_c , and their PDFs are obtained in a similar way as in sections IV.B.1 and IV.C.1.

The PDF of the random variable expressing the jammed bits is written as

$$f_{\Gamma_{b_{k_j}}}(\gamma_{b_{k_j}}) = \frac{2}{\Gamma(m)} \left(m \overline{\gamma_{b_j}} \right)^m \gamma_{b_{k_j}}^{2m-1} e^{-\left(m \overline{\gamma_{b_j}} \right) \gamma_{b_{k_j}}^2}, \quad \gamma_{b_{k_j}} \geq 0 \quad (5.18)$$

where

$$\overline{\gamma_{b_j}} = \frac{1}{r} \left[\left(\frac{E_b}{N_o} \right)^{-1} + \frac{1}{\rho} \left(\frac{E_b}{N_l} \right)^{-1} \right] \quad (5.19)$$

and the PDF of the random variable expressing the non-jammed bits is expressed as

$$f_{\Gamma_{b_{k_o}}}(\gamma_{b_{k_o}}) = \frac{2}{\Gamma(m)} \left(m \overline{\gamma_{b_o}} \right)^m \gamma_{b_{k_o}}^{2m-1} e^{-\left(m \overline{\gamma_{b_o}} \right) \gamma_{b_{k_o}}^2}, \quad \gamma_{b_{k_o}} \geq 0 \quad (5.20)$$

where

$$\overline{\gamma_{b_o}} = \frac{1}{r} \left(\frac{E_b}{N_o} \right)^{-1}. \quad (5.21)$$

Next, the evaluation of the PDF $f_{\Gamma_b}(\gamma_b)$ is done following a procedure analogous to the one described in section III.C.1. First, the LTs of $f_{\Gamma_{b_{k_j}}}(\gamma_{b_{k_j}})$ and $f_{\Gamma_{b_{k_o}}}(\gamma_{b_{k_o}})$ need to be evaluated. This is done numerically by using the LT definition as

$$\begin{aligned}
F_{\Gamma_{b_{k_j}}}(s) &= \int_0^\infty f_{\Gamma_{b_{k_j}}}(\gamma_{b_{k_j}}) e^{-s\gamma_{b_{k_j}}} d\gamma_{b_{k_j}} \\
F_{\Gamma_{b_{k_o}}}(s) &= \int_0^\infty f_{\Gamma_{b_{k_o}}}(\gamma_{b_{k_o}}) e^{-s\gamma_{b_{k_o}}} d\gamma_{b_{k_o}}.
\end{aligned} \tag{5.22}$$

Next, the LTs of the PDFs of the random variables γ_{b_j} and γ_{b_o} are obtained as

$$\begin{aligned}
F_{\Gamma_{b_j}}(s) &= \left(F_{\Gamma_{b_{k_j}}}(s) \right)^i = \left[\int_0^\infty f_{\Gamma_{b_{k_j}}}(\gamma_{b_{k_j}}) e^{-s\gamma_{b_{k_j}}} d\gamma_{b_{k_j}} \right]^i \\
F_{\Gamma_{b_o}}(s) &= \left(F_{\Gamma_{b_{k_o}}}(s) \right)^{d-i} = \left[\int_0^\infty f_{\Gamma_{b_{k_o}}}(\gamma_{b_{k_o}}) e^{-s\gamma_{b_{k_o}}} d\gamma_{b_{k_o}} \right]^{d-i}.
\end{aligned} \tag{5.23}$$

Since the random variable γ_b is defined in Equation (5.13) as the summation of γ_{b_j} and γ_{b_o} , the LT of the PDF of the random variable γ_b is obtained from

$$F_{\Gamma_b}(s) = F_{\Gamma_{b_j}}(s) F_{\Gamma_{b_o}}(s) = \left[\int_0^\infty f_{\Gamma_{b_{k_j}}}(\gamma_{b_{k_j}}) e^{-s\gamma_{b_{k_j}}} d\gamma_{b_{k_j}} \right]^i \left[\int_0^\infty f_{\Gamma_{b_{k_o}}}(\gamma_{b_{k_o}}) e^{-s\gamma_{b_{k_o}}} d\gamma_{b_{k_o}} \right]^{d-i}. \tag{5.24}$$

Finally, the PDF of the random variable γ_b is obtained numerically by evaluating the ILT of $F_{\Gamma_b}(s)$. The numerical evaluation is done using Equation (4.22).

Following these steps and combining Equations (4.8), (4.27), and (4.28), the BER of the noise-normalized sub-optimum receiver is obtained for BPSK/QPSK with PNJ operating in a fading environment.

The special case when the noise-normalized receiver is operating with no fading is examined next. As already discussed, the BER of the noise-normalized sub-optimum receiver is obtained combining Equations (4.8), (4.27), and (4.28), where the conditional probability $P_{d_i}(\gamma_b)$ is found by combining Equations (5.10) and (5.12) to get

$$P_{d_i}(\gamma_b) = Q \left(\sqrt{\frac{2}{d}} \left(\sum_{k=1}^i \frac{a_c}{\sigma_{x_j}} + \sum_{k=1}^{d-i} \frac{a_c}{\sigma_{x_o}} \right) \right). \tag{5.25}$$

However, in the non-fading scenario the amplitude of the received signal is constant, noted as A_c . Therefore substituting a_c with A_c in Equation (5.25), the probability P_{d_i} is no longer conditional and the BER of the optimum receiver is obtained from Equations (4.8) and (4.27), where Equation (5.25) can be simplified as follows:

$$\begin{aligned}
P_{d_i} &= Q \left(\sqrt{\frac{2}{d}} \left(\sum_{k=1}^i \frac{A_c}{\sigma_{x_j}} + \sum_{k=1}^{d-i} \frac{A_c}{\sigma_{x_o}} \right) \right) = Q \left(\sqrt{\frac{2}{d}} \left(i \frac{A_c}{\sigma_{x_j}} + (d-i) \frac{A_c}{\sigma_{x_o}} \right) \right) \\
&= Q \left(\sqrt{\frac{2}{d}} \left(i \sqrt{\frac{A_c^2}{\sigma_{x_j}^2}} + (d-i) \sqrt{\frac{A_c^2}{\sigma_{x_o}^2}} \right) \right)
\end{aligned} \tag{5.26}$$

or

$$\begin{aligned}
P_{d_i} &= Q \left(\sqrt{\frac{2}{d}} \left(\sum_{k=1}^i \frac{A_c}{\sigma_{x_j}} + \sum_{k=1}^{d-i} \frac{A_c}{\sigma_{x_o}} \right) \right) = Q \left(\sqrt{\frac{2}{d}} \left(i \frac{A_c}{\sigma_{x_j}} + (d-i) \frac{A_c}{\sigma_{x_o}} \right) \right) \\
&= Q \left(\sqrt{\frac{2}{d}} r \left(i \sqrt{\gamma_{b_j}} + (d-i) \sqrt{\gamma_{b_o}} \right) \right)
\end{aligned} \tag{5.27}$$

where $\overline{\gamma_{b_j}}$ and $\overline{\gamma_{b_o}}$ are given by Equations (4.44) and (5.21), respectively.

a. Data Rates of 6 and 12 Mbps

For bit rates of 6 and 12 Mbps, a code rate of $r=1/2$ is specified and BPSK and QPSK are used, respectively. Therefore, using $k=1$ and $r=1/2$ into the method described in the previous sub-section and using the values of B_d and d_{free} specified in Table 2, the BER of the noise-normalized sub-optimum receiver is obtained numerically.

The special case when the receiver is operating without the effect of fading is examined first. In Figure 56, the BER of the noise-normalized sub-optimum receiver is illustrated along with the BERs of the optimum and sub-optimum receiver obtained in section IV.C. It is obvious that, when there is no fading, the performance of the noise-normalized sub-optimum receiver is identical to that of the optimum receiver while is significantly better than the sub-optimum receiver for $E_b/N_f \leq 10$ dB. This behavior can be explained because when no fading exists, the noise-normalization completely de-emphasizes the jammed bits, resulting in optimum decision statistics. That being the case, the performance of the noise-normalized sub-optimum receiver will be discussed when

the receiver operates in a severe to moderate fading channel (i.e., for a fading figure $0.5 \leq m \leq 2$) with $E_b/N_o = 15$ dB and $\rho = 0.5$.

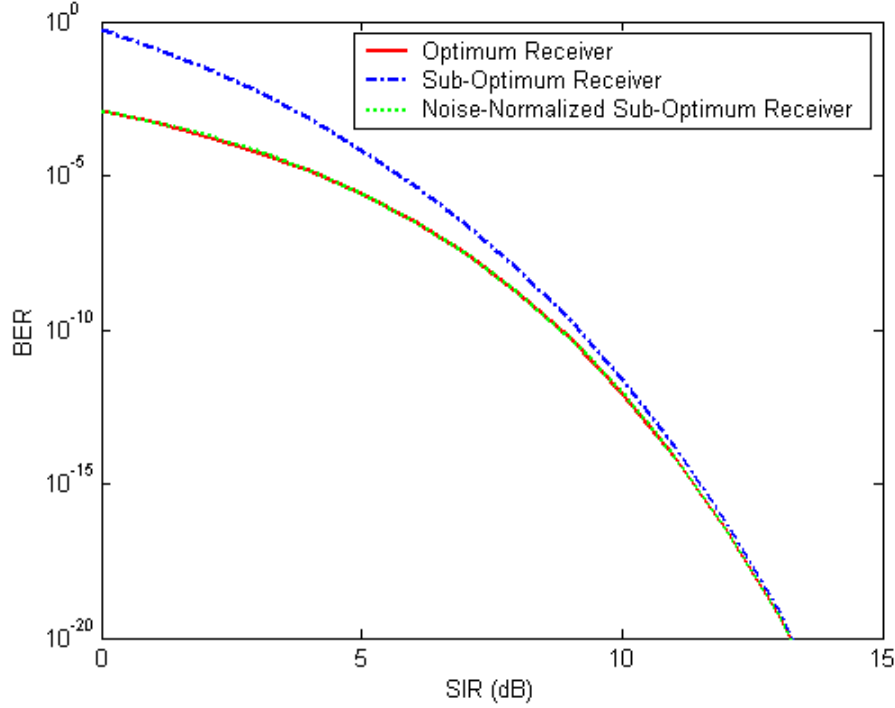


Figure 56. Noise-normalized sub-optimum receiver BER vs. optimum receiver BER with PNJ without fading for data rates of 6 and 12 Mbps.

Next, the BER of the noise-normalized sub-optimum receiver is plotted in Figure 57 as a function of SIR at the receiver. In order to gain some perspective for the performance of the sub-optimum receiver, the BER performance curves of the optimum and the sub-optimum receiver obtained in Chapter III for the same fading conditions are also plotted. For these calculations, the SNR is assumed to be $E_b/N_o = 15$ dB and the coefficient ρ that defines the fraction of time that the jammer is operational is set to $1/2$.

Next, we investigate the effect that the coefficient ρ has on receiver performance. In Figure 58 we plot the BER of the receiver for different values of ρ , keeping in mind the limitation $0 < \rho \leq 1$, with $E_b/N_o = 15$ dB and $m = 1$.

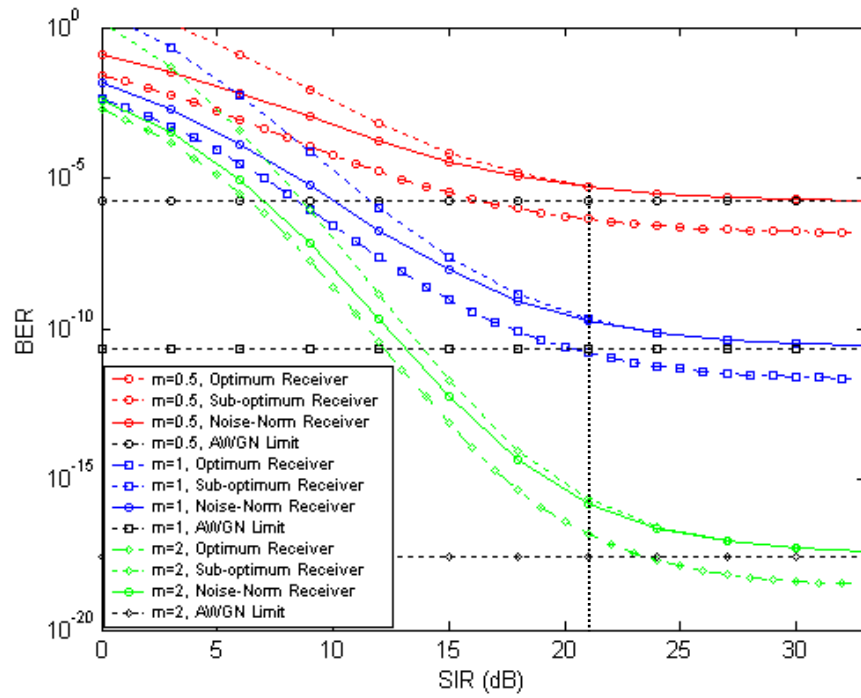


Figure 57. BER performance of an *IEEE 802.11a* noise-normalized sub-optimum receiver with PNJ for data rates of 6 and 12 Mbps.

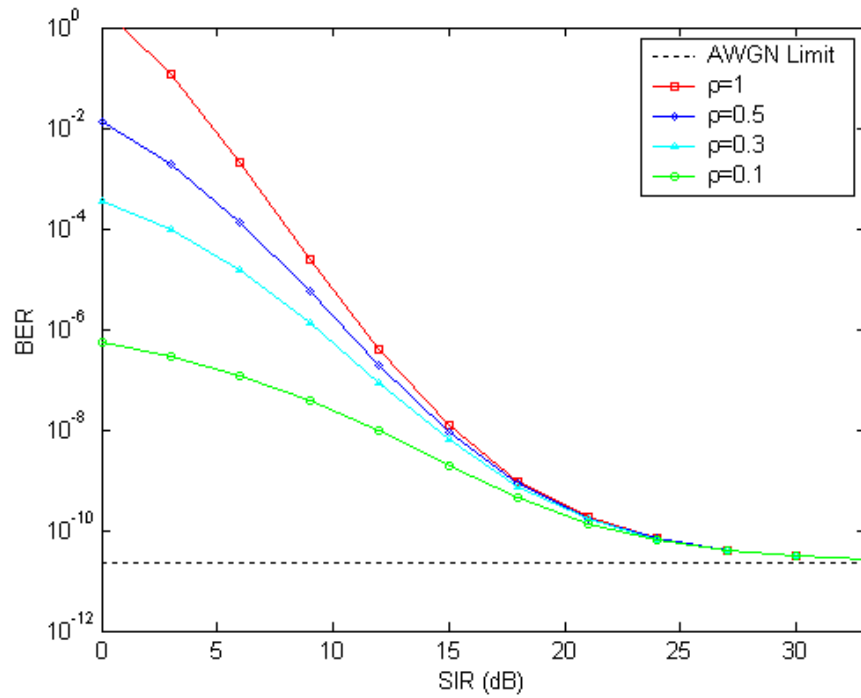


Figure 58. BER performance of an *IEEE 802.11a* noise-normalized sub-optimum receiver with PNJ for various ρ and for data rates of 6 and 12 Mbps.

b. Data Rates of 9 and 18 Mbps

For bit rates of 9 and 18 Mbps, a code rate of $r=3/4$ is specified and BPSK and QPSK are used, respectively. Therefore, using the values $k=1$ and $r=3/4$, we can numerically determine the BER of the noise-normalized sub-optimum receiver. In Figure 59 the resulting BER is plotted with respect to SIR at the receiver for different fading conditions. For these calculations, $E_b/N_o=15$ dB and $\rho=0.5$ are used, while the BER performance curves of the optimum and sub-optimum receiver obtained in Chapter III, for the same fading conditions, are also plotted.

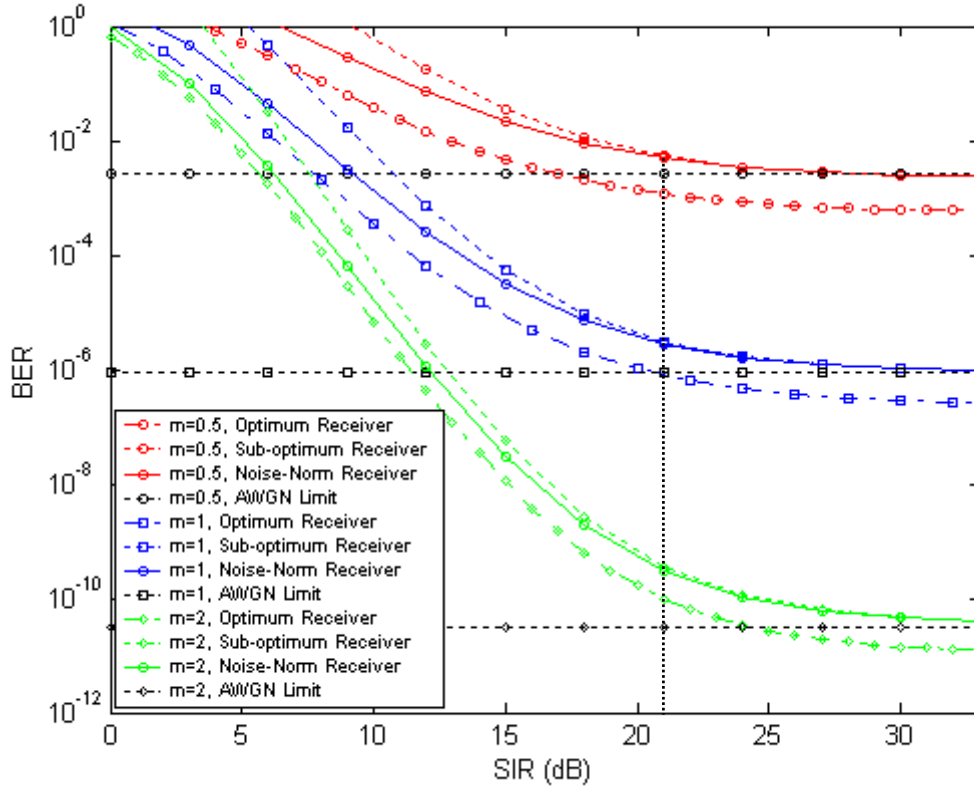


Figure 59. BER performance of an *IEEE 802.11a* noise-normalized sub-optimum receiver with PNJ for data rates of 9 and 18 Mbps.

Finally, in Figure 60 we plot the BER of the receiver for different values of ρ , with $E_b/N_o=15$ dB and $m=1$.

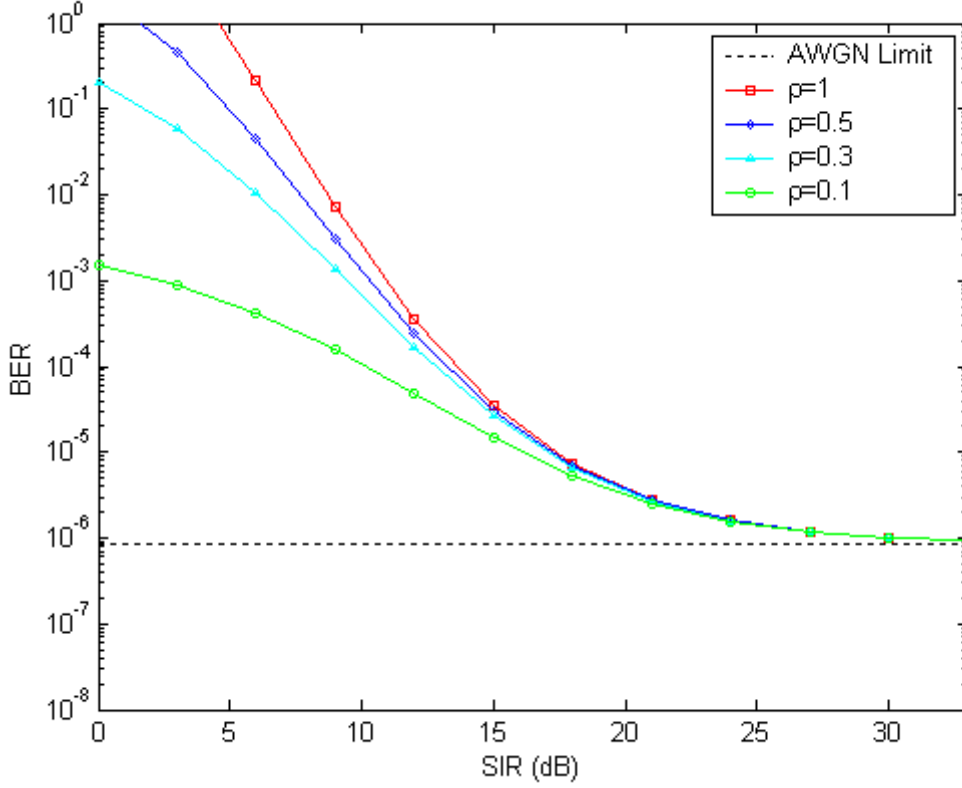


Figure 60. BER performance of an *IEEE 802.11a* noise-normalized sub-optimum receiver with PNJ for various ρ and for data rates of 9 and 18 Mbps.

2. Non-binary Modulation

Following the method discussed in the previous section, the BER of the noise-normalized sub-optimum *IEEE 802.11a* receiver can be obtained when MQAM is utilized. Combining Equations (4.8), (4.27), and (4.28) and inserting the PDF $f_{\gamma_b}(\gamma_b)$, the BER of an *IEEE 802.11a* noise-normalized sub-optimum receiver operating with PNJ is obtained when MQAM is used.

When non-binary modulation is used, the conditional probability $P_{d_i}(\gamma_b)$ is no longer expressed by Equation (5.10). Keeping in mind the assumption made previously in Chapter II, that the information bits keep the “soft” information that the demodulated symbol that represented the bits had, we see that the conditional probability of selecting a weight output sequence $P_d(\gamma_b)$ is given by

$$P_{d_i}(\gamma_b) = \frac{4}{q} Q \left(\sqrt{\frac{3q}{d(M-1)}} \gamma_b \right) \quad (5.28)$$

where q is the number of information bits per symbol and M is the number of symbols.

Next, the performance of the noise-normalized sub-optimum receiver in terms of BER is examined with PNJ and for all higher data rates specified by the *IEEE 802.11a* standard.

a. Data Rate of 24 Mbps

The receiver performance when data are transferred with a rate of 24 Mbps is examined. For this data rate 16QAM is used along with $r = 1/2$ FEC. Using the values $M = 16$, $q = 4$, and $r = 1/2$ along with the values of d_{free} and B_d specified in Table 2, we get the upper bound on BER, plotted in Figure 61 with respect to SIR at the receiver and for different fading conditions. For these calculations, the SIR is assumed to be $E_b/N_o = 15$ dB and the coefficient ρ that defines the fraction of time that the jammer is operational is $1/2$. Additionally, the BER performance curves of the optimum and sub-optimum receiver obtained in Chapter III for the same fading conditions are also plotted. Next, in Figure 62 we plot the BER of the receiver for different values of ρ , with $E_b/N_o = 15$ dB and $m = 1$.

b. Data Rate of 36 Mbps

Substituting $M = 16$, $q = 4$, and $r = 3/4$, we get the upper bound on BER of the optimum receiver for the 36 Mbps data rate. The estimated BER is plotted in Figure 63, along with the BERs of the optimum and sub-optimum receiver, with respect to SIR at the receiver and for different fading conditions. For these calculations, the SNR is assumed to be $E_b/N_o = 15$ dB and $\rho = 0.5$.

In Figure 64 we plot the BER of the receiver for different values of ρ , with $E_b/N_o = 15$ dB and $m = 1$.

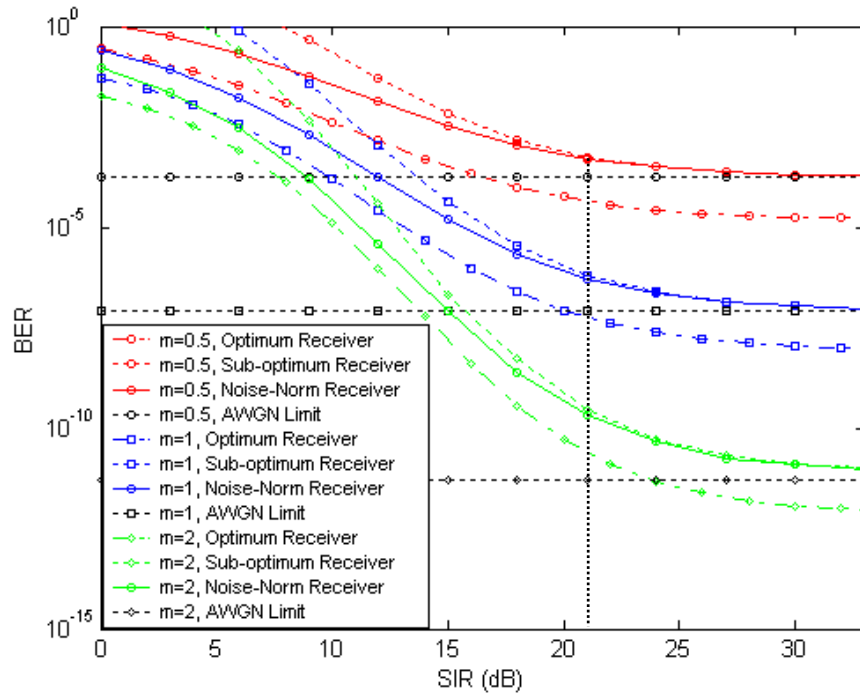


Figure 61. BER performance of an *IEEE 802.11a* noise-normalized sub-optimum receiver with PNJ for data rate of 24 Mbps.

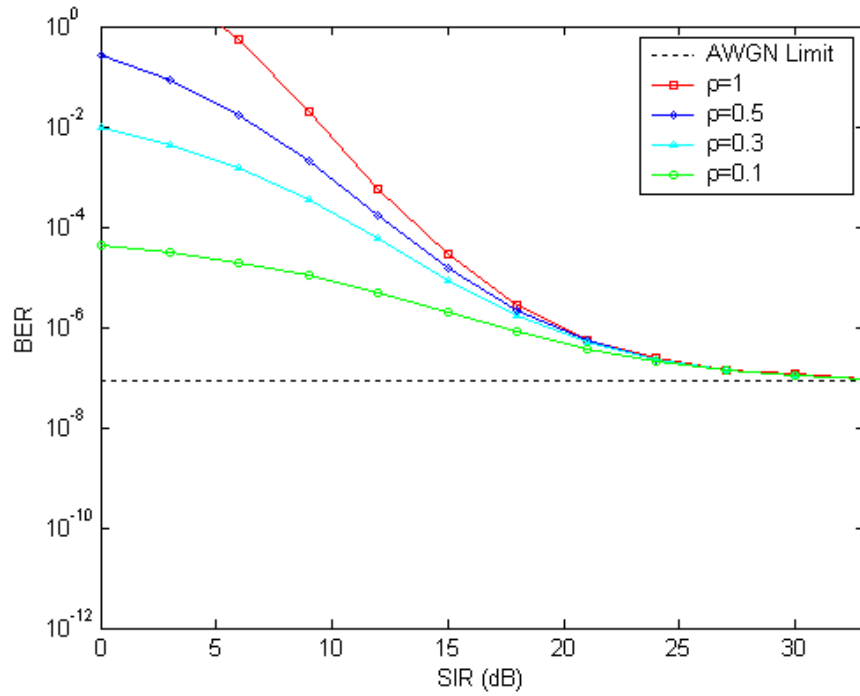


Figure 62. BER performance of an *IEEE 802.11a* noise-normalized sub-optimum receiver with PNJ for various ρ and for data rate of 24 Mbps.

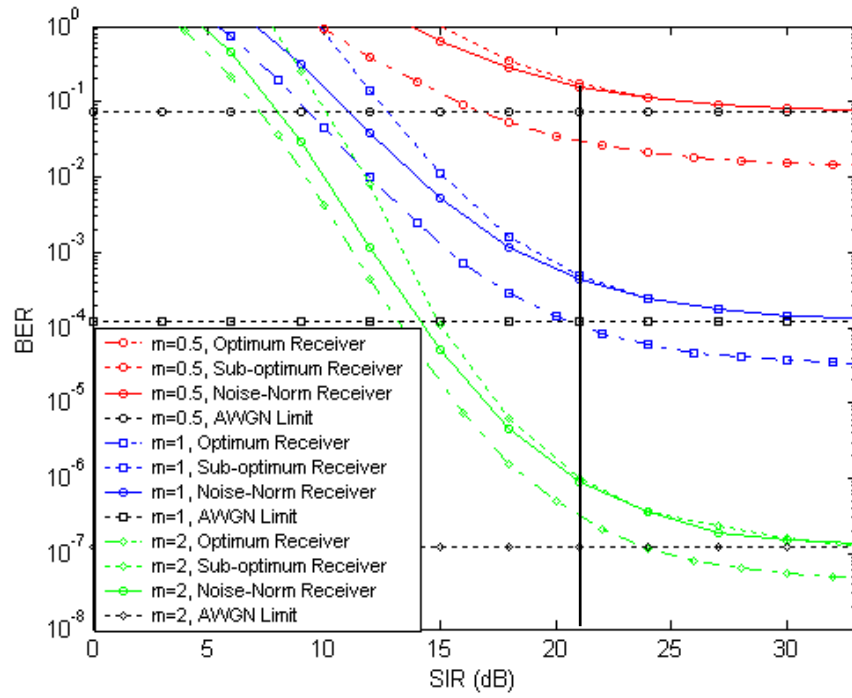


Figure 63. BER performance of an *IEEE 802.11a* noise-normalized sub-optimum receiver with PNJ for data rate of 36 Mbps.

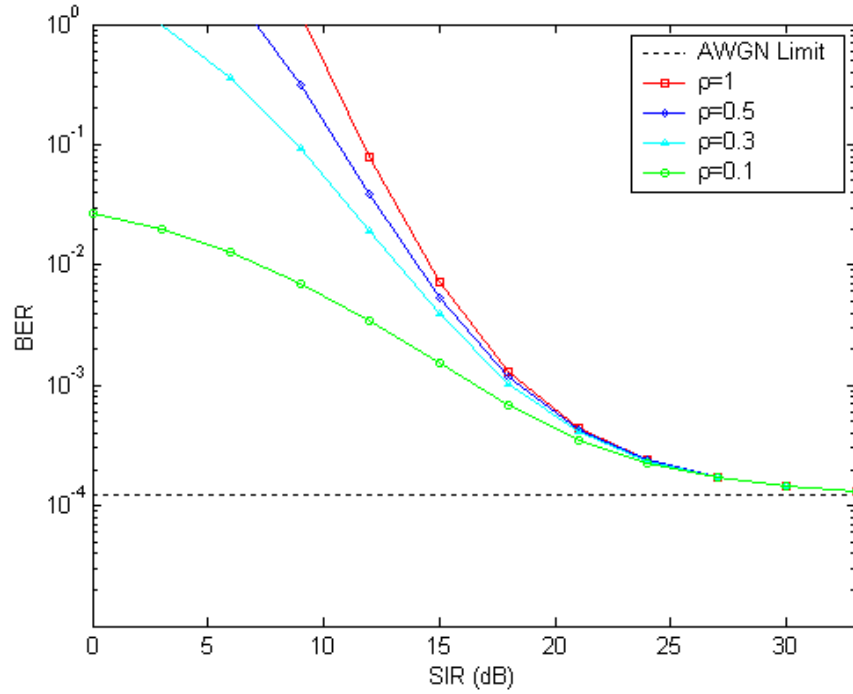


Figure 64. BER performance of an *IEEE 802.11a* noise-normalized sub-optimum receiver with PNJ for various ρ and for data rate of 36 Mbps.

c. Data Rate of 48 Mbps

For a data rate of 48 Mbps, 64QAM is used with a code rate of $r = 2/3$. Using $M = 64$, $q = 6$, and $r = 2/3$ we get the upper bound on BER, plotted in Figure 65, along with the BERs of the optimum and sub-optimum receiver with respect to SIR at the receiver, while SNR is assumed to be $E_b/N_o = 15$ dB and $\rho = 0.5$. In Figure 66, we plot the BER of the receiver for different values of ρ , with $E_b/N_o = 15$ dB and $m = 1$.

d. Data Rate of 54 Mbps

The highest data rate of 54 Mbps is achieved by using 64QAM and a FEC with $r = 3/4$. Using $M = 64$, $q = 6$, and $r = 3/4$ we get the upper bound on BER, plotted in Figure 67 with respect to SIR at the receiver and for different fading conditions. The SNR is assumed to be $E_b/N_o = 15$ dB and $\rho = 0.5$, and the BERs of the optimum and sub-optimum receiver are also plotted. Finally, in Figure 68 we plot the BER of the receiver for different values of ρ , with $E_b/N_o = 15$ dB and $m = 1$.

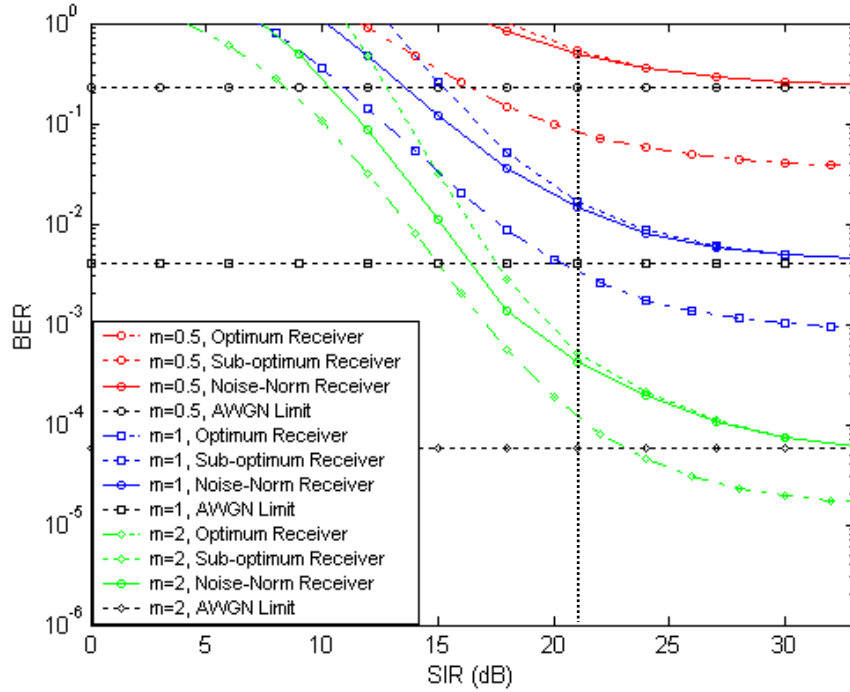


Figure 65. BER performance of an *IEEE 802.11a* noise-normalized sub-optimum receiver with PNJ for data rate of 48 Mbps.

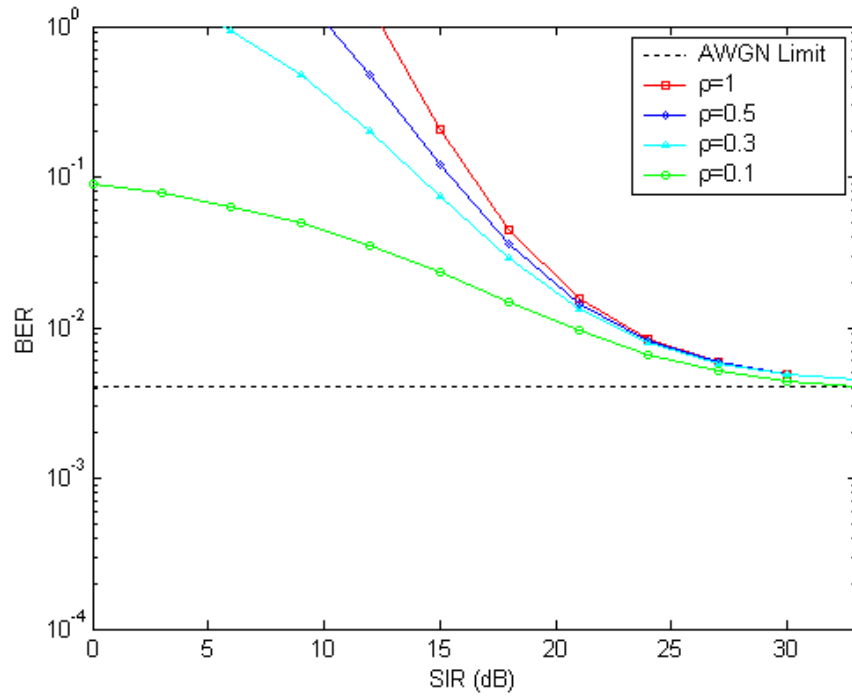


Figure 66. BER performance of an *IEEE 802.11a* noise-normalized sub-optimum receiver with PNJ for various ρ and for data rate of 48 Mbps.

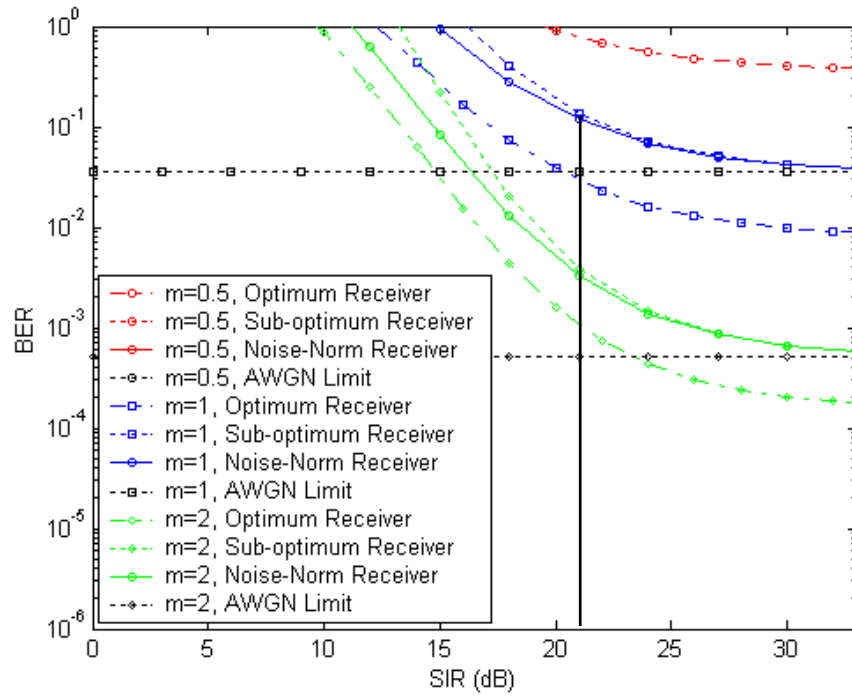


Figure 67. BER performance of an *IEEE 802.11a* noise-normalized sub-optimum receiver with PNJ for data rate of 54 Mbps.

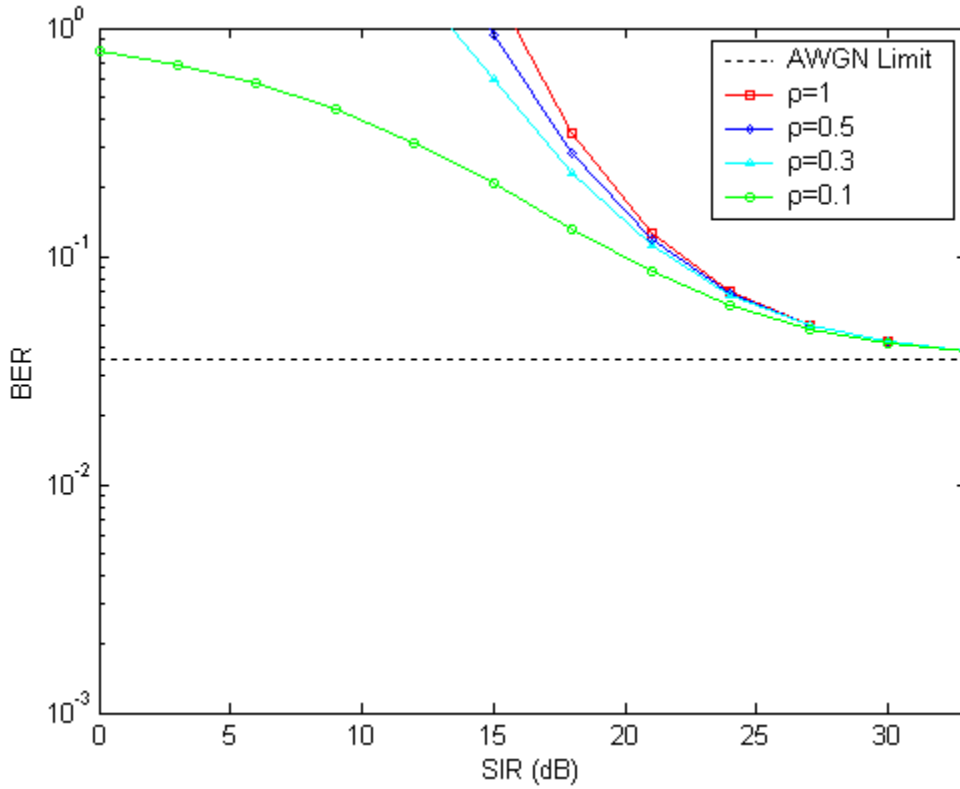


Figure 68. BER performance of an *IEEE 802.11a* noise-normalized sub-optimum receiver with PNJ for various ρ and for data rate of 54 Mbps.

3. Conclusions on the Effect of a Hostile PNJ on an IEEE 802.11a Noise-Normalized Sub-optimum Receiver

Summarizing, the overall performance of a noise-normalized sub-optimum receiver was discussed for all specified operational data rates when operating under the effect of PNJ.

First, we comment generally on the noise-normalized sub-optimum receiver performance. The BER of the noise-normalized sub-optimum receiver obviously follows a pattern analogous to the BERs of the optimum and sub-optimum receivers, regardless of the modulation or the code rate used (Figures 57, 59, 61, 63, 65, and 67). Therefore, the general conclusions made for the optimum and sub-optimum receiver with PNJ in sections III.C.3 and IV.C.3 apply here also. Summarizing, the noise-normalized receiver performance improves as we move from severe to moderate fading conditions. For severe fading conditions, receiver performance is affected mainly by the code rate used, while

the fading environment affects the receiver less when lower code rates are used. Moreover, as SIR increases, the performance of the noise-normalized sub-optimum receiver is improved up to the point where the AWGN power dominates. As a result, for values of $E_b/N_I > 30$ dB and for $E_b/N_o = 15$ dB, the performance of the receiver converges to a limit determined by AWGN.

Second, we compare the noise-normalized sub-optimum receiver performance to the optimum and sub-optimum receiver studied in Chapters III and IV, respectively.

Comparing the noise-normalized sub-optimum receiver BER to the optimum receiver BER (Figures 57, 59, 61, 63, 65, and 67), we see that the noise-normalized sub-optimum receiver BER is worse than that of the optimum receiver. However, this difference between the two receivers' performance lessens as the fading conditions become less severe. For all specified data rates, we see that the difference between the two performance curves decreases as m gets bigger. Moreover, it was proven that for no fading (i.e., $m \rightarrow \infty$) the performance of the two receivers are identical. This phenomenon occurs because, as the fading conditions improve, the jammed bits are increasingly de-emphasized due to the noise-normalization, resulting in better decision statistics. In the limiting case where $m \rightarrow \infty$, the jammed bits are completely de-emphasized, and the receiver is optimum (Figure 56).

Next, comparing the noise-normalized sub-optimum receiver BER to the sub-optimum receiver BER (Figures 57, 59, 61, 63, 65, and 67), we see that the noise-normalized sub-optimum receiver BER is significantly worse than the sub-optimum receiver BER for low SIR (i.e., $E_b/N_I < 21$ dB). However, as SIR increases, the two sub-optimum receivers' performance converges, asymptotically approaching the limit determined by AWGN. This behavior indicates that for low SIR, noise-normalization significantly improves the receiver's ability to reject PNJ and leads to better overall performance. On the other hand, when SIR increases, the AWGN dictates receiver performance and no further improvement is possible.

It also important to note that the value of SIR below which the noise-normalized sub-optimum receiver BER is worse (compared to the sub-optimum receiver BER) does not depend on either the modulation utilized or the code rate used. For all specified data

rates with $E_b/N_o = 15$ dB and $\rho = 0.5$, the SIR value below which the noise-normalized sub-optimum receiver BER is worse is $E_b/N_I = 21$ dB (Figures 57, 59, 61, 63, 65, and 67). Moreover, this difference in the two receivers is maintained even for the no fading scenario (Figure 56).

In Figures 58, 60, 62, 64, 66, and 68, the effect that the coefficient ρ has on receiver performance was investigated. It is clear that varying ρ affects the receiver performance significantly just as it does in the optimum receiver scenario. It can be seen that the worst case PNJ against the noise-normalized sub-optimum receiver is achieved when $\rho = 1$. Essentially, this means that the jammer is operational at all times, and the receiver is subjected to barrage jamming instead of pulsed jamming. Therefore, we conclude that BNJ is more effective against the noise-normalized sub-optimum receiver than a PNJ. Furthermore, we see that as ρ approaches zero (i.e., for $\rho = 0$ the jammer is not operating), the receiver performance tends to be constant and approaches the AWGN limit.

This behavior is explained by the fact that noise-normalization is implemented at the sub-optimum receiver. When the jamming power is spread to only a number of the received bits, those bits are de-emphasized, and the receiver is able to make decisions using primarily the non-jammed bits, resulting in better performance. On the other hand, when the jamming power has been spread to all received bits, even if all the bits are de-emphasized, the receiver is still forced to make a decision using all received, jammed bits and, because of this fact, is more likely to reach a wrong decision. In other words, from the receiver perspective, the larger the ρ , the poorer the receiver performance.

From the analysis made for both sub-optimum receivers on how the coefficient ρ affects receiver performance, it was found that the two receivers behave differently. The sub-optimum receiver with linear combining is affected the most when ρ is small, while in the noise-normalized scenario, worst case jamming is achieved for large ρ . In order to further investigate this behavior, in Figures 58 through 68 the BERs of the two receivers are plotted for all specified data rates for $\rho = 0.1$ and $\rho = 1.0$ with $E_b/N_o = 15$ dB.

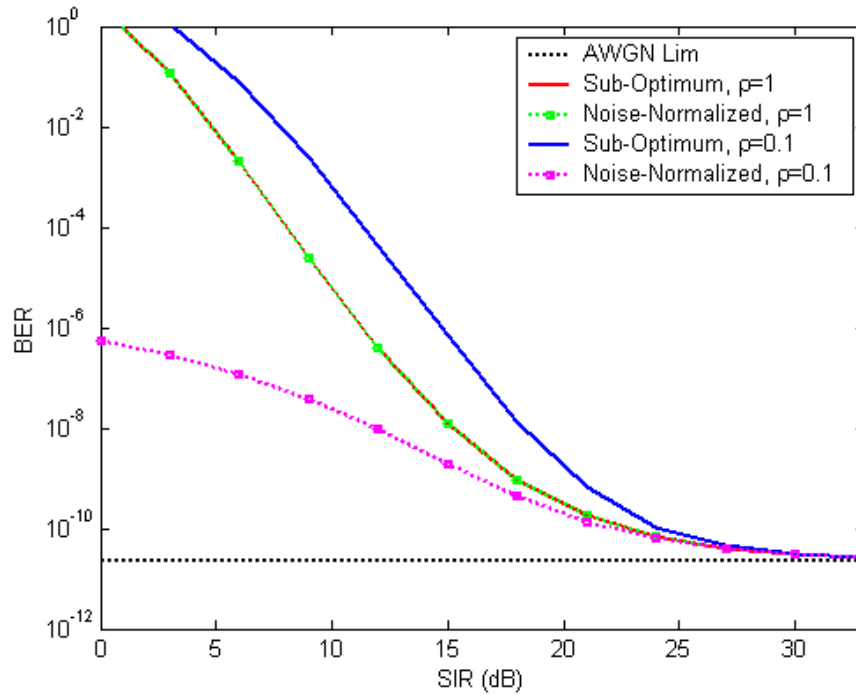


Figure 69. Noise-normalized sub-optimum receiver vs. linear-combining sub-optimum receiver with PNJ for $\rho = 0.1$ and 1.0 and for data rates of 6, 12 Mbps.

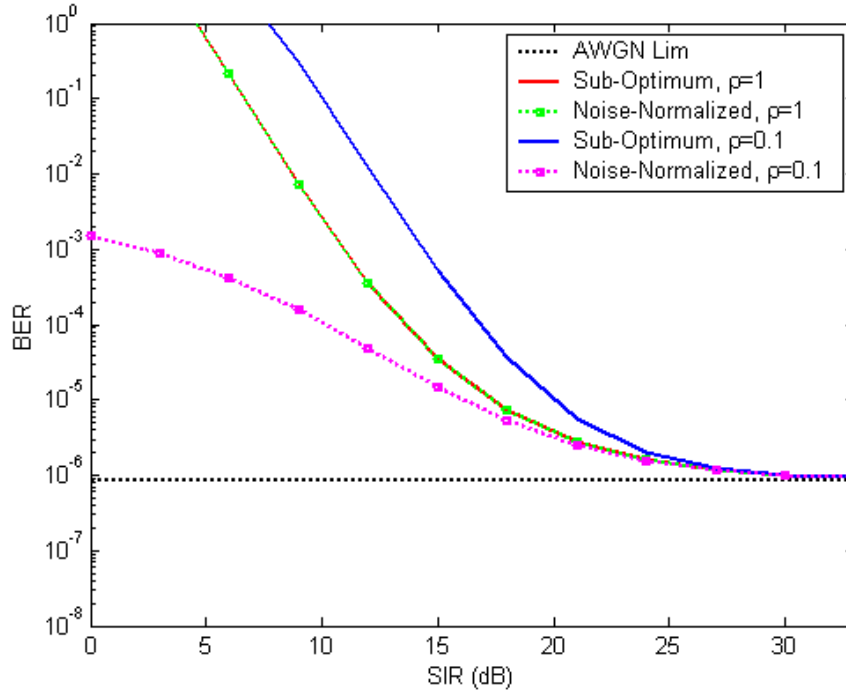


Figure 70. Noise-normalized sub-optimum receiver vs. linear-combining sub-optimum receiver with PNJ for $\rho = 0.1$ and 1.0 and for data rates of 9, 18 Mbps.

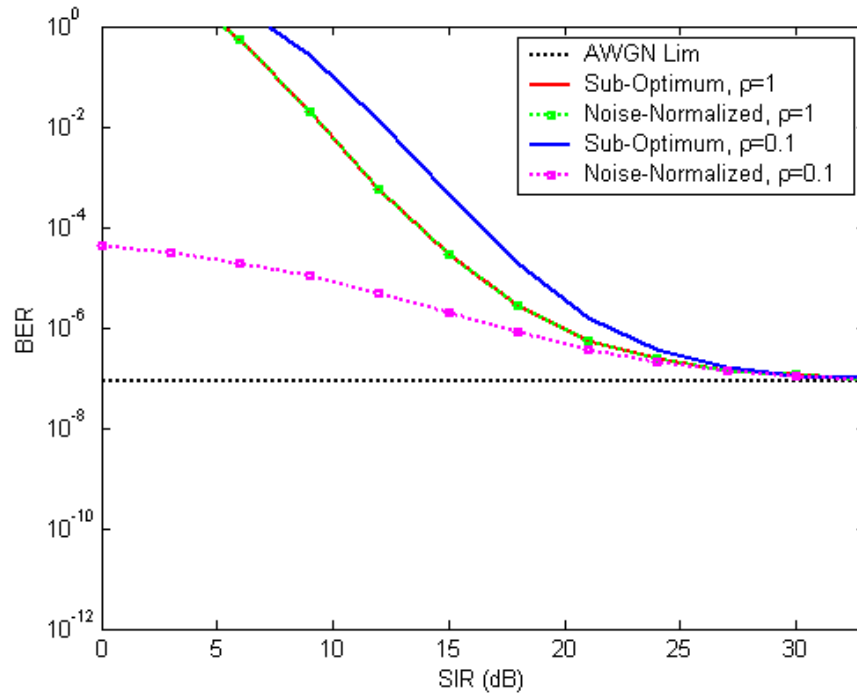


Figure 71. Noise-normalized sub-optimum receiver vs. linear-combining sub-optimum receiver with PNJ for $\rho = 0.1$ and 1.0 and for data rate of 24 Mbps.

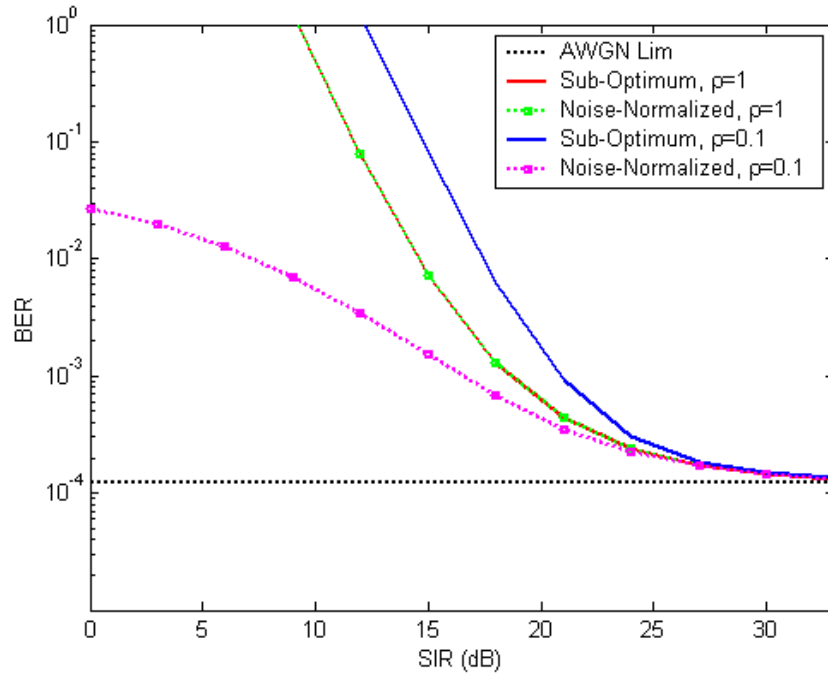


Figure 72. Noise-normalized sub-optimum receiver vs. linear-combining sub-optimum receiver with PNJ for $\rho = 0.1$ and 1.0 and for data rate of 36 Mbps.

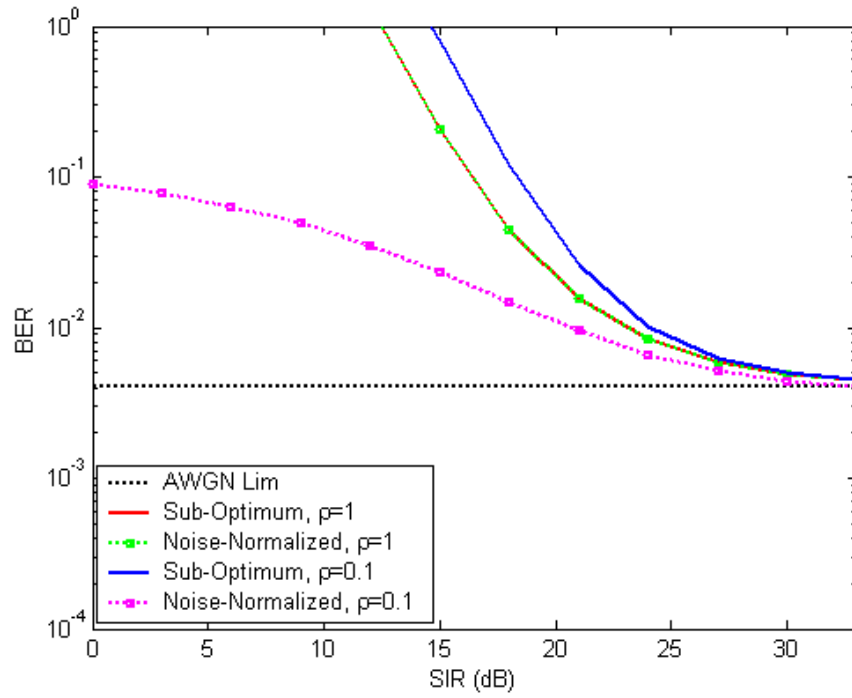


Figure 73. Noise-normalized sub-optimum receiver vs. linear-combining sub-optimum receiver with PNJ for $\rho = 0.1$ and 1.0 and for data rate of 48 Mbps.

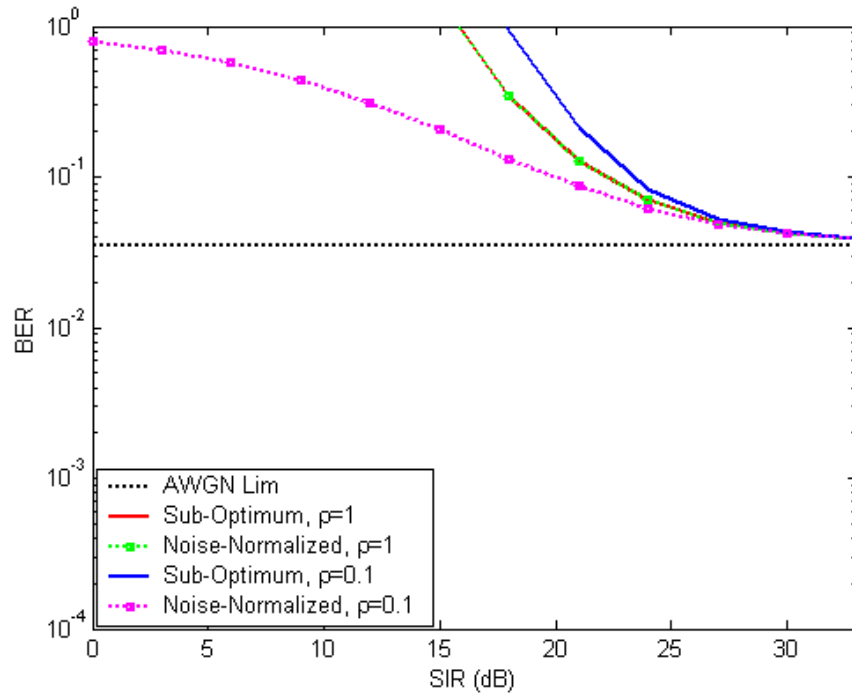


Figure 74. Noise-normalized sub-optimum receiver vs. linear-combining sub-optimum receiver with PNJ for $\rho = 0.1$ and 1.0 and for data rate of 54 Mbps.

From Figures 69 through 74, it is clear that, for all specified data rates, when a BNJ is operational (i.e., $\rho = 1$) both receivers have the same performance. This assumption is explained since in the BNJ scenario the jamming power has been spread to all received bits, and the effect of noise-normalization diminishes.

On the other hand, when ρ gets smaller, for low SIR the implementation of noise-normalization drastically improves the receiver performance, while for larger SIR both receivers' performance converges to a limit dictated by the AWGN. Therefore, for low SIR under the effect of PNJ, a noise-normalized sub-optimum receiver is a more reliable wireless communication scheme.

Having examined the performance of the noise-normalized sub-optimum receiver, we conclude our analysis with comments on the performance of the three receivers examined in Chapters III, IV and V.

THIS PAGE INTENTIONALLY LEFT BLANK

VI. CONCLUSIONS

The performance of the *IEEE 802.11a* WLAN standard receiver over flat fading Nakagami channels in a worst case, pulse-noise jamming environment was investigated in this thesis for the different combinations of modulation type (binary and non-binary modulation) and code rate specified by the WLAN standard. Receiver performance with Viterbi SDD was analyzed for AWGN alone and for AWGN plus PNJ. Moreover, the performance of the *IEEE 802.11a* WLAN standard receiver was examined both for the scenario where perfect side information was considered to be available (optimum receiver) and when it was not (sub-optimum receiver). In the sub-optimum receiver scenario, the receiver performance was examined both when linear combining was specified and when noise-normalization was utilized. In this closing chapter, the main conclusions of the analysis are summarized together with suggestions for future work.

A. SUMMARY OF THESIS FINDINGS

The performance of each *IEEE 802.11a* WLAN standard receiver (i.e., optimum receiver, sub-optimum receiver with linear combining, and noise-normalized sub-optimum receiver) was examined both for AWGN alone and for AWGN plus PNJ.

1. Conclusions on the Effect of AWGN

The first comment about the effect of AWGN on receiver performance is that in the sub-optimum receiver scenario, the implementation of noise-normalization has no effect on performance. When only AWGN is present, the noise power is uniform for all received bits. Therefore, the performance of the sub-optimum receiver without noise normalization is identical to the noise-normalized sub-optimum receiver when only AWGN is present.

The performance of the optimum and sub-optimum receiver was examined and each was assumed to operate in various fading conditions, from severe and moderate conditions to the ideal case of no fading. It was proven analytically that when there is no

fading, the two receivers have identical performance. In other words, for an ideal channel without fading, all receivers examined have optimum performance.

In the more realistic scenario where the receivers are operating in a fading channel, the optimum receiver outperforms – as expected – the sub-optimum receiver, regardless of the modulation utilized or the code rate used, especially when the fading conditions are severe (i.e., $m \rightarrow 0.5$). However, the performance of these two receivers tends to converge as the fading conditions improve (i.e., m gets larger).

Moreover, it is important to note that the BERs of both the optimum and sub-optimum receiver follow a very similar pattern for all specified data rates. Therefore, the following comments apply to both receivers: the fading environment affects the receiver less when lower code rates are used, while for severe fading conditions the sub-optimum receiver performance is mainly affected by the code rate used. For less severe fading conditions, receiver performance is mainly affected by the modulation utilized. As a result, even though in general non-binary modulation is known to have poorer performance, some higher data rates (i.e., 36 Mbps) appear to have better performance in severe fading conditions than lower data rates (i.e., 24 Mbps).

2. Conclusions on the Effect of PNJ

As in the AWGN only scenario, the performance of the optimum and two sub-optimum receivers was examined when each was assumed to operate in various fading conditions, from severe and moderate conditions to the ideal case of no fading.

One general comment is that the optimum receiver outperforms both sub-optimum receivers for all specified data rates and for all fading conditions while the sub-optimum receiver with linear combining has the poorest performance. In the special case where no fading conditions are assumed, the noise-normalized sub-optimum receiver is optimum, while for large SIR the sub-optimum receiver with linear combining is also optimum. On the other hand, for lower SIR the sub-optimum receiver with linear combining is significantly worse (Figure 56). The value of SIR below which the sub-optimum receiver with linear combining is worse depends on the SNR used. Particularly, for $E_b/N_o = 15$ dB, this value of SIR was found to be $E_b/N_f = 10$ dB.

Another finding that applies to all receivers is the fact that as the signal strength increases (i.e., SIR increases) each receiver's performance converges to a limit determined by the AWGN power (i.e., the SNR used) regardless of the fading conditions. This limit for any particular m is smaller for the optimum receiver while it is the same for the two sub-optimum receivers. Comparing the two sub-optimum receivers, we see that for low SIR the receiver with linear combining performs worse than the noise-normalized while for larger SIR both BERs converge.

Besides the differences already noted, the BERs of the three receivers follow a very similar pattern regardless of the fading conditions or the data rate at which the receiver operates. Commenting on all three receivers, we note that each receiver's performance improves as we move from severe to moderate fading conditions. For severe fading conditions, receiver performance is affected mainly by the code rate used, while the fading environment affects the receiver less when lower code rates are used.

It obvious that for all three receivers there is a tradeoff between BER and data rate. The higher the data rate, the poorer the performance. So, in order to maintain reliable communication for higher data rates (i.e., achieving $P_b \leq 10^{-4}$), more signal power is required. The additional signal power required is significantly more for the sub-optimum receiver with linear combining when SIR is small since this receiver performance is the worse. When $E_b/N_o = 15$ dB and $m = 1$, it was found that the maximum data rate that a sub-optimum receiver with linear combining can reliably process is 24 Mbps, while an optimum receiver can go up to 36 Mbps.

Another important finding is how the parameter ρ affects each receiver performance. It was found that the worst case jamming for the optimum and the noise-normalized sub-optimum receiver is the BNJ (i.e., $\rho = 1$), while for the sub-optimum receiver with linear combining, the worst case jamming is achieved as $\rho \rightarrow 0$. Moreover, it is important to note that, when $\rho = 1$, the two sub-optimum receivers have the same performance. In other words, the noise-normalized receiver worst jamming scenario is similar to the receiver with linear combining best jamming scenario; with BNJ both sub-optimum receivers have the same performance (noise-normalization loses its advantage).

Summarizing, the optimum receiver results in the best performance with PNJ but cannot be realized in practice since perfect side information is not available. On the other hand, the more practical sub-optimum receiver with linear combining results in significantly poorer performance, especially when SIR is small. This disadvantage can be compensated for by the implementation of noise-normalization. However, this increases the complexity of the receiver since the noise power must be accurately measured. Therefore, if we need to improve receiver performance, a more complex and more expensive receiver is required.

B. FUTURE WORK

There are several areas in which follow-on research is recommended. Since the computation of the BER of the sub-optimum receivers is done numerically, a derivation of analytical closed form expressions would help reduce the time required to obtain results.

Furthermore, the performance of the receivers can be examined for other types of jammers, such as a tone jammer.

Finally, the development of circuitry that could accurately measure the noise power in order to implement noise-normalization would be of great importance.

C. CLOSING COMMENTS

The *IEEE 802.11a* WLAN standard is a proven and widely used communication scheme in both commercial and military applications. The analysis in this thesis will prove beneficial to those utilizing the *IEEE 802.11a* WLAN standard. The performance of this widely used standard was examined for all specified data rates, for a wide range of fading conditions, and for both ideal and more practical receivers.

The fact that the *IEEE 802.11a* WLAN standard was examined in the presence of BNJ and PNJ makes this research beneficial to those utilizing the standard for military applications, where systems are more likely to operate in a hostile environment.

APPENDIX A. THE TWO-SIDED LAPLACE TRANSFORM

The evaluation of an alternative, more efficient method to estimate the ILT of a function is discussed in [8] and discussed in this APPENDIX A for convenience. Consider the function $f_X(x)$. The two-sided LT of $f_X(x)$ is defined as

$$F_X(s) = \int_{-\infty}^{\infty} f_X(x) e^{-sx} dx \quad (\text{A.1})$$

where $s = c + j\omega$ and c must be within the strip of convergence of $F_X(s)$.

The inverse two-sided LT is given by definition by [10]

$$f_X(x) = \frac{1}{2\pi j} \int_{c-j\omega}^{c+j\omega} F_X(s) e^{sx} ds. \quad (\text{A.2})$$

Rewriting Equation (A.2) as an integral over ω , we get

$$f_X(x) = \frac{1}{2\pi} \int_{-\infty}^{+\infty} F_X(c + j\omega) e^{(c+j\omega)x} d\omega \quad (\text{A.3})$$

where

$$\begin{aligned} F_X(c + j\omega) e^{(c+j\omega)x} &= \left[\text{Re}\{F_X(c + j\omega)\} + j \text{Im}\{F_X(c + j\omega)\} \right] \\ &\quad \times e^{cx} \left[\cos(\omega x) + j \sin(\omega x) \right]. \end{aligned} \quad (\text{A.4})$$

If $f_X(x)$ is a real function, then the real part of $F_X(s)$ is even and the imaginary part of $F_X(s)$ is odd. As a result, the imaginary part of $F_X(c + j\omega) e^{(c+j\omega)x}$ is odd and, as required for a real function, does not contribute to Equation (A.3). The real part of the integrand is expressed as

$$\text{Re}\{F_X(c + j\omega) e^{(c+j\omega)x}\} = e^{cx} \left[\text{Re}\{F_X(c + j\omega)\} \cos(\omega x) - \text{Im}\{F_X(c + j\omega)\} \sin(\omega x) \right]. \quad (\text{A.5})$$

Substituting Equation (A.5) into (A.3), we get

$$f_X(x) = \frac{e^{cx}}{2\pi} \int_{-\infty}^{+\infty} \left[\text{Re}\{F_X(c + j\omega)\} \cos(\omega x) - \text{Im}\{F_X(c + j\omega)\} \sin(\omega x) \right] d\omega. \quad (\text{A.6})$$

Next, we perform the change of variables

$$\omega = \frac{cu}{\sqrt{(1-u^2)^3}} \quad (\text{A.7})$$

which yields

$$d\omega = \frac{c du}{\sqrt{(1-u^2)^3}}. \quad (\text{A.8})$$

Equation (A.6) can now written as

$$\begin{aligned} f_X(x) = \frac{e^{cx}}{2\pi} \int_{-1}^1 & \left[\operatorname{Re} \left\{ F_X \left(c + j \frac{cu}{\sqrt{1-u^2}} \right) \right\} \cos\left(\frac{cux}{\sqrt{1-u^2}}\right) \right. \\ & \left. - \operatorname{Im} \left\{ F_X \left(c + j \frac{cu}{\sqrt{1-u^2}} \right) \right\} \sin\left(\frac{cux}{\sqrt{1-u^2}}\right) \right] \frac{c du}{\sqrt{(1-u^2)^3}}. \end{aligned} \quad (\text{A.9})$$

In order to simplify Equation (A.9), we perform a second change of variables

$$\tan(\varphi) = \frac{u}{\sqrt{1-u^2}} \quad (\text{A.10})$$

which yields

$$d\varphi = \frac{du}{\sqrt{1-u^2}}. \quad (\text{A.11})$$

Finally, substituting Equations (A.10) and (A.11) into (A.9), we get

$$\begin{aligned} f_X(x) = \frac{ce^{cx}}{\pi} \int_0^{\pi/2} & \left[\operatorname{Re} \{ F_X(c + jc \tan(\varphi)) \} \cos(cx \tan(\varphi)) \right. \\ & \left. - \operatorname{Im} \{ F_X(c + jc \tan(\varphi)) \} \sin(cx \tan(\varphi)) \right] \sec^2(\varphi) d\varphi \end{aligned} \quad (\text{A.12})$$

where

$$\sec^2(\varphi) = \frac{1}{\sqrt{1-u^2}} \quad (\text{A.13})$$

The advantage of Equation (A.12) is the fact that the integral with infinite limits (Equation (A.1)) has been transformed into one with finite limits. Therefore, the expression in Equation (A.12) can be numerically computed more easily.

THIS PAGE INTENTIONALLY LEFT BLANK

LIST OF REFERENCES

- [1] Count, A., Patrick, "Performance Analysis of OFDM in Frequency-selective, Slowly Fading Nakagami Channels," Master's thesis, Naval Postgraduate School, Monterey, CA, 2001.
- [2] Kosa, Irfan, "Performance of IEEE 802.11a Wireless LAN Standard over Frequency-Selective, Slowly Fading Nakagami Channels in a Pulsed Jamming Environment," Master's thesis, Naval Postgraduate School, Monterey, CA, 2002.
- [3] Institute of Electrical and Electronics Engineers Standard, 802.11a, *Wireless LAN Medium Access Control (MAC) and Physical Layer (PHY) Specifications: High-Speed Physical Layer Extension in the 5 GHz Band*, IEEE, New York, 16 September 1999.
- [4] Proakis, J.G., *Digital Communications*, 4th edition, McGraw Hill, New York, NY, 2001.
- [5] Wicker, S.B., *Error Control Systems for Digital Communication and Storage*, Prentice Hall, Upper Saddle River, NJ, 1995.
- [6] Rappaport, S. Theodore, *Wireless Communications Principles and Practice*, 2nd edition, Prentice Hall, Upper Saddle River, NJ, 2002.
- [7] Sklar, B., *Digital Communications: Fundamental and Applications.*, 2nd edition, Prentice Hall, Upper Saddle River, NJ, 2001.
- [8] Robertson, Clark, Notes for EC4550 (*M*-ary Digital Communication Systems), Naval Postgraduate School, Monterey, CA, 2001 (unpublished).
- [9] Hippenstiel, D. Ralph, *Detection Theory: Applications and Digital Signal Processing.*, CRC Press LLC, Boca Raton, FL, 2000.
- [10] Leon-Garcia, A., *Probability and Random Processes for Electrical Engineering.* 2nd edition, Addison Wesley, Reading, MA, 1994.
- [11] Gradshteyn, I.S. and Ryzhik, I.M., *Tables of Integrals, Series, and Products*, Academic Press, New York, NY, 1980.

THIS PAGE INTENTIONALLY LEFT BLANK

INITIAL DISTRIBUTION LIST

1. Defense Technical Information Center
Ft. Belvoir, Virginia
2. Dudley Knox Library
Naval Postgraduate School
Monterey, California
3. Chairman, Code EC/Po
Department of Electrical and Computing Engineering
Naval Postgraduate School
Monterey, California
4. Chairman, Code IS/Bo
Department of Information Sciences
Naval Postgraduate School
Monterey, California
5. Professor Clark Robertson, Code EC/Rc
Department of Electrical and Computing Engineering
Naval Postgraduate School
Monterey, California
6. Professor Don Wadsworth, Code EC/Wd
Department of Electrical and Computing Engineering
Naval Postgraduate School
Monterey, California
7. Embassy of Greece, Naval Attaché
Washington, DC
8. Christos Kalogrias
Mpotsari 73,75
Piraeus, GREECE
TK: 18537